

DOTTORATO DI RICERCA IN SCIENZE CHIMICHE - XXV CICLO

Settore Concorsuale di afferenza: 03/B1 Fondamenti delle Scienze Chimiche e Sistemi Inorganici

Settore Scientifico disciplinare: CHIM/03 – Chimica Generale ed Inorganica

**DESIGN, SYNTHESIS AND
CHEMICAL-PHYSICAL CHARACTERIZATION OF
PHOTOCATALYTIC INORGANIC NANOCRYSTALS
FOR INNOVATIVE
TECHNOLOGICAL APPLICATIONS**

Presentata da:
Dott. Marco Marchetti

Relatore:
Prof. Norberto Roveri

Coordinatore Dottorato:
Prof.ssa Adriana Bigi

INDEX

	Page
ABSTRACT	1
CHAPTER 1	
INTRODUCTION	3
1.1 - TITANIUM DIOXIDE	3
1.1.1 - Structure of Titanium Dioxide	7
<i>1.1.1.1 – Rutile</i>	<i>8</i>
<i>1.1.1.2 – Anatase</i>	<i>10</i>
<i>1.1.1.3 – Brookite</i>	<i>11</i>
1.2 - SEMICONDUCTOR MATERIALS	13
1.2.1– Density of Electron and Gaps in a Semiconductor	15
1.2.2 – Semiconductors and photocatalytic activity	16
1.3– PHOTOCATALYSIS	19
1.3.1 – Mechanism	20
1.4 - SYNTHESIS OF TITANIUM DIOXIDE NANOPARTICLES	24
1.4.1 - Hydrothermal synthesis	24

1.5.2 - Sol-Gel Method	27
1.5 TITANIUM DIOXIDE FUNCTIONALIZATION	29
1.5.1 - Functionalization with inorganic nanoparticles	30
1.6.1.1 – <i>Hydroxiapatite</i>	30
1.5.2 - Functionalization with organic molecules	32
1.6.2.1 – <i>Resorcinol</i>	33
CHAPTER 2	
EXPERIMENTAL SECTION	34
2.1 - SYNTHESSES	34
2.1.1- Hydrothermal Synthesis of titanium dioxide particles	34
2.1.1.1 – <i>Operation mode</i>	35
2.1.1.2 – <i>Materials</i>	35
2.1.1.3 – <i>Syntheses</i>	35
2.1.2 – Synthesis in water	38
2.1.2.1 – <i>Materials</i>	38
2.1.2.2 – <i>Synthesis</i>	38
2.1.3 – Functionalization of Titanium Dioxide Nanoparticles	39
2.1.3.1 – <i>Functionalization with hydroxyapatite</i>	39
2.1.3.1.2 - <i>Synthesis of hydroxyapatite microcrystals</i>	40
2.1.3.1.2.1 – <i>Materials</i>	40
2.1.3.1.2.2 – <i>Synthesis</i>	40
2.1.3.1.3 – <i>Synthesis of titanium dioxide – hydroxyapatite</i>	

<i>microcrystals</i>	40
2.1.3.2 – <i>Functionalization with oxidized resorcinol</i>	41
2.1.3.2.1 - <i>Resorcinol oxidation</i>	41
2.1.3.2.1.1 – <i>Materials</i>	41
2.1.3.2.1.2 – <i>Synthesis</i>	41
2.1.3.2.2 - <i>TiO₂ nanoparticles surface complexed by oxidized resorcinol</i>	42
2.1.4. – <i>Synthesis water less</i>	42
2.1.4.1. – <i>Materials</i>	42
2.1.4.2. – <i>Synthesis</i>	42
2.2 – CHEMICAL-PHYSICAL CHARACTERIZATION	44
2.2.1 - X-ray diffraction (XRD)	44
2.2.1.1 - <i>Operating Procedure</i>	46
2.2.2 - UV Visible Spectroscopy	47
2.2.2.1 - <i>Operating Procedure</i>	49
2.2.3 - Infrared spectroscopy (FT-IR)	52
2.2.3.1 - <i>Operating Procedure</i>	54
2.2.4 - Scanning Electron Microscope (SEM)	55
2.2.5 - Tunneling Electron Microscopy (TEM)	59
2.2.5.1 - <i>Operating Procedure</i>	60
2.2.6 – Surface Area	60
2.2.7 - Thermal Analysis	60
2.2.7.1 - <i>Thermogravimetric Analysis (TGA)</i>	61
2.3 – PHOTOCATALYTICAL TESTS	62
2.3.1 - Degradation of methylene blue	62
2.3.1.1 - <i>Mechanistic aspects of degradation</i>	65

2.3.1.2 – Procedure	66
2.3.2 - Degradation of NO _x	67
2.3.3 - Antibacterial test	68
2.4 – BIOLOGICAL TESTS	70
2.4.1 – Antioxidant capacity	70
2.4.2 – Toxicity Test	71
2.4.2.1 -Test of hemolysis	71
2.4.2.2. - Test of cell viability by staining with Trypan blue	72
2.4.2.3 - Production of Nitrite in THP-1 cells	72
2.4.2.4 - Cytotoxicity assay by determination of LDH	72
CHAPTER 3	
RESULTS AND DISCUSSION	74
3.1 – HYDROTHERMAL SYNTHESSES	74
3. 1.2 – DRX Characterization	74
3. 1. 2 .1 – Synthesis 1	74
3. 1. 2. 2 - Synthesis 2	75
3. 1. 2. 3 - Synthesis 3	75
3. 1.2 .4 - Synthesis 4	76
3. 1.2 .5 - Synthesis 5	76
3. 1.2 .6 - Synthesis 6	77
3. 1.2 .7 - Synthesis 7	77

3. 1.2 .8 - <i>Synthesis 7 heat-treated</i>	78
3. 1.2 .9 - <i>Synthesis 4 heat-treated</i>	78
3. 1.2 .10 - <i>Synthesis 6 with ultrasound treatment</i>	79
3.1.2. 11. - <i>Comparison of the products obtained</i>	79
3.1.2.12 – <i>Thermal treatment</i>	81
3.1.2.13 - <i>Use of ultrasound</i>	84
3.1.2 – Morphologic Characterization	85
3.1.3 – FT-IR Characterization	90
3.1.4 - Photocatalytic Test	94
3.1.4.1 – <i>Degradation of Methylene Blue</i>	94
3.1.5 – Discussion	96
3.2 – SYNTHESIS IN WATER	99
3.2.1 – XRD Characterization	99
3.2.2 – Morphological Characterization	100
3.2.3 – Surface area	101
3.2.4 – FT-IR Characterization	102
3.2.5 - Photocatalytic test	102
3.2.5.1 – <i>Degradation of methylene blue</i>	<i>102</i>
3.2.5.2 – <i>Degradation of NOx</i>	<i>104</i>
3.3 – SYNTHESIS OF HYDROXYAPATITE	105
3.3.1 – DRX Characterization	105
3.3.2 – FT-IR Characterization	105
3.3.3 – Morphological Characterization	106
3.6 – FUNCTIONALIZATION WITH HYDROXYAPATITE	107
3.6.1- XRD Characterization	107

3.6.2- FT-IR Characterization	108
3.6.3 – Surface Area	109
3.6.4 – Morphologic Characterization	109
3.6.5 – Thermal Analysis	111
3.6.3 Photocatalytic Test	112
3.6.3.1 – Degradation of Methylene Blue	112
3.6.3.2 – Degradation of NO_x	114
3.6.3.3 -Antibacterial effect	116
3.6.4 – Biological and cellular tests	117
3.6.4.1 - Antioxidant Activity	117
3.6.4.2 - Toxic activity	118
3.6.5 – Discussion	120
3.6.2 – Functionalization with oxidized resorcinol	121
3.6.2. 1. - XRD Characterization	121
3.6.2.2 - FT-IR Characterization	122
3.6.3 – Morphologic characterization	124
3.6.4 – Thermal treatment	124
3.6.4.1 – Thermogravimetric analysis	125
3.6.4.2 –XRD Characterization	125
3.6.4.3 - FT-IR Characterization	126
3.6.5 - Photocatalytic Test	127
3.6.5.1 - Degradation of Methylene Blue	127
3.6.5.2 - NO_x degradation	128
3.6. 6 – Discussion	129
3.7- SYNTHESIS WATERLESS	131
3.7.1 - DRX- Characterization	131
3.7.2 -FT-IR Characterization	133
3.7.3 - Morphologic Characterization	134

3.7.4 – Surface Area	135
3.7.5 - Photocatalitical test	136
<i>3.7.5.1 - Degradation of Methylene Blue</i>	<i>136</i>
3.7.6. – Thermal treatment	136
<i>3.7.6.1.– XRD Characterization</i>	<i>137</i>
<i>3.7.6.2 – FT-IR Characterization</i>	<i>138</i>
<i>3.7.7.1-Photocatalytic Test</i>	<i>139</i>
<i>3.7.7.1.1- Degradation of Methylene blue</i>	<i>139</i>
3.7.7 – Discussion	140

CHAPTER 4

CONCLUSIONS	142
--------------------	------------

REFERENCES	146
-------------------	------------

ABSTRACT

This doctoral thesis has been developed on the study of the synthesis and characterization of novel inorganic nanocrystals with peculiar properties for applications in technological and biomedical fields.

In particular, the work has been focused on innovative inorganic nanocrystals with photo-catalytic properties like titanium dioxide. Starting to synthesis, and then by varying parameters and type of production of the crystals and their functionalization which influence the chemical-physical properties, we have studied the correlation between the latter and photocatalytic properties of the nanocrystals.

At first the work studied the correlation between fluctuations in the parameters of the synthesis and physico-chemical properties, then we continued investigating new types of synthesis and finally the functionalization of the crystals both with other inorganic materials and with organic molecules to obtain a greater photo-catalytic efficiency.

We have develop hydrothermal syntheses for nanocrystalline TiO₂ anatase varying some synthetic processes and some specific parameters like some reactants, pH, temperature and duration of the reaction, in order to optimize the characteristics of the photocatalytic TiO₂ nanocrystals obtained.

Sequencely the method and the optimal parameters for the synthesis of nanocrystalline TiO₂ have been further refined and a water-alcohol suspension of inorganic microparticles and nanostructured functionalized surface with nanocrystals TiO₂ able to produce innovative photocatalytic properties has been developed.

It also were conducted studies on the functionalization of titanium dioxide nanoparticles with organic molecules.

To ensure that there is a greater adhesion and functionalizing effect on the nanoparticles, it is sought to develop a new type of synthesis or a synthesis in which the formation of titanium dioxide occurs without water, not passing through hydrolysis of alkoxide precursor of TiO_2 , but through an esterification between formic acid and octanol. The result is a material that consists of a single crystalline phase, which is anatase, directly from synthesis without the need for heat treatments, where the surface presents carboxylic residues able to bind most organic molecules.

CHAPTER 1 - INTRODUCTION

1.1 - TITANIUM DIOXIDE

Titanium dioxide (Fig. 1) still represents one of the most known and important materials used in various fields and applications, for its excellent optical properties consisting of a high reflective index that brings a powder hiding and whiteness, chemical stability and relatively low production cost.



Fig. 1 – Titanium dioxide

Titanium dioxide is present in nature in three different minerals: rutile, anatase and brookite. In addition to these, there are two other phases that formed in conditions of high pressures and have respectively monoclinic form similar to that of baddeleyite (zirconium oxide, ZrO_2), an orthorhombic form similar to α - PbO_2 . The most common form is that of rutile which is also the most thermodynamically stable form. The other 2 stages, anatase and brookite, are metastable phases and may be converted into rutile through thermal processes.

Oxides of titanium may be extracted in nature and used as a source of titanium for commercial use. Titanium metal can be extracted from other minerals such as ilmenite (FeTiO_3) or leucoxene.

Crystalline TiO_2 is used to improve materials and device in many fields.

Titanium dioxide is a preferred system for experimentalists because it is well-suited for many experimental techniques.

Titanium dioxide is a semiconductor; following irradiation with UV light or sunlight hole-electron pair is created which can be separated and then the charge carriers can migrate to the surface where they can react with the adsorbed water and oxygen to produce radical species. These species can attack a wide range of organic molecules and reduce and decompose them to H_2O and CO_2 .

Because of this behavior, the titanium dioxide has found a wide range of applications in many areas such as processes of purification of waste water [1]; disinfection based on the bactericidal properties of TiO_2 [2] (for example, in operating theaters in hospitals), use of self-cleaning coatings on glass, car windshields [3], for protective coatings of marble to preserve statues and monuments [4], coatings of houses, buildings and road tunnels. (Fig. 2)

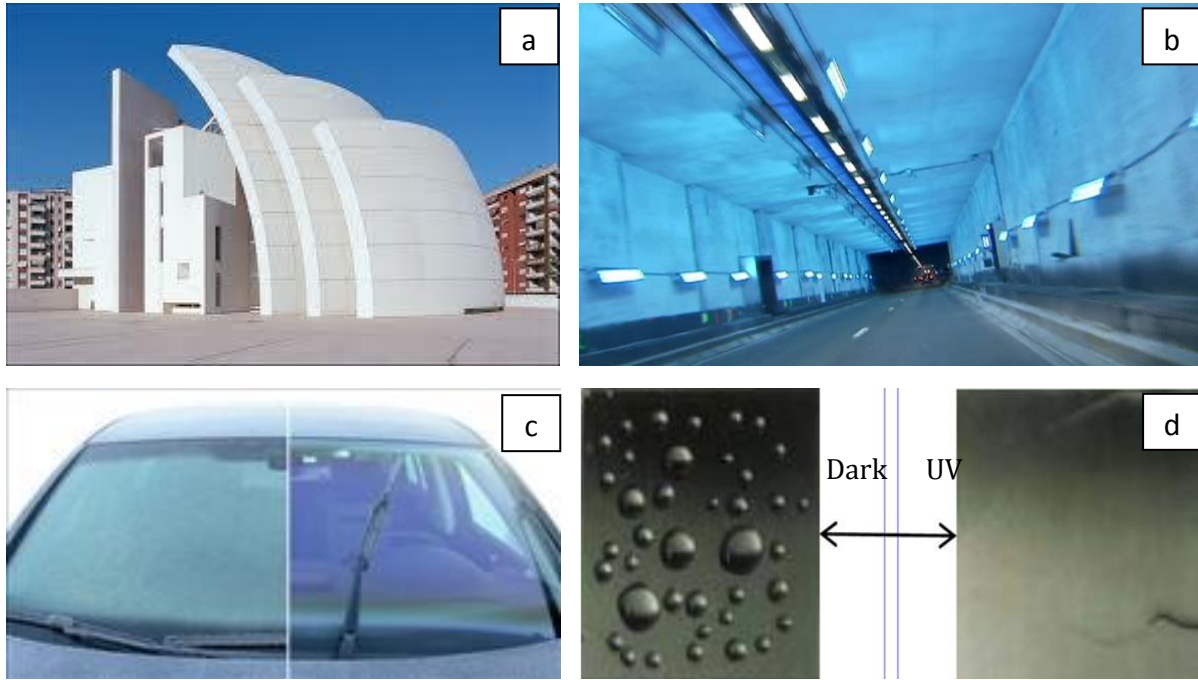


Fig. 2 - Examples of Titanium dioxide applications: coating of building(a), coating of road tunnel(b), self-cleaning coatings on car(c), self-cleaning coatings on car(d)

Furthermore, titanium dioxide has also found applications in the medical field. Some studies conducted in rats show that subcutaneous injection of a paste composed of titanium dioxide followed by exposure to UV light may reduce, close or block the development and proliferation of tumor cells [5,6,7].

In scientific literature there are several scientific studies and papers documenting the superficial work and photocatalytic activity of titanium dioxide [1,8,9,10,11,12].

Some metal oxide semiconductors are able to change their conductivity on the basis of adsorption of different types of gases and gas concentrations. These changes can be transformed into electric signals and this property is today used to create gas detectors based on oxide semiconductors [13]. In this context, the titanium dioxide is not used as much as other oxides like SnO_2 and ZnO , but has received some attention as gas sensor containing oxygen, in the automotive industry to control the composition of the mixture air / fuel in car engines [14,15].

Titanium dioxide is used widely as an industrial pigment. Currently, the volume of TiO₂ pigmented products throughout the world is approximately 4 million tons per year [16].

Titanium dioxide is used as a pigment especially in production of paints thanks to its high degree of whiteness. In addition, TiO₂ is not toxic and is stable and can be easily dispersed in solvents and aqueous media [16]. It is also used as a food additive [17], in the pharmaceutical and cosmetics industry [18].

Titanium dioxide is also used in many other technological applications especially in the energy field. In fact, there has been a strong growth in this sector due to the discovery of the photovoltaic cells called “of third generation” DSSC (dye-sensitized solar cell) developed by the Swiss scientist and Nobel laureate Michael Grätzel who used titanium dioxide as an electron acceptor and organic dye as photosensitizers.[19] (Fig. 3)

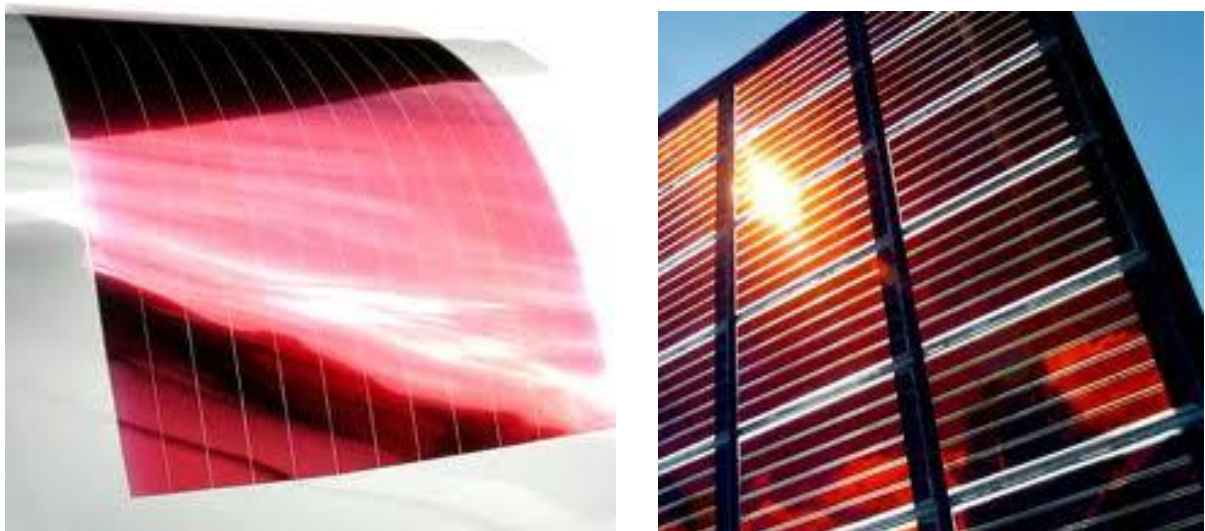


Fig. 3 – Examples of DSSC Cells

1.1.1 - Structure of Titanium Dioxide

Titanium dioxide exists in 3 different crystalline phases: anatase (tetragonal crystal structure cell), rutile (tetragonal cell) and brookite (orthorhombic cell with 2.96 eV gap). (fig 4)

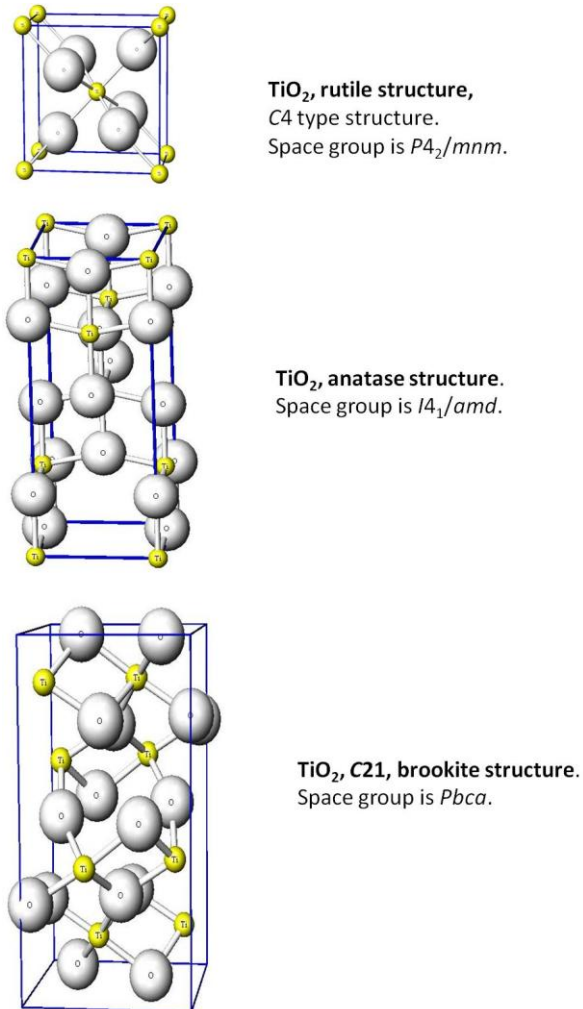


Fig. 4 - TiO₂ phase structures: rutile (a), anatase (b) and brookite (c)

Among the 3 phases, the rutile phase is the most stable [20], whereas the other two phases can be converted in rutile by heating.

The rutile and anatase have trigonal structures, while the brookite has a rhombohedral structure. The rutile and anatase phases are ever more widely studied. In both, the basic structure is made of a titanium atom surrounded by six oxygen atoms which assume a distorted octahedral conformation depending on the type of phase. In both phases, the two bonds between the titanium and oxygen atoms are slightly different from those that would be found in a perfectly octahedral cell; in fact they are slightly longer, giving rise to slightly distorted octahedral cells.

1.1.1.1 - Rutile

Rutile is a mineral composed primarily of titanium dioxide, TiO_2 . Its refractive index is one of the highest among the known minerals; it also shows a high leakage. The natural rutile may contain up to 10% iron and a substantial amount of niobium and tantalum.

Its name derives from the Latin *Rutilus*, red, referring to the deep red color observed in some specimens when viewed against the light. (Fig. 5)

Rutile is present in metamorphic rocks produced at high temperature and pressure and in igneous rocks. Rutile is the most abundant polymorph at room temperature and ambient pressure because it has the lowest molecular volume among the three polymorphs.



Fig. 5 – Rutile minerals

Rutile is a common mineral in igneous rocks Plutonic, even if it is occasionally in igneous effusive rocks, in particular those present in the earth's mantle which kimberlites and lamproiti. Anatase and brookite are found in igneous rocks as products of alteration during the cooling of the plutonic rocks.

The unit cell of the rutile is tetragonal, with cell parameters $a = 4.584\text{\AA}$ and $c = 2.953\text{\AA}$. The titanium cations have a coordination number 6: are surrounded by an octahedron of 6 oxygen atoms.

The main uses for rutile are the manufacture of refractory ceramic, as a pigment, and for the production of titanium.

The finely divided powder of rutile is a brilliant white pigment and is used in paints, plastics, paper, ceramics, cosmetics, food, and other applications which require a bright white colour. Nanoscale particles are transparent to visible light, but they are very effective at absorbing ultraviolet radiation; in fact, they are used in sunscreens to protect the skin from ultraviolet rays.

Synthetic rutile was first synthesized in 1948, it is pure transparent and almost colourless (slightly yellow). It can get it coloured by doping rutile. However, the rutile is rarely used in jewellery as it is not very hard (scratch resistant), measuring only 6 on the Mohs scale.

1.1.1.2 - Anatase

This is always in the form of small crystals and it crystallizes in the tetragonal system; but, despite the same degree of symmetry for both, there is no relationship between the interfacial angles of the two minerals. The word anatase comes from the greek "anataxis" (extension) as the vertical axis of the crystal is the longer axis of the rutile (Fig. 6). It is not very hard ($H = 5 \frac{1}{2} - 6$) or dense (specific gravity 3.9), it has a greater gloss of rutile.

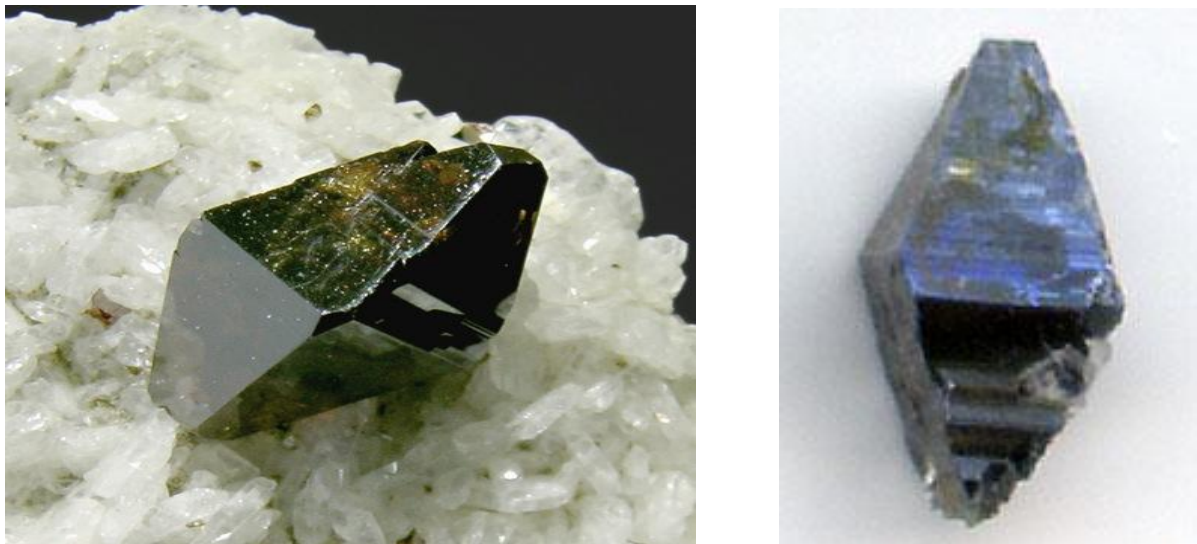


Fig. 6 – Anatase mineral

It is well known that TiO_2 anatase usually shows better photocatalytic activity than TiO_2 rutile, the mixture of TiO_2 anatase and rutile demonstrates ‘magic’ effects on carrier transfer in photocatalysis applications. For example, Kawahara et al. evidenced the electron transfer from anatase conduction band to rutile conduction band in the patterned anatase–rutile bilayer-type photocatalyst and

consequently much higher photodecomposition efficiency of CH₃CHO than pure anatase or rutile photocatalyst.

Among the TiO₂ found in nature, anatase exhibits a higher activity than other polymorphs[21].

TiO₂ with well-defined (001) facets is particularly useful for solar energy applications [22]. However, the most stable and frequently observed surface on anatase has a (101) orientation[23,24].

The (001) is only a minority surface due to its high surface energy (0.90 J/m²) compared to that of the (101) surface (0.44 J/m²)[22].

Up to now, surface science investigations have yielded an amazing degree of atomic-scale structural and chemical information on rutile TiO₂ (110), whereas work on anatase is scarce, [23, 25, 26] mainly because of the difficulty in growing large anatase single-crystals.

Although there are general and qualitative rules that can assess the stability of oxide surfaces according to first-principle calculations, controlling the shape of TiO₂ single-crystals exposed with reactive {001} facets is still a great challenge. Most available experimental information on the structure surface chemistry of anatase single-crystals is still based on studies of dispersed samples. Moreover, the use of different preparation techniques has led to samples with various morphologies and impurity contents.

1.1.1.3 – Brookite

Brookite (Fig. 7) has a composition identical to rutile and anatase, but crystallizes in the orthorhombic system. It is the rarest of the three polymorphs and, unlike the other two, has no photocatalytic activity. At high temperatures, around 750 °C, it transforms into rutile.



Fig. 7 – Brookite structure

1.2 - SEMICONDUCTOR MATERIALS

The distribution of the electrons in a solid is described by the model which is usually called bands models: a model obtained from the treatment of the quantum energy levels in the atoms and molecules.

From two overlapping orbitals, whether atomic or molecular, also identical, is obtain two new wave functions characterized by different energies. In solids the situation is rendered more complex by the fact that it has not in fact to do with small numbers of overlap between orbitals, as happens for example in the molecules, but the overlay covers all components of the crystal lattice: if a crystal is formed atoms from 10^{22} there will be a equal order of energy levels.

In fact from this complex orbital overlap derives a simplest situation: there are in fact two groups of energy levels, called bands (hence the name of the theoretical model) inside of which the outermost electrons can go to be arranged: the band at less energy is called the "valence band" that higher energy "conduction band".

In each band energy levels are very close and the two bands are separated by an interval of energy GAP called "band gap" or, more commonly "band gap", the amplitude of which depends on the structure of the lattice and by the nature of the atoms.

The difference between the energy of the lowest level of the conduction band (E_c) and the energy of the highest level of the valence band (E_v) is the width of the band gap, classifying substances in insulators, semiconductors and conductors:

1. In the conductors, as for example metals, the valence band is partially occupied or superimposed on the conduction band, then the application of an electric field, also weak, the electrons move in the levels of the conduction band, allowing the material to conduct .

2. Insulation materials there is a clear and wide separation (EGAP ~ 6 eV for diamond) between the valence band, filled with electrons, and the conduction band, blank. Furthermore, the application of an external electric field is not sufficient to promote electrons from the valence band to the conduction band, making it impossible to run.

3. In semiconductors the band gap has a relatively modest (EGAP ~ 0.785 eV for Ge, EGAP ~ 1.21 eV for Si). For these substances has not run at low temperature. The conductivity occurs at higher temperatures and is strictly dependent on the temperature itself. In fact for thermal excitation (or optical) the electrons pass from the valence band to the conduction and the substance becomes a modest conductor.

Each electron passing in the conduction band leaves free an energy level in the valence band is called gap or hole. The shortcomings of charge can give rise to a unique mechanism of electrical conduction: other electrons are filled in the gaps creating new gaps, overall there has been a "motion of gaps." It is usual to describe the gap as a positive charge that moves freely within the valence band.

The lower energy level that a gap can occupy is the level to greater energy of the valence band. Consider the possibility that any inner electron to the valence band is captured by a species in solution, creating a blank layer, which is a shortcoming. The electrons levels slightly higher in energy immediately occupy the gap by moving this to the higher energy level of the valence band.

The possibility of conduction of electrical current by a solid is guaranteed by the possible motion of electrons in the conduction band or holes in the valence band.

The presence of defects in a solid affects the structure and properties (electronic, optical and magnetic properties) of the material by changing the process of electron-hole recombination and, consequently, there is an improvement of the chemical qualities that depend on the charge transfer. It is known, moreover,

that the adsorbed molecules are often linked to surface defects which notes a charge transfer of these species surface [27].

1.2.1 – Density of Electron and Gaps in a Semiconductor

In physics, particularly in quantum mechanics, the Fermi energy is the energy of the highest occupied level in a system of fermions at absolute zero temperature, and describes the ways in which electrons and holes are to occupy the energy levels in solids; in other words, all the energy levels up to the level that has the Fermi energy are occupied by electrons.

More accurate results from the Fermi-Dirac distribution function which indicates the probability that a level at energy E is occupied by an electron:

$$f = \frac{1}{1 + e^{\left(\frac{E-E_F}{kT}\right)}}$$

Where E_F is the Fermi Energy, k is the *Boltzmann constant* and T is the temperature. The Fermi level is, therefore, the energy level having a probability equal to $\frac{1}{2}$ of being populated; this probability decreases rapidly for energy levels to greater than E_F and grows rapidly to lower levels.

You have information on the nature of the solid from the position of the Fermi level, as can be seen from the following figure (fig. 8):

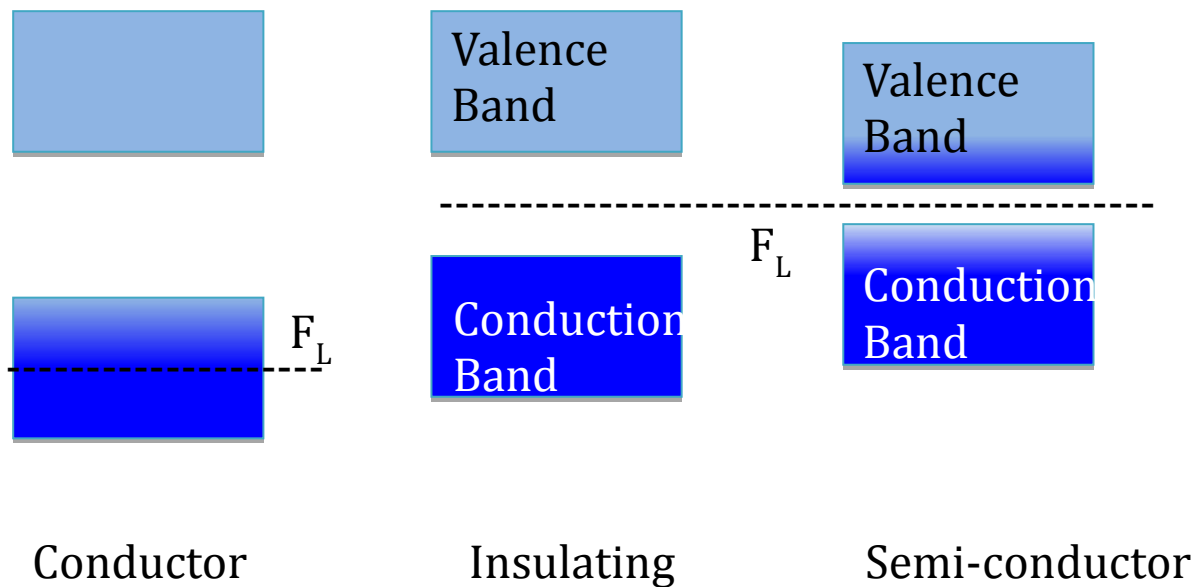


Fig.8 - Position of Fermi level in different materials

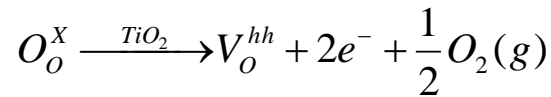
The Fermi energy is a parameter that describes the degree of occupation of the various levels under conditions of thermodynamic equilibrium; semiconductors are often in different conditions, for example if hit by radiation with energies greater than EGAP and, therefore, it is necessary to use appropriate equations that take into account these non-equilibrium conditions vacancies.

1.2.2 – Semiconductors and photocatalytic activity

In the oxides or chalcogenides of metals in general, the electronic properties are modified by defects in their stoichiometric composition, producing a kind of "internal doping". The presence of vacancies of oxygen atoms in the crystal lattice produces an excess of positive charges, due to Ti (IV), which must be compensated for by an excess of electrons; in fact, the real composition is TiO_{2-x} . This classifies the TiO_2 (but also ZnO , V_2O_5 , MoO_3 and) as n-type semiconductor.

Cu₂O, NiO and Cr₂O₃ are included among the p-type semiconductors; in this case it is likely that in the crystal lattice sites are present in which the metal has an oxidation number higher than normal.

The oxygen vacancies are formed according to the following reaction:



Kröger-Vink notation is used to explain that in the TiO₂ you create a vacance (V_o^{hh}) following the release of two electrons and molecular oxygen. For example, this reaction can be induced by heating in oxygen-poor environment.

The difference in the lattice structure of the two main polymorphs (rutile and anatase) causes a different electronic band structure and consequently a different band gap [28, 29,30]:

Titanium Dioxide Phase	Energy Gap (eV)
Rutile	3,02
Anatase	3,20

Using the following equations:

$$E = h\nu = \frac{hc}{\lambda} = \frac{(4,13566733 \times 10^{-15} eV \cdot s) \cdot (299792458 m/s)}{\lambda}$$

$$E(eV) \approx \frac{1240 eV \cdot nm}{\lambda(nm)}$$

a threshold of absorption (expressed as a wavelength of absorption) of about 387 nm and 410 nm for the anatase to rutile is obtained.

The values just expressed concern single crystals or samples almost perfectly crystallized. Usually higher values are obtained for thin films, little crystalline [31, 32] or nanometric materials [33, 34].

1.3 - PHOTOCATALYSIS

If during the process the photocatalytic semiconductor remains intact and the charge transfer to the species adsorbed on the surface is continuous the process is said exothermic heterogeneous photocatalysis.

Typically, the photocatalytic reactions can be summarized by the following:



The sign, negative or positive, the Gibbs free energy (ΔG°) of the above reaction, the ranking as photocatalysis and photosynthesis, respectively [35]. In inert solvents or in the absence of solvents, the functional groups of organic compounds can undergo transformations (mainly oxidation), which can be used in organic synthesis if the product obtained has a high yield.

In most of the photosynthetic reactions that involve the use of TiO_2 , ΔG° is negative, then photocatalytic reactions are obtained rather than photosynthesis.

A semiconductor photocatalyst to be efficient it is necessary that the different electronic processes involving interfacial e_{cd} and h_{bv+} compete effectively with the main deactivation processes (recombination of e_{cd} and h_{bv+}), which can occur in bulk or on the surface. Following the excitation, e_{cd} and h_{bv+} progress through different paths

The electron transfer photoinduced to species and organic or inorganic adsorbed or to the solvent is the result of migration of gaps (h_{VB+}) and electrons (E_{CD}) on the surface of the semiconductor; such transfer process is more efficient if the species are pre-adsorbed on the surface [36].

The semiconductor can donate e_{cd} migrated to the surface to reduce a species acceptor of electrons (generally oxygen in an aerated solution), or electrons from the donor species can be combined with (h_{VB+}) migrated to the surface.

The probability and the rate of the process of charge transfer depend on the positions of the valence bands and conduction than the redox potential of the adsorbed species.

In competition with the above process, there is the recombination of electrons and holes on the surface, or in bulk, with release of heat.

Ideally, a semiconductor photocatalyst should be:

- Able to effectively catalyze the reactions
- Chemically and biologically inert
- Stable photocatalytically
- Easy to produce and use
- Easily activated by sunlight
- Cheap
- Not hazardous to the environment and human health

The titanium dioxide is close to being an ideal photocatalyst, possessing almost all of the above properties. The only exception is that it does not absorb visible light. Both crystal structures, anatase and rutile, are used as photocatalysts.

1.3.1 - Mechanism

Each functional group with lone electron pairs or having π conjugation can oxidize in the presence of TiO_2 as we go toward dehydrogenation, oxygen or oxidative cleavage. The reductive transformation of organic lead, which can occur in the presence under suitable experimental conditions (absence of oxygen, the source of protons)[37], is usually less efficient for two reasons:

- The reducing power of the electrons of the conduction band is remarkably lower than the oxidizing power of the holes in the valence band
- Most organic substrates reducible not kinetically compete with oxygen for the acquisition of photogenerated electrons trapped in the conduction band

As a direct result, there has been research into the fundamental nature of the photocatalytic reduction. However, reductive processes may be convenient in organic synthesis because they are selective in respect of the functional groups.[38, 39]

If water is used as solvent, the selectivity of the photocatalytic process favours a partial/complete photodegradation of the organic substrate (instead of photosynthesis), due to the formation of hydroxyl radicals ($\text{OH} \cdot$) strongly oxidizing which you can add to the substrate or extract hydrogens. Any organic compound can be completely mineralized by TiO_2 irradiated with a few exceptions.

The term "photo-degradation", usually refers to the complete oxidative mineralization: conversion of organic compounds H_2O , CO_2 , NO_3^- , PO_4^{2-} , ions halide, etc. Often the degradation begins with a partial oxidation; a complete oxidative destruction can also be carried out in inert solvents, but the efficiency is lower.[40]

Generally, under the same conditions, oxygenates and aromatic compounds are more easily photocatalyzed of hydrocarbons and aliphatic compounds, respectively.

With respect to aromatic compounds, it has been observed that, in general, the time required to obtain the removal of aromatic is less than the time required to eliminate the products resulting from the rupture of the aromatic ring. Their photodegradation is influenced by the nature and position of the substituents in the aromatic ring. In general, the photocatalytic degradation of organic

pollutants is fast for compounds with electron-donor substituents, due to the activation of the aromatic ring toward electrophilic attack of OH · radical. The aromatic elimination is fast even in the case of deactivating substituents [41].

After formation of phenolic[42, 43] and quinonic derivatives[43], the rupture of the aromatic ring with formation of products aliphatic is obtained, such as adipic acid, acetic, oxalic, formic and maleic before the complete mineralization [45, 46]. The hydroxyl radical preferably attacks the aromatic portion, but can also attack the alkyl chains, converting them into aldehydes and acids, with subsequent decarboxylation [47, 48].

A similar oxidative route is also possible for aliphatic chains linked to nitrogen atoms [49].

The release of halides in solution by compounds such fluoroalkenes[50], fluoroaromatic[51] and molecules containing chlorine [52, 53], takes place, usually, the faster the mineralization to CO₂.

Molecules containing nitrogen are mineralized to NO₃ [54], but it has proved also the presence of ammonium ion (NH₄). Ammonium ions are relatively stable and ratio ammonium / nitrate depends mainly on the initial content of nitrogen and the irradiation time [55]. With a long time of irradiation, a conversion of ammonium ion to nitrate [52, 56, 57, 58, 59] is observed.

For compounds containing nitrogen rings, the production of a high concentration of nitrate (compared with the ammonium ion) is observed unlike the compounds with the nitrogen rings linked or in side chains [56].

Compounds containing sulfur are mineralized to sulphate[42, 43, 56, 58, 59], which is deposited on the surface of TiO₂ leading to a partial inhibition of the reaction [42].

Organophosphorus pesticides produce phosphate ions [57], which can remain adsorbed on the surface of TiO₂ [60].

The photodegradation of pollutants by TiO₂ is one of the most promising applications of heterogeneous photocatalysis, but cannot be proposed as a

method without a detailed knowledge of the process, as it may form toxic intermediates before complete mineralization.

1.4 - SYNTHESIS OF TITANIUM DIOXIDE NANOPARTICLES

Synthetic methods to obtain titanium dioxide nanoparticles in very important because the synthetic method can change the physical-chemical characteristics and consequently the photocatalytic efficiency.

In fact, photocatalytic activity of TiO₂ anatase is strictly related to the synthetic conditions which can allow to obtain nanosized TiO₂ powder with different chemical-physical properties, such as surface area, crystallinity, surface composition and reactivity.

Normally, nano-sized powders have been prepared by sol–gel process [64] and [65], chemical co-precipitation [66], metalorganic decomposition (MOD) [67], plasma enhanced chemical vapor deposition (PECVD) [68], atmospheric-pressure chemical vapor deposition (APCVD) [69], physical vapor deposition (PVD) [70] and [71], low-pressure flame deposition (LPFD) [72], and laser ablation [73]. Besides the above methods, the high-energy ball milling or mechanical alloying [73] has been proved to be a very effective route in preparing nano-sized solid solution for gas-sensing application recently [75], [76], [77], [78] and [79].

1.4.1 - Hydrothermal synthesis

One of synthetic method investigated in this work is a hydrothermal method.

With the hydrothermal synthesis particular temperature and pressure conditions are recreated, that have influence on the final product. In particular, in the synthesis of crystals and inorganic nanoparticles, these conditions will affect both the size and the morphology.

The hydrothermal synthesis is carried out within particular reactors.

Within the reactor a pressure develops proportional to the tension of the vapor of the solvent of the solution inside and at the temperature according to curve pressure / temperature.

The use of the methodology of the hydrothermal synthesis for the particles of titanium dioxide is carried out in order to be able to have a synthesis in which the given conditions are obtained at the end of a crystalline material.

The method is based on the ability of water and aqueous solutions to dilute at high temperature (200-500°C) and pressure (10-80 MPa, sometimes up to 300 MPa) substances practically insoluble under normal conditions: some oxides, silicates, sulphides. The main parameters of hydrothermal synthesis, which define both the processes, kinetics and the properties of resulting products, are the initial pH of the medium, the duration and temperature of synthesis, and the pressure in the system. The synthesis is carried out in autoclaves which are sealed steel cylinders that can withstand high temperatures and pressure for a long time.

Nanopowders are normally produced by means of either high temperature hydrolysis reactions of various compounds directly in the autoclave or hydrothermal treatment of reaction products at room temperature; the latter case is based on the sharp increase in the rate of crystallization of many amorphous phases in hydrothermal conditions. In the first case the autoclave is loaded with aqueous solution of precursor salts, in the second case – with suspension of products derived from solution reactions flowing under normal conditions.

There is normally no need to use special equipment and maintain a temperature gradient (Fig. 9)



Fig.9 – Instrument utilized for hydrothermal synthesis

Advantages of the hydrothermal synthesis method include the ability to synthesize crystals of substances which are unstable near the melting point, and the ability to synthesize large crystals of high quality. Disadvantages are the high cost of equipment and the inability to monitor crystals in the process of their growth. Hydrothermal synthesis can be affected both under temperatures and pressures below the critical point for a specific solvent above which differences between liquid and vapour disappear. The solubility of many oxides in hydrothermal solutions of salts is much higher than in pure water; such salts are called mineralizers. There is also a group of solvothermal synthesis methods, relational to hydrothermal methods; this group of methods is based on the use of organic solvents and supercritical CO₂. Substantial enhancement of the hydrothermal method facilitates the use of additional external factors to control the reaction medium during the synthesis process. This approach is implemented in the hydrothermal-microwave, hydrothermal-ultrasonic, hydrothermal-electrochemical and hydrothermal-mechanochemical synthesis methods.

One of the most widely known nanomaterials produced by the hydrothermal

method are synthetic zeolites. A necessary condition for their production is the presence in the solution of some surface active agents (SAA) that actively influence the morphological evolution of oxide compounds in hydrothermal solutions. The choice of synthesis conditions and type of surfactants can ensure the production of targeted porous nanomaterials with given pore size controlled in a fairly wide range of values.

1.4.2 - Sol-Gel Method

Another synthetic method investigated in this work is the sol-gel method.

In fact, sol-gel hydrolysis and polycondensation reactions of Ti(IV)-alkoxide represent the synthetic method usually utilized to prepare nanosized TiO₂ crystals. Titanium alkoxides are readily hydrolyzed by water due to their susceptibility to nucleophilic attack [80, 81].

The relative rate of the hydrolysis/polycondensation reactions during the sol-gel processing can be controlled by various methods like oligomerization, alcohol interchange, acid/base catalysis, steric hindrance and by using organic chelating agents such as acetyl acetone[82] bialkanol amines[83], diols [84] and acetic acid [85] to replace alkoxide groups on the central metal atom.

In this work, the hydrolysis of titanium alkoxides in water is studied, first using isopropyl alcohol as capping agent; a new type of sol-gel synthesis has also been studied.

A type of sol-gel synthesis has also been studied starting from the idea to obtain well crystalline anatase like unique phase using a waterless synthetic method by an esterification between formic acid and octanol.

In fact, M. Ivanda in 1998[86] proposed the hydroxylation of Ti(IV)-isopropoxide with water molecules generated “in situ” by an esterification between carboxylic acid (acetic acid) and alcohol providing excellent control of the hydrolysis and condensation rate. However, according to the Ivanda’s synthetic method the TiO₂ powder has been obtained like an amorphous phase

which could be only partially crystallized into anatase by heat treatment at temperature ranging from 370 °C to 480 °C.

In this work the way to a crystalline anatase phase without any further heat treatment is studied.

1.5 - TITANIUM DIOXIDE FUNCTIONALIZATION

One of the major objectives that are currently being studied about the titanium dioxide is to increase the photocatalytic efficiency, to obtain kinetics of degradation faster, lower of the band gap so as to be able to have phenomena of photocatalysis with wavelengths higher than the UV ones, which fall in the visible spectrum so as to be able to use a majority of wavelengths of the solar spectrum and to increase the yield.

To obtain these effects, we studied doping with metals, with synthesis gas, hybrids with other types of oxides and finally the photocatalytic functionalization of particles of titanium dioxide with molecules used as photosensitizers capable of increasing the photocatalytic yield .

Titanium dioxide photosensitization involves surface modification with appropriate species requiring a visible light-induced electron or hole injection into conduction or valence band, respectively. Two types of the charge injection mechanisms may be distinguished:

- 1) charge is transferred from the excited state of the sensitizer molecule to the conduction or valence band
- 2) charge transfer takes place directly from molecule to band (MBCT). The MBCT process can be realized by surface Ti (IV) complexes with various organic and inorganic ligands. Catechol, phthalic acid or salicylic acid derivatives, as cyanometallate anions, upon chemisorption at TiO₂ surface constitute an especially interesting group of ligands to yield various Ti(IV) surface complexes.

Loading of metal particles such as Pt, Cu, Ni and Ag on the surface of TiO₂ can inhibit charge recombination. Metal ion doping on TiO₂ can expand its photo response to visible region through formation of impure energy levels. The effect of red shift is negligible and doped ions tend to become recombination centers limiting the benefit of metal ion doping.

The use of Ti (IV) complexes with organic ligands as photosensitizers may be considered only when long term activity is not required. In fact, surface complexes of titanium (IV) are not photostable in the presence of oxygen and complexation of organic pollutants at the photocatalyst surface facilitates their oxidation.

1.5.1 - Functionalization with inorganic nanoparticles

Recently many studies have been directed to the functionalization of titanium dioxide with inorganic crystals, especially with biocompatible and biomimetic materials to obtain composite materials of interest for biomedical or have synergistic effect and increased photocatalytic efficiency against pollutants and bacteria.

Among these materials one of the most used is the hydroxyapatite.

In fact this material, in addition to its uses in the biomedical field, has been studied to be applied also in the killing of bacteria, [87] and [88]. It was also discovered that HA replaced with ions Ag^+ and Ti^{4+} exhibit excellent antimicrobial effects [89] and [90].

Thus, the combination of hydroxyapatite with TiO_2 to obtain materials having the capacity to absorb and decompose shows very promising.

1.5.1.1 - Hydroxiapatite

Calcium phosphate is the inorganic component of many biological hard tissues, the most important being bones and teeth.

In fact 69% of the weight of bone tissue is hydroxyapatite, as is 75% and 95% of dentine tooth enamel. Hydroxyapatite chemical formula is $\text{Ca}_5(\text{PO}_4)_3\text{OH}$. (Fig. 10)

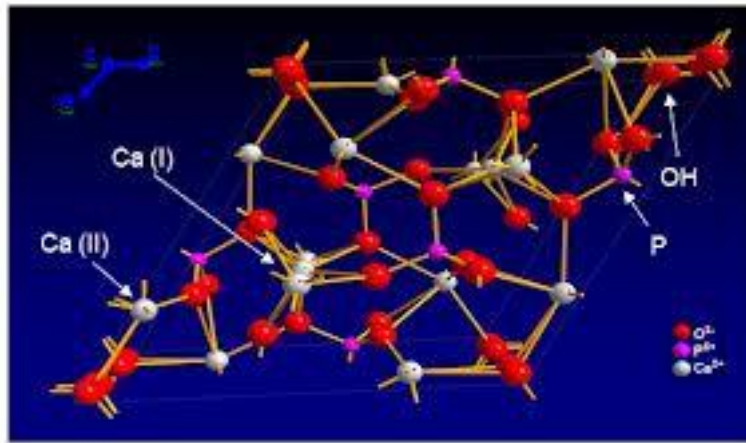


Fig. 10 – Structure of Hydroxyapatite

The mineral phase of bone and teeth is made up of hydroxyapatite crystals with a length of about 100 nm, a width of 20-30 nm, and the thickness of 3-6 nm and having low crystallinity, disorder crystalline surface, and non stoichiometric composition especially for the presence of carbonate ions in the crystal structure.

Due its high biocompatibility, calcium phosphate is studied in many works, in order to provide a synthetic method to obtain biomimetic hydroxyapatite that need to be prepared with similar morphology, size, and structural and chemical characteristics of the biological ones. In fact, the excellent biological properties of crystals of calcium phosphates, such as the lack of toxicity, inflammatory responses and immunity, and high bioresorbability can be significantly increased by improving their similarity with those.

Numerous synthetic strategies for the realization of stoichiometric hydroxyapatite have been studied.

The principal methods are wet precipitation, hydrothermal methods and ultrasonic nebulization, electrodeposition, sol-gel and solid state synthesis [91-97].

These researches on synthetic methods are focused to obtain crystals of hydroxyapatite that may be biomimetic and at the same time exhibit size, morphology, degree of crystallinity and surface properties but with the

possibility to modulate these properties, in order to improve and optimize the surface functionalization for specific molecules.

In fact it is well known that hydroxyapatite, thanks to its capacity and surface property, is able to bind a wide variety of molecules and therapeutic agents such as anticancer drugs for the treatment of bone diseases. The absorption and release of bioactive molecules depends not only on the characteristics of the molecule, but above all on the characteristics of the apatite used as substrate [98].

For this reason, in this work hydroxyapatite to be functionalized with titanium dioxide has been chosen.

In fact, nanoparticles of titanium dioxide are arranged neatly on the surface of hydroxyapatite crystals. In this way TiO_2 nanoparticles are coordinated in order to obtain a greater efficiency compared to a crystal of the same size consisting entirely of titanium dioxide.

1.5.2 - Functionalization with organic molecules

Adsorption of ions or molecules to the surface of a semiconductors is known to induce a change in the flat band potential.[99]

Since the doping level and band gap are usually insensitive to surface adsorption, the energetic positions of the conduction and valence bands shift in parallel relative to a reference potential.

For example, this kind of functionalization, is used to increase photocatalytic efficiency. Gratzel reported an increase in an open circuit voltage enhancement of 280 mV, corresponding to an 8.5% global conversion efficiency, after functionalization of mesoporous nanocrystalline (anatase) TiO_2 with 4-tert-butylpyridine (TBP).[100]

1.5.2.1 - Resorcinol

There are three isomeric compounds of dihydroxybenzene molecule structure, which all have traditional names respectively. The ortho (1,2) isomer is called catechol (also known as catechin; pyrocatechol; pyrocatechuic acid), which forms clear crystals used as a photographic developer in solution and as a starting material to produce synthetic catecholamines which have important physiological effects as neurotransmitters and hormonesany (such as epinephrine, adrenaline, norepinephrine, and dopamine). The meta (1,3) isomer is resorcinol (also known as resorcin), which forms clear needle crystals used in the production of diazo dyes and plasticizers. (Fig. 11)

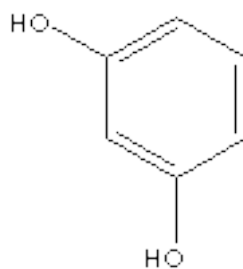


Fig. 11 - Structure of resorcinol

It is produced by sulfonating benzene with fuming sulfuric acid and fusing the resulting benzene disulfonic acid with caustic soda. Resorcinol is used in resins as an UV absorber. It is used in manufacturing fluorescent and leather dyes and adhesives. Reaction with formaldehyde produces resins (resorcinol formaldehyde resins) used to make rayon and nylon. It is used as a pharmaceutical to treat acne and other greasy skin conditions in combination with other acne treatments such as sulfur. It is used as an anti-dandruff agent in shampoo and sunscreen cosmetics.

CHAPTER 2 – EXPERIMENTAL SECTION

2.1 - SYNTHESSES

2.1.1- Hydrothermal Synthesis of titanium dioxide particles

In the first phase, this work focused on the synthesis of titanium dioxide nanoparticles obtained by hydrothermal synthesis.

A synthesis methodology is used where the hydrolysis of a titanium alkoxide in water forms titanium dioxide and the corresponding alcohol, as described in the following reaction (Fig. 12):

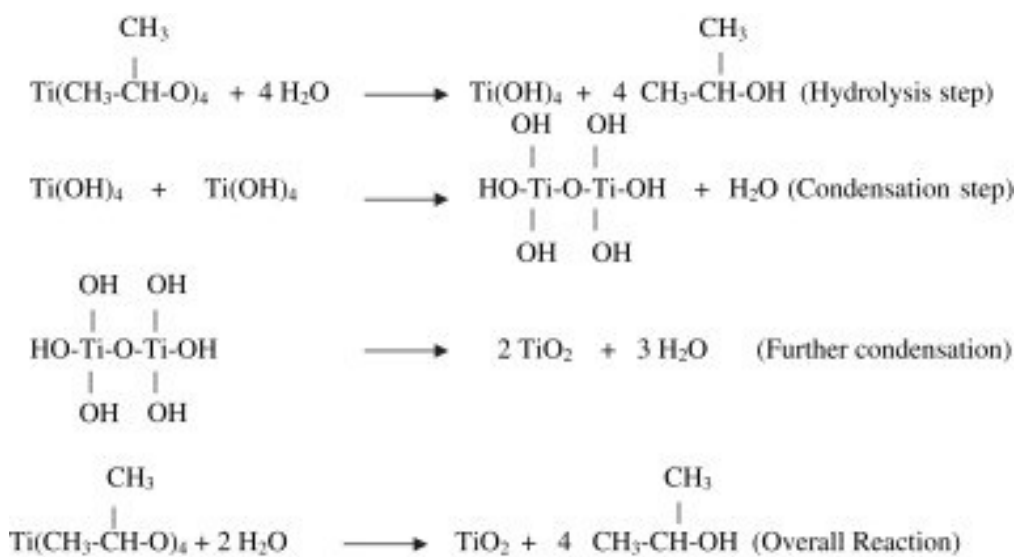


Fig. 12 – Example of mechanism of hydrolysis reaction of Ti(IV)Isopropoxide with water

In this synthesis triethanolamine is used as stabilizing and capping agent of the Ti (IV); such agent is also able to act on the morphology of the nanoparticles.

[101]

2.1.1.2 – Operation mode

In the synthesis tuning, the formation of a solution of Ti^{4+} obtained by mixing titanium alkoxide (IV) (eg. isopropoxide) (TYPE: $Ti(OCH(CH_3)_2)_4$) with triethanolamine (TEOA: $N(CH_2CH_2OH)_3$) in a molar fraction of [TYPE]: [TEOA] = 1:2. A stable complex Ti^{4+} is obtained, which does not give hydrolysis at room temperature. [101, 102] Hydrolysis by adding water is then obtained; this is added very slowly by dripping.

The solution is stirred for 2 hours at 100 °C forming a gel. At the end of this treatment, the product is washed with water, centrifuged and dried. In some cases the product is subject to a thermic treatment

2.1.1.2 – Materials

To obtain this synthesis, the reagents used were the following:

- Titanium (IV) n- Butoxide, 99% (Acros Organics)
- Titanium (IV) – Isopropoxide 97% (Sigma –Aldrich)
- Triethanolamine 99% (Fisher Chemical)
-

2.1.1.3 – Syntheses

SYNTHESIS N° 1	
Titanium Alkoxide	Ti(IV)-Butoxide (0,5 M)
Stabilizer	Triethanolamine (TEOA) (1M)
pH	9.70
Stirrer temperature (°C)	100
Stirrer Time (min)	60
Use of Ultrasound	-
Hydrothermal Reaction Time (min)	840
Hydrothermal Reaction Temperature (°C)	160

SYNTHESIS N° 2	
Titanium Alkoxide	Ti(IV)-Butoxide (0,5 M)
Stabilizer	Triethanolamine (TEOA) (1M)
pH	9.70
Stirrer temperature (°C)	100
Stirrer Time (min)	60
Use of Ultrasound	-
Hydrothermal Reaction Time (min)	120
Hydrothermal Reaction Temperature (°C)	160

SYNTHESIS N° 3	
Titanium Alkoxide	Ti(IV)-Butoxide (0,5 M)
Stabilizer	Triethanolamine (TEOA) (1M)
pH	11.25
Stirrer temperature (°C)	100
Stirrer Time (min)	60
Use of Ultrasound	-
Hydrothermal Reaction Time (min)	840
Hydrothermal Reaction Temperature (°C)	160

SYNTHESIS N° 4	
Titanium Alkoxide	Ti(IV)-Isopropoxide (0,5 M)
Stabilizer	Triethanolamine (TEOA) (1M)
pH	9.70
Stirrer temperature (°C)	100
Stirrer Time (min)	60
Use of Ultrasound	-
Hydrothermal Reaction Time (min)	840
Hydrothermal Reaction Temperature (°C)	160

SYNTHESIS N° 5	
Titanium Alkoxide	Ti(IV)-Isopropoxide (0,5 M)
Stabilizer	Triethanolamine (TEOA) (1M)
pH	11.20
Stirrer temperature (°C)	100
Stirrer Time (min)	60
Use of Ultrasound	-
Hydrothermal Reaction Time (min)	840
Hydrothermal Reaction Temperature (°C)	160

SYNTHESIS N° 6	
Titanium Alkoxide	Ti(IV)-Isopropoxide (0,5 M)
Stabilizer	Triethanolamine (TEOA) (1M)
pH	9.70
Stirrer temperature (°C)	100
Stirrer Time (min)	60
Use of Ultrasound	-
Hydrothermal Reaction Time (min)	120
Hydrothermal Reaction Temperature (°C)	160

SYNTHESIS N° 7	
Titanium Alkoxide	Ti(IV)-Isopropoxide (0,5 M)
Stabilizer	Triethanolamine (TEOA) (1M)
pH	9.70
Stirrer temperature (°C)	100
Stirrer Time (min)	60
Use of Ultrasound	-
Hydrothermal Reaction Time (min)	120
Hydrothermal Reaction Temperature (°C)	120

In this work we tried to use ultrasounds; infact, in sol-gel polymerization, ultrasounds (US) affected the preparation of titanium nanoparticles [104] US effectively lead to reduce the particle size of solid reactants thereby increasing the reactive surface area [104, 105].

SYNTHESIS N° 7 US	
Titanium Alkoxide	Ti(IV)-Isopropoxide (0,5 M)
Stabilizer	Triethanolamine (TEOA) (1M)
pH	9.70
Stirrer temperature (°C)	100
Stirrer Time (min)	60
Use of Ultrasound	o
Hydrothermal Reaction Time (min)	120
Hydrothermal Reaction Temperature (°C)	160

In order to evaluate possible interferences caused by residual unreacted ethanolamine or adsorbed on the surface of the particles of the titanium dioxide obtained, a part of the product obtained by the synthesis No. 4, was heat-treated using a circular oven with a temperature of 450 °C and for 240 minutes.

To evaluate crystalline phase conversion of gel, in synthesis No. 7 a circular oven was used with a temperature of 400 °C and for 240 minutes.

2.1.2 – Synthesis in water

In this work, it is developed a new type of sol-gel synthesis of titanium dioxide has been developed, which is able to obtained directly crystalline anatase phase, contrary to the classical sol-gel synthesis method, in which an amorphous material that must be necessary heat-treated is obtained.

2.1.2.1 – Materials

In the synthesis the following reagents have been used:

- Titanium (IV) – Isopropoxide, 97% (Sigma –Aldrich)
- Isopropyl alcohol $\geq 99.7\%$, (Sigma –Aldrich)

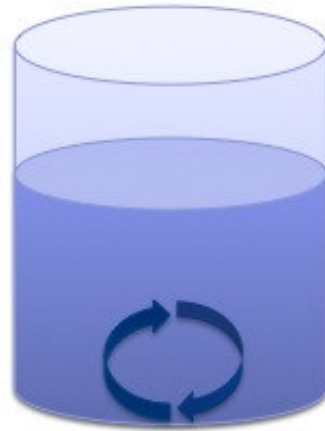
2.1.2.2 - Synthesis

The synthesis is carried out using Ti (IV)-isopropoxide as precursor of titanium, and isoprophyl alcohol as stabilizing and capping agent.

The hydrolysis of titanium isopropoxide takes place with water, but contrary to the mode found in the literature [106], the synthesis tuning involves very slow addition of adduct isprophilic alcohol/titanium isopropoxide to a volume of water previously heated to 80 °C in vigorous stirrer as described in the following scheme (Fig. 13):

Titanium isopropoxide 0,153 mol + 150 ml Isopropanol

Drop to drop (45 min)



450 ml Distilled Water 80°C

Stirring time 3 hours
Room Temperature

Fig. 13 – Synthesis method Scheme

2.1.3 – Functionalization of Titanium Dioxide Nanoparticles

2.1.3.1 – Functionalization with hydroxyapatite

Nanoparticles obtained with sol-gel method, are functionalized with hydroxyapatite microcrystals in order to obtain a composite material with a core of hydroxyapatite surface functionalized with titanium dioxide nanoparticles.

2.1.3.1.2 - Synthesis of hydroxyapatite microcrystals

2.1.3.1.2.1 - Materials

In the synthesis of Zn substituted hydroxyapatite the following reagents have been used:

- Calcium Hydroxide Ca (OH) ₂ puriss. p.a. from Riedel-de Haën
- Phosphoric acid H₃PO₄ 85% m / m from Riedel-de Haën
- Zinc Carbonate from Sigma Aldrich

2.1.3.1.2.2 - Synthesis

This type of synthesis is based on a neutralization reaction.

A solution of 600 ml of 0.15 M phosphoric acid (88.8 g of phosphoric acid to '85% wt) was prepared and dropwise added, with a rate of flow of 1-2 drops per second, into a suspension of 1 L of 0.17 M calcium hydroxide (100 g of calcium hydroxide) and zinc carbonate 0,03 M which was kept under mechanical stirring and at a temperature of 37 °C.



Once the dripping ended, the suspension was kept under stirring and at a constant temperature of 37 °C for 2 hours. Then the agitation was turned off and the product was left to mature for other 2 hours.

After that, the product was slowly stirred for 8 hours at 50 °C temperature in order to obtain nanocrystals aggregation in a microcluster structure.

2.1.3.1.3 – Synthesis of titanium dioxide – hydroxyapatite microcrystals.

10 % m/m of aqueous suspension of hydroxyapatite microcrystals (30% solid phase) was added to the hydro-alcoholic suspension of titanium dioxide nanoparticles by dripping.

Total suspension was stirred for 4 hours at 60 °C of temperature.

Later, the product was slowly stirred at room temperature for 4 hours, centrifuged and dried.

2.1.3.2 – Functionalization with oxidized resorcinol

2.1.3.2.1 - Resorcinol oxidation

2.1.3.2.1.1 – Materials

In the synthesis the following reagents have been used:

- Ethanol, 96% (Sigma-Aldrich)
- Resorcinol, 99% (Sigma-Aldrich)
- Sodium hydroxide reagent grade, $\geq 98\%$, pellets (anhydrous) (Sigma – Aldrich)
- Copper(II) nitrate hemi(pentahydrate), 98% (Sigma – Aldrich)

2.1.3.2.1.2 - Synthesis

A 35 ml ethanol (96%v/v) solution of resorcinol (0.57 M) was mixed to 10 ml of a water solution of $\text{Cu}(\text{NO}_3)_2 \cdot 2.5\text{H}_2\text{O}$ (1M). A solution obtained adding 5 ml of ethanol (96%v/v) to 2 ml of NaOH (10 M) water solution was dropped in ten minutes into this mixture kept under reflux. Other 5 ml of ethanol (96%v/v) have been used to rinse the filling funnel. During the dropping an ochre precipitate formed while the liquid phase turned from green to dark red. The reflux lasted for 3 hours at 105 °C before cooling to room temperature. The

ochre precipitate deposited at the bottom of the flask has been separated by centrifugation at 5000 rpm for 5 minutes, washed 4 times with ethanol (96%v/v) and dried under vacuum at 90 °C. The transparent dark red liquid phase was stored in a falcon tube at room temperature.

2.1.3.2.2 - TiO₂ nanoparticles surface complexed by oxidized resorcinol

5 ml of the transparent dark red liquid phase solution over described has been diluted up to 10 ml with water and mixed to 189 mg of anatase previously prepared. The heterogeneous mixture has been sonicated for few seconds and stirred for 5 minutes. A purple red precipitate has been allowed to deposit at the bottom of the tube without centrifugation, isolated and air dried at 110 °C obtaining an ochre residue.

2.1.4. – Synthesis water less

2.1.4.1. – Materials

- Titanium(IV) n-butoxide, 99% (Acros Organics)
- Formic acid EmsureMerk 98÷100% (ACS Reagent)
- 1-Octanol 99% (Acros Organics)

2.1.4.2. – Synthesis

Titanium dioxide nanoparticles with anatase structure and different chemical-physical properties have been prepared according to a modification of the synthetic method proposed by M. Ivanda [86] varying the reagent molecular ratio in order to observe the influence of the reagent molecular ratio on the chemical-physical properties of the final product.

Titanium(IV) n-butoxide, 99% was used as a source of titanium.

Formic acid EmsureMerk 98÷100% was added drop by drop to a solution of Titanium(IV) n-butoxide and 1-Octanol 99% in different molar ratio.

The reaction mixture was stirred for 30 minutes at room temperature in a two

necked round bottom flask provided with a bubbled reflux condenser and a thermometer.

The reaction mixture was heated with an oil bath kept at about 185 °C and refluxed for 1 hour.

On heating, the gels were converted into a white precipitate. After cooling at room temperature, the white precipitates were separated from the liquid phase by centrifugation at 5000 rpm for 10 to 15 minutes, washed with absolute ethanol (30*5 ml) to remove octane and then with diethylether.

The synthesis obtained using different formic acid / octanol are the following:

Sample	FA/ Oc
a	2,50
b	1,25
c	0,80
d	0,40
e	0,17

2.2 – CHEMICAL-PHYSICAL CHARACTERIZATION

2.2.1 - X-ray diffraction (XRD)

The theory of X-ray diffraction from single crystals was developed in the early twentieth century, ie a few years after the discovery of radiation, in order to explain the diffraction patterns generated by crystal lattices irradiated by radiation X.

The modern theory is mainly due to scientists such as Laue (1912), Ewald (1913) and father and son Bragg (1915-1935), each of which went with a different approach to explain the phenomenon.

The physics of X-ray diffraction is in part based on the physics of diffraction of light waves by gratings and slits on the theory of reflection "simple."

Clearly a crystal lattice has similarities with a lattice of slits (for example the translational periodicity of its "constituents").

However, the analogy between an atom and a slit may not seem obvious. It should be remembered that a slit to receive a certain incident wave becomes (at every point), secondary source of radiation.

An X-ray beam is produced from collisions of electrons with a certain energy on a metal; this will emit a characteristic X radiation mainly formed by 3 components: two peaks ($K\alpha$ and $K\beta$) and a background radiation more or less high, said bremsstrahlung.

X-rays colliding on a crystal will be reflected according to the well-known Bragg's law:

$$2d_{hkl}\sin\theta = n\lambda$$

Operationally, there are several diffraction techniques, but the most frequently used for dust is the Debye-Scherrer method, with all its subsequent amendments.

This method of analysis of the powder is also called Hull-Debye-Scherrer method, because it was developed independently by Hull in the United States and by Debye and Scherrer in Germany between 1915 and 1917. The incident beam is passed through a filter to remove the $K\beta$ radiation characteristic, after which the $K\alpha$ radiation is collimated by a collimation system. The close brush rays resulting irradiates the sample and the sections of the various diffracted cones are intercepted by the X-ray detector disposed cylindrically. The main advantages of the Debye-Scherrer method are:

- the small amount of powder required for the analysis (up to 0.1 mg)
- receiving almost full of all the reflections produced by the sample
- the relative simplicity of the equipment and technology required

Currently the photographic detection methods are practically in disuse and are used to counter diffractometers, more complex and expensive, but faster, accurate, and easily automated.

Scherrer's formula:

$$D_p = \frac{0.94\lambda}{\beta_{1/2} \cos \theta}$$

D is the average size of the crystallites, K is the shape factor, λ is the wavelength of the incident radiation, β is the integral of the peak and θ is the angle of diffraction. The quantity in the formula assumes numerical values different from a minimum of 0.70 to a maximum of 1.70, in dependence of a number of factors which include:

- the shape of the crystallites
- the indices (hkl) of the reflecting planes
- the particular definition of which is adopted (or full width at half height of a peak),
- definition of the particular, the size of the crystallites that is adopted.

2.2.1.1 - Operating Procedure

The powdered sample is placed using light pressure on a slide specimen holder which is then placed on the axis of the goniometric circle which is focused on the radiation diffracted X and records the spectrum. The spectra are obtained with an X-ray diffractometer for powders Philips 1050/81-PW1710: $K\alpha$ radiation of copper ($\lambda = 1.5406 \text{ \AA}$); working voltage of 40 kV, -40 mA. The instrument is equipped with a graphite monochromator on the diffracted beam and proportional counter. It were carried collected data using two different conditions.

- The scans are performed with steps of 0.05° , of 3 seconds each, in a range between 5° and 60° to make the recognition of the crystalline phases present.
- It have been determined, the average size of the crystals along the orthogonal axis to it by the width at half height of the peaks (002) and (003) the HA. In this case a collection speed of 0.1° per minute in intervals of 2θ between 24.5° and 27.5° (reflection 002) and between 37° and 44° (reflection 310) are used.

The analysis of the RX diffractograms performed on the powders of HA has allowed us to calculate:

- The size of nanocrystals. In particular, using the half-height width of the peak at $2\theta = 26^\circ$, (002) it was possible to calculate the size of crystallite along the c-axis, while using the peak at $2\theta = 39^\circ$. It have been calculated from the dimensions of nanocrystals along the diagonal between the axis a and b. The formula used is as follows:

$$\text{Crystal Size} = \frac{k\lambda}{w \cos \vartheta}$$

Where W size is the difference between w_s and w_b , w_b is the width at half height of the peak considered, w_s is the enlargement at half height of the standard (silicon), k is a shape factor and λ is the wavelength.

- The degree of crystallinity, corresponding to the fraction of crystalline phase present in the quantity by volume taken into consideration. This was calculated using the peak at $2\theta = 26^\circ$, using the formula:

$$B_{002} \sqrt[3]{x_c} = k$$

For the display of diffractograms and for the recognition of the phases the following programs were used: APD, PDF2 and the software of the Xpert, associated to Philips diffractometer.

2.2.2 - UV Visible Spectroscopy

The absorption spectrophotometry is concerned within the phenomena of absorption of the electromagnetic radiation in the region of the electromagnetic spectrum belonging to the visible range (350 - 700 nm) and near ultraviolet (200 - 350 nm).

The absorption of these types of radiation on the part of the molecules is capable of producing the energy transitions of the outer electrons of the molecules.

These electrons may be (Fig. 14):

- type of sigma (σ), consisting of a electron cloud thickened along the axis joining the nuclei of the atoms involved in the bond (the links are of simple type σ);

- in-greek pi (π), consist of pairs of electrons whose greatest electron density is located outside the axis joining the nuclei (such as in double or triple bonds).

π electrons are 'less connected' and are therefore more easily excitable than σ .

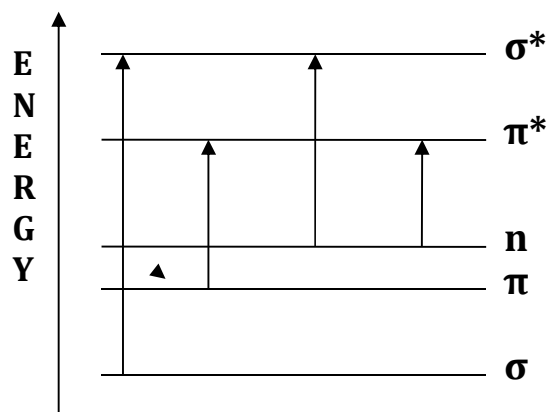


Fig. 14 – Energetic scheme of electrons

If conjugated double bonds are present in a molecule, an electron delocalization occurs with consequent energy decrease between a level and the other. A radiation of lower energy, like those in the visible range will be needed to make transitions.

TRANSITION	NECESSARY WAVELENGTH TO ABTAIN TRANSITION
$\sigma \rightarrow \sigma^*$	110 – 135 nm
$\pi \rightarrow \pi^*$	160 – 255 nm
$n \rightarrow \sigma^*$	
$n \rightarrow \pi^*$	> 285 nm

Therefore, electrons are usually delocalized to come into play, for example those participating in the π bond in the double bond carbon - carbon, and those of the doublet free nitrogen and oxygen.

The spectra in the visible (that are band spectra, since these transitions are generally accompanied in both vibrational transitions that rotational, so that the absorptions are constituted by many very close lines, so as to appear a continuous, ie a band) are then due to the bonding electrons more or less extensively delocalized π .

Such relocation may be extended to the whole molecule or may be limited to particular groupings, separated from each other in the molecule by a set of fully saturated bonds which act as an insulator and which therefore prevent the relocation.

In the first case the absorption spectrum is unique and difficult to interpret according to simple rules; in the second case, instead, it can be considered as the sum of absorptions due to the various unsaturated groups which are called "chromophores".

A 'chromophore' is therefore intended to be an unsaturated chemical group responsible for an absorption located in the region of wavelengths between 180 and 1000 nm.

2.2.2.1 - Operating Procedure

To perform quantitative analyzes, use is made of monochromatic rays, ie constituted by radiation of a single frequency. In practice, given the difficulty of having rays with this property, we use radiation beams including a very narrow band of the spectrum, ie almost monochromatic beams.

The quantitative determinations are based on the fact that, when a radiation passes through a solution, it is absorbed more or less intensely depending on the concentration, in other words the absorption depends on the concentration.

Thus providing tools to measure the absorption easily to the concentration of the solution.

In fact, if it is passed through a solution to unknown concentration monochromatic radiation (ie in a specific λ) and of intensity I_0 , beyond the solution will be found a radiation intensity I , which will be less than if a part of the radiation I_0 was absorbed by the solution itself, or equal to I_0 if no has been no absorption.

Suitable devices (detectors) are capable of measuring the intensity of the luminous flux; in particular are measured:

- I_0 : intensity of the light flux at the cell with the sample
- I : intensity of the luminous flux output of the cell with the sample

The fraction of the transmitted light, compared to that incident, is defined TRANSMITTANCE T , and is given by:

$$T = I / I_0$$

This quantity expressed as a fraction of the incident light has passed through the sample without being absorbed, and can assume values between 0 and 1, and this ratio is much smaller than the greater was the absorption.

Commonly used, however, the TRANSMISSION RATE, who will have values between 0 and 100:

$$\%T = T \cdot 100 = (I / I_0) \cdot 100$$

where $\% T = 100$ means that the beam has not undergone any weakening, ie there was no absorption by the substance, and $\% T = 0$ means that the beam has been completely absorbed.

The amount of radiation absorbed is more commonly known as absorbency (A), and is equal to the logarithm of the reciprocal of the transmittance:

$$A = \log (1/T) = \log (I/I_0) = \log (100 / \%T) = 2 - \log \%T$$

To calculate the concentration of the sample due to its absorption using the Beer-Lambert law:

$$A = \varepsilon \cdot c \cdot d$$

where:

A = absorbance of the sample

ε = molar extinction coefficient, specific for each substance

d = optical path length (cm)

c = concentration (mol / l)

According to the law of Lambert - Beer, the absorbance A is proportional both to the concentration of the absorbing substance, it is the thickness of the layer, so that the higher the concentration of the molecules that pass from the ground state to the excited, the greater will be the absorbance (the greater the decrease in the intensity of the incident ray).

The molar extinction coefficient ε indicates the absorbance value of the test compound when [d = 1] cm and [c = 1], and its value depends on the wavelength of the absorbed radiation, the nature of the solvent, the pH and the chemical species that absorbs, but not by temperature.

The law of Lambert - Beer is only an abstraction, and is valid only to dilute many conditions, because if the sample concentration is low, there is proportionality between A and C, while if the concentration is too high the law undergoes a detour and the proportionality fails.

With increasing concentration of the solute significant deviations occur resulting in poor reliability of analytical data.

About the causes of these deviations, the more hypothesized is the one that with increasing concentration increases the number of particles in solution, and also

increases the number of collisions between these; interionic forces and / or intermolecular increase and molecules or aggregates of more complex particles may be formed, different in structure from those under consideration, for which it can have a shift of the absorption maximum.

For this reason, the working conditions customary foresee that the solutions are always diluted to the maximum, consistent with the sensitivity of the instrument, to be of acceptable values of absorbance.

The instrument used in this work was a UV-VIS spectrophotometer Cary 300 Bio VARIAN with proprietary software.

2.2.3 - Infrared spectroscopy (FT-IR)

Spectrophotometry (IR) is a well known technique in the chemistry, it is a technique of molecular analysis in which transitions between vibrational energy levels are measured, which require energy corresponding to radiation in the infrared region of the electromagnetic spectrum, namely between 1 and 500 microns.

With this technique it is possible to obtain information on the functional groups present in the molecules that make up the sample and thus, indirectly, the molecules themselves. The information is primarily qualitative, the quantitative aspect is poorly exploited.

Each vibrational transition, such as electronic and rotational, has a specific energy that gives rise to an absorption of the infrared region in a specific region. Each functional group can have several vibrational modes which correspond to different energies; at the same time the absorptions of different functional groups correspond to similar energies although present in different molecules.

It should be considered that, despite the vibration modes of a molecule can be different, the rules of quantum mechanics tell us that the absorption of energy, and therefore the transition between two vibrational energy states, takes place

only if the vibration implies a change in the dipolar moment of the molecule. In the jargon of quantum mechanics, this equates to indicate a vibration mode active or permission.

- the frequency that corresponds to a given vibration is determined by the strength of the bonds and the mass of the atoms involved. Some general rules are the following: the stretching frequencies are higher than the bending ones, because less energy is required to bend a bond rather than to lengthen it.
- the bonds with hydrogen have stretching frequencies higher than those with heavier atoms
- the triple bonds have stretching frequencies higher than those of the corresponding double bonds, in turn higher than the corresponding single bonds, eg.

- C-C \Rightarrow 700-1200 cm^{-1}
- C=C \Rightarrow 1620-1680 cm^{-1}
- C \equiv C \Rightarrow 2260-3030 cm^{-1}

- The main functional groups are illustrated in the figure below in relation to the absorption frequencies. (Fig. 15)

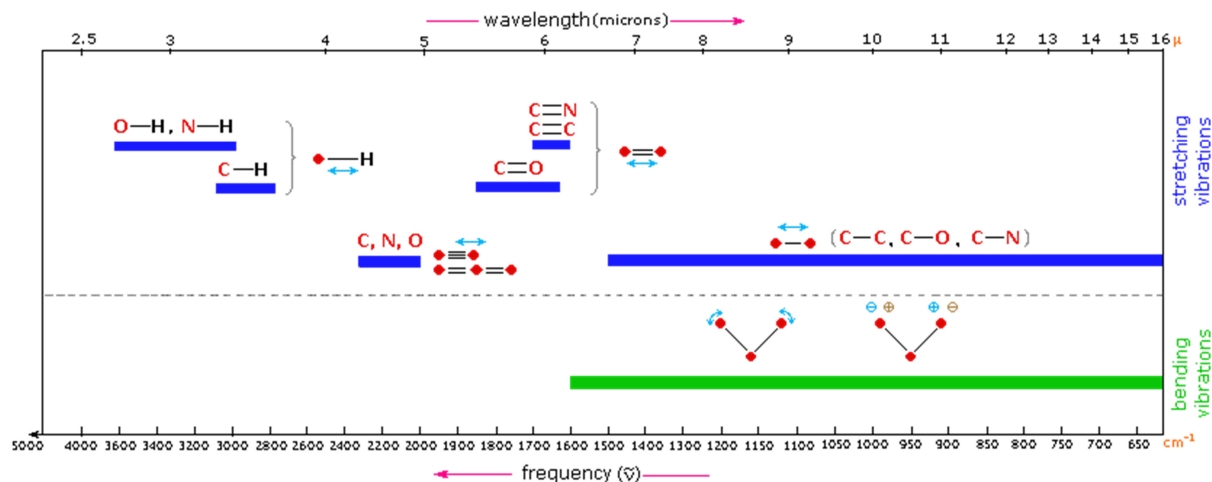


Fig. 15 - IR frequency of various functional groups

2.2.3.1 - Operating Procedure

The sample is irradiated with a more or less wide range of λ ; the λ absorbed correspond to the functional groups of the molecules. The answer is in the form of visible absorption spectrum or transmittance.

The most common IR spectrophotometers are the Fourier Transform, in which, through a system of light radiation collection known as Michelson interferometer and based on a mirror moving, the IR spectrum is recorded simultaneously around the required range.

The IR analysis can be carried out on samples of different nature:

- liquid samples: a drop is deposited on a transparent support
- samples with soluble film-forming properties: a film is generated by evaporation of a solution
- samples or insoluble solids: spray and capsule embedding in KBr
- solids material: surface analysis

In this thesis the preparation of the samples was carried out by grinding with a mortar a mixture containing 1 mg of the sample and 10 mg of KBr in order to homogenize the two materials; the powder thus obtained is pressed with a press to obtain a tablet that is then analyzed.

For these analyzes a spectrometer FT-IR Nicolet 380 THERMO ELECTRON CORPORATION is used; for the visualization of data the EZ Omnic software has been used.

2.2.4 - Scanning Electron Microscope SEM

Scanning electron microscope (Scanning Electron Microscopy, SEM)

The Scanning Electron Microscope (SEM) is an electro-optical system which allows to analyze the signals issued from the interaction of the electrons of the beam with the sample under examination, following the emission of a beam of electrons.

The processing of these signals makes it possible to obtain a wide range of information not only morphological but also compositional and structural relating to various parts of which compose the sample.

In fact, despite being born as a microscope with high resolution and three-dimensionality, in recent years SEM has proved to be very effective also in the analysis of chemical composition and crystallographic orientation of a sample, allowing accurate analysis and area, both qualitative and quantitative. The extreme versatility of this instrument is also guaranteed by the many types of samples that can be analyzed, both in terms of their nature (only materials containing fluids are not analyzable) that their shape and size (of any form, up to about one cubic decimeter), as well as for the easy preparation of the samples, which, if they are not naturally conductive (metal) must only be covered by a thin layer of a conducting element (graphite or gold).

SEM is schematically constituted by the following elements:

- 1) a column address, where the electron beam is created;
- 2) a vacuum chamber, where the electron beam interacts with the sample;
- 3) a series of electromagnetic lenses to direct the electron beam;

- 4) various types of detectors, which acquire the signals from the interacting beam and transfer them to the computer;
- 5) a screen, reconstructing the image from the signal.

The electronic source on top of the column generates the electron beam, by means of a filament (commonly tungsten) which produces electrons by thermionic effect once led to high temperature. The electrons are then accelerated at variable energy between a few hundreds and some tens of thousands of eV (typically from 200 eV to 30 keV) thanks to an anode placed under the filament.

The beam which emerges from the source is divergent, but is converged again and focused by a series of electromagnetic lenses and slits within the column. At the lower end of the column, a series of coils deflects the beam scanning and setting it in motion alternately along parallel and equidistant lines, so that it goes to cover a predefined area, once it reaches the surface of the sample.

Finally, the beam is focused by the final lens present in the column and hits the sample within the vacuum chamber. As the electrons in the beam penetrate the sample, they lose energy, which is re-emitted by the sample in various forms. Each type of emission is potentially a signal from which an image is created.

Beam-sample interaction and production of signals

In the instant the electron beam strikes the surface of the sample, the electrons of the beam begin to interact with the nuclei and the electron clouds of atoms in the sample, through two principal mechanisms: diffusion elastic and inelastic scattering.

The result of these processes is the production of a considerable variety of signals:

- secondary electrons

- backscattered electrons
- electrons absorbed
- transmitted electrons
- Auger electron
- electron-hole pairs
- electromagnetic radiation (in the spectrum UV-IR)
- X-ray emission

The region of the sample where the signals of interaction with the beam originates and from where these come out to be detected is known as the volume of interaction.

The shape and size of this volume depend on the characteristics of the beam incident and on the composition of the sample and, in many cases, are more extensive in the beam diameter, thereby determining the limit of resolution.

Typically, SEM is equipped with three different detectors for the acquisition of three of the signals listed above, and exactly:

- 1) secondary electrons (Secondary Electrons, SE)
- 2) backscattered electrons (Backscatter Electrons, BSE)
- 3) X-ray

1) Secondary electrons are electrons of low energy (up to a few tens of eV) originating from the most superficial portion of the sample (a few nm). The main property of this type of signal is to be strongly controlled by the morphology of the sample, therefore, the resulting image will be the image in black and white area affected by beam scanning where the contrast of shades of gray will highlight the appearance three-dimensional objects under examination. The use of this type of signal is devoted to the study of the morphological characteristics of three-dimensional objects or their structural relationships.

2) The backscattered electrons are high-energy (50 eV energy of the electrons of the beam) products up to a certain depth of the sample (a few microns). Their energy is directly dependent on the energy of the beam incident and the chemical composition (more precisely, the atomic weight average) of the material of which the sample is constituted, then the resulting image will be in black and white area affected by scanning the beam in which the contrast of gray tones emphasize the diversity of chemical composition of the different parts making the sample. In particular, it will become relatively more clear parts made of a material with a high average atomic weight and darker share to lower average atomic weight, the extreme case is the black as the not issued (a blank portion of the sample).

3) Unlike the first two types of signal (electrons), the X radiation does not provide an image linked to a topographical contrast (SE) or compositional (BSE) in the area affected by the scan.

In fact, the purpose of microanalysis RX is to obtain accurate chemical analysis of an object under examination.

The resulting image will be a spectrum of X-ray from which the material analyzed can be traced back to chemical composition, since each spectrum peak is due to a precise atomic species.

The scanning fact allows the beam to strike the surface of the sample line per line, up to cover the area to be examined, and the signals so generated vary in intensity, point by point, as a function of the morphological, chemical and structural anisotropies of the sample.

These signals are measured by the detectors and converted from analog digital signals to be processed in a timely manner.

In this work a Carl Zeiss SEM Evo MA 10 equipped with Oxford Microanalysis has been used. (Fig. 16)



Fig. 16 – SEM Zeiss Evo MA10

2.2.5 - Tunneling electron microscopy (TEM)

The instrument used is a Philips CM 100. The voltage work is 80 kV. The TEM images are obtained using electrons instead of visible light that is used in the common optical instruments, such as the optical microscope. In this technique, the electrons compared to photons depend on the fact that they can move with smaller wavelengths of light. This allows magnification with high resolution up to 800 times greater than the best optical microscope: the theoretical limit of magnification for a light microscope is about 1200x, while a TEM microscope can magnify and resolve over a sample 1.000.000x. This technique allows to obtain, from a sample sufficiently thinned (<0.1 mM), high-resolution images (<10 Å) produced by high-energy electrons (100 keV), broadcast on digital camera.

The TEM is used in materials science for the study and characterization of microphases and interfaces. Particularly important is the possibility of obtaining information on lattice parameters through electron diffraction and high resolution images. You can carry out studies on:

- morphology: the shape, size and arrangement of microcrystals or of particles observed on the sample, the degree of order and the detection of defects on an atomic scale (a few nanometers in diameter).
- composition: the elements present in the sample and their reports, in areas of a few nanometers in diameter.

2.2.5.1 - Operating Procedure

The sample was prepared by placing a bit of substance, in distilled water in the case of apatites and in acetone in the case of functionalized apatites. The suspension was allowed to settle on the grid for a few minutes and then the excess solvent was removed from the grid by means of filter paper. The mixture was sonicated for one minute. A drop of the suspension was put on a special grid, consisting of a micro-copper grid covered with a thin layer of carbon. The suspension was allowed to settle on the grid for a few minutes and then the excess solvent was removed from the grid by means of filter paper.

2.2.6 – Surface Area

Specific surface area measurements were taken using a Carlo Erba Sorpty 1750 instrument by measuring N₂ adsorption at 77 K and adopting the well-known Brunauer–Emmett–Teller (BET) procedure [107].

2.2.7 - Thermal Analysis

The methods of thermal analysis include a group of techniques in which a physical property of a substance, and / or its reaction products, is measured as a function of temperature, while the substance is subject to a program of temperature controlled variation.

The synthesized gels have been characterized also with these techniques by performing two types of analysis:

2.2.7.1 - Thermogravimetric Analysis (TGA)

The basic principle of thermogravimetry is simple: the sample to be tested is placed on a balance or weighing instrument inside an oven or heating device, and here is subjected to a heating program default.

The changes of the mass as a function of time and temperature are recorded continuously.

In this work instruments of the company TA model SDT Q600 were used.

2.3 – PHOTOCATALYTICAL TESTS

2.3.1 - Degradation of methylene blue

The methylene blue is an organic dye with the following molecular structure (Fig. 17):



Fig. 17 – Methylene Blue molecule

Methylene blue shows a main absorption band in the visible region, with an absorption maximum of 668 nm (experimentally were observed deviations from this theoretical value of the order of 2/3 units), with a small shoulder at 615 nm due the dimerization of dye. The absorption of the aromatic rings substituted is observed in the ultraviolet region of the spectrum. The absorbance used for the quantitative analysis is the peak maximum at 663 nm, in the visible region of the spectrum (Fig. 18).

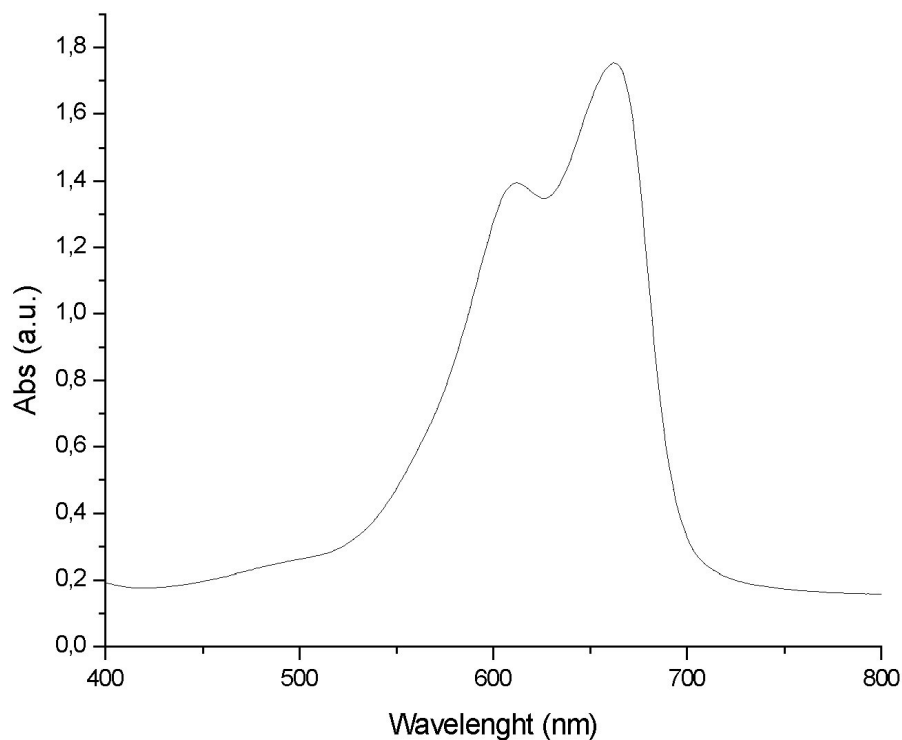
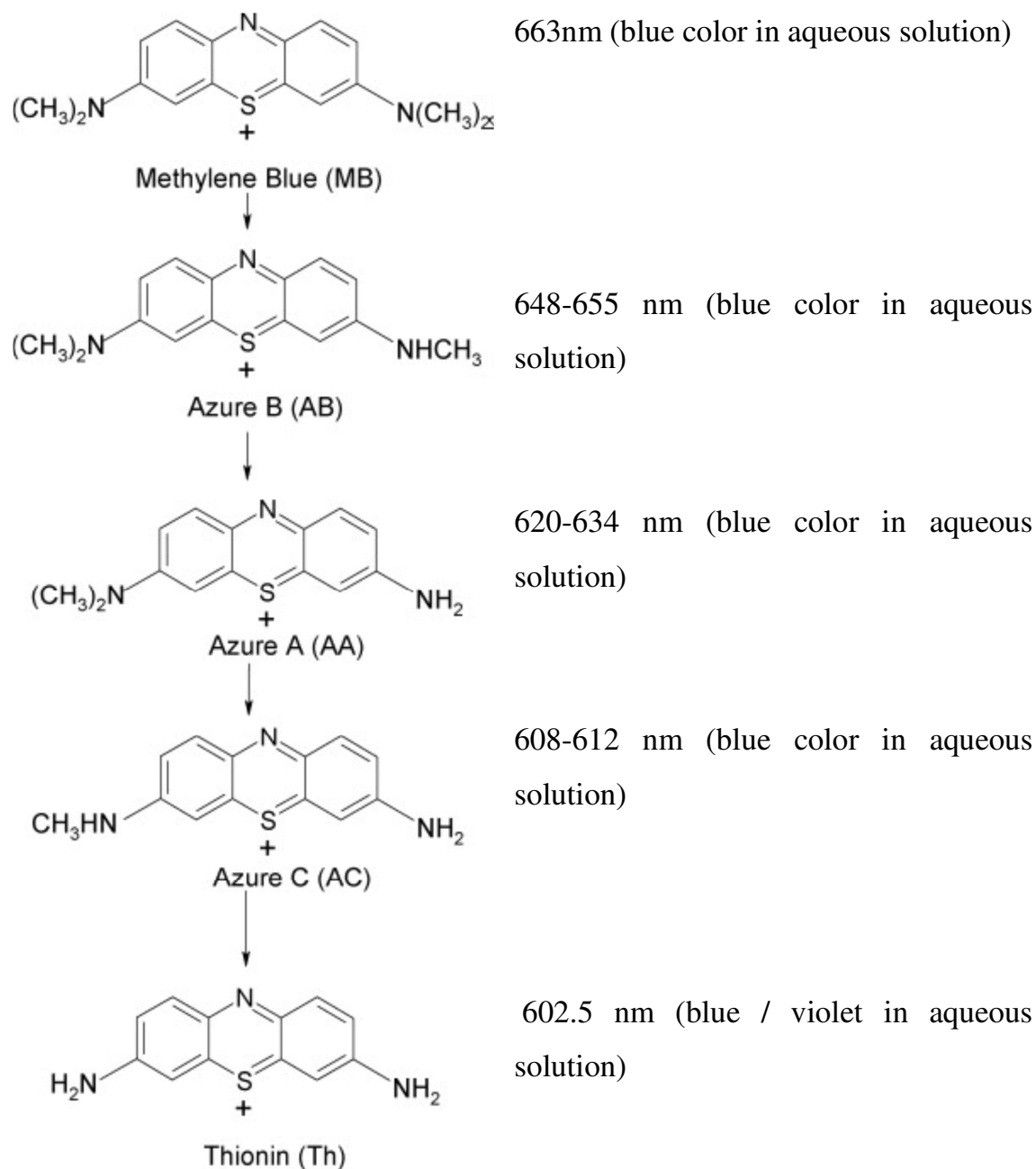


Fig. 18 – Absorbance spectra of Methylene Blue

According to T. Zhang and collaborators [109] the ipsocromic effect, described previously, is related to the degradation of the two auxocromic groups ($-NR_2$), with the formation of compounds responsible for the "blue shift" and with the simultaneous oxidation of MB. In anaerobic environment, spectrum of degradation of MB presents no blue shift, therefore suggesting that the auxocromic groups are not degraded. There are two effects: oxidation of the dye and sequential cleavage of the bonds $N-CH_3$.

The species that are formed are the following:



Further confirmation is given by M.A. Rauf and co-workers [107] who have analyzed the degradation products through HPLC-UV/Vis-MS system

2.3.1.1 - Mechanistic aspects of degradation

The different possible processes which may occur in the system Dye/TiO₂ may be due to exposure to UV-visible radiation [108] (Fig. 19).

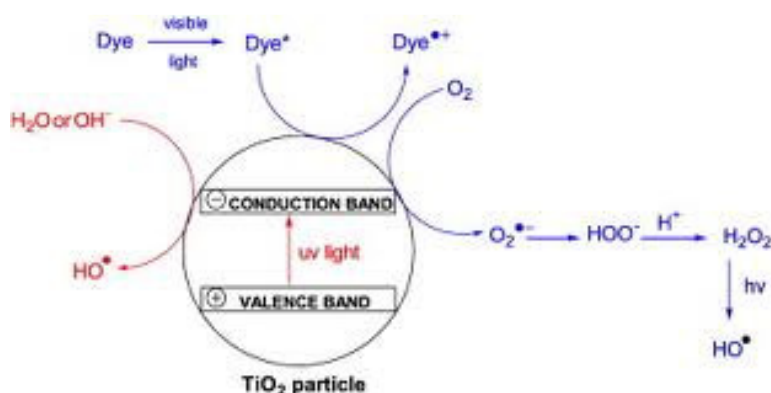
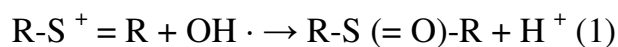


Fig. 19 – Degradation of dyes by TiO₂ nanoparticles

The first initial step is certainly not the reaction gap / MB because the MB is a cationic reagent and not electron-donor. In contrast, the OH · radicals can attack the functional group C-S = C⁺ (FL1²³), which forms a favorable Coulomb interaction with the surface of the catalyst, as previously highlighted by the influence of pH, with formation of the sulfoxide (FL2) :



The electrophilic attack regards the doublet free heteroatom S, oxidizing it. However this oxidation requires the preservation of conjugation of the double bond, which then induces the central opening of the aromatic ring. H atoms necessary to form the bond CH and NH may result from the reduction of protons present in solution by electron capture photogenerated:



A large number of experimental results indicate that the photocatalytic oxidation of various dyes work of TiO₂ activated by UV radiation and in the presence of oxygen is in agreement with the kinetic model of Langmuir-Hinshelwood (LH) [109].

Generally, the degradation grows if you increase the amount of catalyst added within the solution as it increases the surface area available for adsorption.

Above a certain value of concentration, however, the opacity of the solution (due to light scattering) increases causing a reduction in the penetration of light in the solution and, consequently, a decrease in the speed of reaction. There is therefore an optimum value.

2.3.1.2 - Procedure

Titanium samples are inserted within an ultrasonic bath and are sonicated for 15 minutes to disperse the nanoparticles

They are inserted by pipette to bubble 1 ml of a solution of BM to 260 ppm within the beaker titanium dioxide suspension, thus obtaining a concentration of MB within the dispersion of 10 ppm, in agreement with the literature [110].

A vigorous stirring is activated to equilibrate the system for 10 minutes; after that the UV lamp is activated.

At regular intervals of time, by micropipette, sampling 1 ml of solution of MB from the reaction mixtures is taken; these are inserted into two separate numbered Eppendorf tubes and centrifuged at 9500 rpm for 15 minutes.

A lamp PL Series by UVP Inc. lamp equipped with 365 nm wavelength and 4W of power is used.

2.3.2 - Degradation of NO_x

The test is performed in a system composed by following equipment (Fig. 20):

- A source of nitrogen oxides (cylinder).
- A compressed air source (cylinder or compressor).
- A reactor.
- A magnetic stirrer.
- A UV lamp HG500.
- A device for the measurement of the chemiluminescent NOX

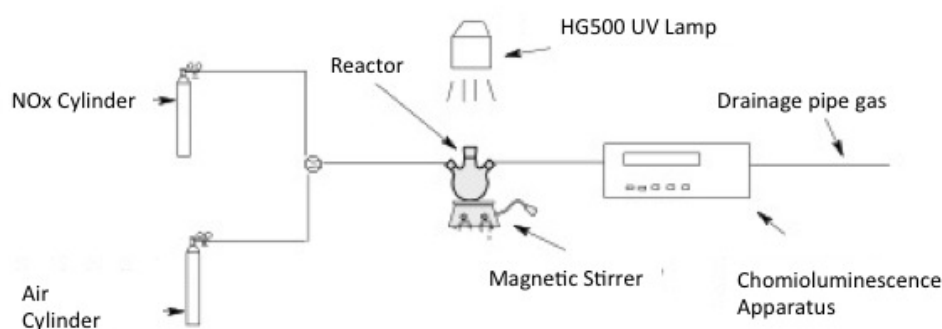


Fig. 20 – NOx degradation test Equipment

This test is performed in a spherical reactor of 20 liters.

It has an input for the gas that is closed at the start of the reaction, a pressure gauge for controlling the vacuum that forms as a result of sampling, an exit for gas sampling, a receipt for the samples of catalyst and support for the same. Within the reactor is also a magnetic stir bar to keep the gas moving. This injection is carried out by placing about 2 bars of pressure from the regulator of the cylinder to the reactor and then flowing into the pipes by a quick flow of compressed air to ensure that all nitrogen oxides come in reactor. At this point, the entrance is closed and the process goes on to make the zero point; then the UV lamp (Jellosil HG500 with a power of 500 W and an emission peak at 364

nm) is switched on and sampling at different times is carry out. After each sampling the gas outlet valve is closed to keep the reactor going in a vacuum. The measurement of the lamp power was carried out by exposing the sol, prepared with the above procedure and placed in a quartz cuvette of dimensions 10x10x20 mm, the lamp placed at predetermined distances, and then measuring the absorbance at 540 nm.

Applying the formula:

$$Y = 1.96 X$$

Where Y is the distance between light source and sample, while X is the energy radiated. Radiated power is obtained for the irradiated millijoules cm^2 exposed surface area; this value and the exposure time (t) in minutes, are given by the following formula :

$$W/\text{m}^2 = X / (60 \times t) \times 10000.$$

The procedure for the actinometrical measurement and for the equation of calibration were found in the literature in Application of TiO_2 sol for UV Radiation Measurements.

2.3.3 - Antibacterial test

To evaluate microbiological activity, Escherichia Coli (ATCC 8739) is used. This bacterial family grows overnight in TSA (Tryptic Soybean agar). Aliquots of these cultures were inoculated in nutrient culture broth (Tryptic Soy Broth) and incubated in aerobic conditions at 37°C until achievement of exponential growth phase. From these cultures the standard suspensions (approximately 10^7 cfu/ml for Escherichia Coli and 10^6 cfu/ml for Staphylococcus Aureus) were obtained by serial dilutions. Then for the tests, 7 ml of aqueous suspension of titanium dioxide were put in Petri Plate (diameter 5.5 cm) and dried for the complete evaporation of liquid part of the sample [111]. Each sample-plate,

covered by TiO₂ nanoparticles, was treated with 2 ml of bacterial suspension at standard titre with 2x10⁷ cfu/ml of Escherichia Coli and put for 3 h under UVA black light with wavelength 366 nm and intensity 12 Watt (220 Volt) [112].

After irradiation, from each treated sample an aliquot was taken (1 ml) suitably diluted and then put in plate with agar for determination of the number of alive bacteria (counted as unit that shape colony, cfu/ml). The inoculated plate was put in an incubator at 37 °C for 24 h and then the bacterial colonies were counted.

To determine the decrease percentage of bacteria colonies these mathematic formulas are followed:

Percent survival colonies: S/S_0

(S= final concentration; S₀= start concentration) x100

Percent of reduction: $1 - [S/S_0] \times 100$.

2.4 – BIOLOGICAL TESTS

2.4.1 – Antioxidant capacity

Total antioxidant activity was determined using a direct measurement of ABTS (2,2-azino-bis-3 ethylbenzothiazoline-6- sulfonic acid). ABTS radical cation (ABTS) was produced by reacting ABTS stock solution (ABTS dissolved in water to a 7 mM concentration) with 2.45 mM potassium persulfate (final concentration) and allowing the mixture to stand in the dark at 4° C for 12–16 h before use until the radical was stable. The ABTS solution was diluted in a hydroalcoholic mixture ethanol–water (50/50) to an absorbance of 0.70 (± 0.02) at 734 nm. 10 mg of the sample was used for the determination. After being suspended in 6 mL of ABTS diluted solution, the mixture was stirred in the dark for 25 min and then centrifuged at 4000 rpm for 2 min. The absorbance was read at 734 nm using as blank the same quantity of the ABTS diluted chromophore in which only cellulose had been suspended. The antioxidant capability (AC) was expressed, using Trolox as standard, as mmol of Trolox Equivalent (TE) per gr. of dried weight (dw), therefore TEAC notation was used. The values are the mean three replicates.

The method TEAC (Trolox equivalent antioxidant capacity) using the ABTS and is based on the ability of antioxidants to reduce the ABTS radical cation (fig. 21), characterized by an intense blue-green color with consequent loss of absorbance.

2.4.2.2. - Test of cell viability by staining with Trypan blue

Cells THP-1 (human monocytic line) are grown in RPMI medium supplemented with 10% FBS at 37 °C, 5% CO₂, and distributed in Constar plates at a concentration of 106 cells / well / ml. The cells are stimulated and accession induced by the addition of phorbol myristate acetate (PMA) at a concentration of 2 mg / ml, treated with sample (300µg/ml) and incubated at 37 °C, 5% CO₂ for 24, 48 and 72h. After each incubation time washes with PBS were performed and the cells were detached by adding 1% trypsin for 5 minutes at 37 °C. Finally the cells were stained with Trypan blue. Cell viability was determined with the following formula: $N^{\circ} \text{ viable cells} / N^{\circ} \text{ viable cells} + \text{non-viable cells} \times 100$. [113]

2.4.2.3 - Production of Nitrite in THP-1 cells

Cells THP-1 (human monocytic line) are grown in RPMI medium supplemented with 10% FBS at 37 °C, 5% CO₂, and distributed in Constar plates at a concentration of 106 cells / well / ml. The cells are stimulated and accession induced by the addition of phorbol myristate acetate (PMA) at a concentration of 2 mg / ml, treated with sample (300µg/ml) and incubated at 37 °C, 5% CO₂ for 24, 48 and 72h. The positive control was done by stimulating the THP-1 cells with LPS (10µg/ml). The supernatants recovered after each incubation time were treated with the Griess reagent and the absorbance was read at 490nm. [113]

2.4.2.4 - Cytotoxicity assay by determination of LDH

The release intracellular enzyme lactate dehydrogenase (LDH) was used as the endpoint for the study of cell toxicity, and used as a marker for cell necrosis. THP-1 cells are grown in RPMI medium supplemented with 10% FBS at 37 °C, 5% CO₂, and distributed in Constar plates at a concentration of 106 cells / well /

ml Non-Radioactive Cytotoxicity Assay(PROMEGA). Such cells are induced for accession by the addition of phorbol myristate acetate (PMA) at a concentration of 2 mg / ml, treated with sample (300µg/ml) and incubated at 37 °C, 5% CO₂ for 24 , 48 and 72h. The test for the assay of LDH was conducted using the kit CytoTox96 not-Radioactive Cytotoxicity Assay (Promega).

CHAPTER 3 - RESULTS AND DISCUSSION

3.1 – HYDROTHERMAL SYNTHESSES

The synthesis obtained by hydrothermal process, have been characterized in order to correlate the chemical-physical characteristics with the variation of the synthesis parameters and to evaluate the influence that these variations have on the characteristics of the nanoparticles obtained.

3.1.2 – DRX Characterization

3.1.2.1 – Synthesis 1

The XRD pattern (Fig. 22) shows how this type of synthesis has been achieved with a single step reread characteristic of anatase. Is in fact observed characteristic reflections of anatase with well defined peaks defined. The reference used is ICSD collection code 202242 (01-084-1285).

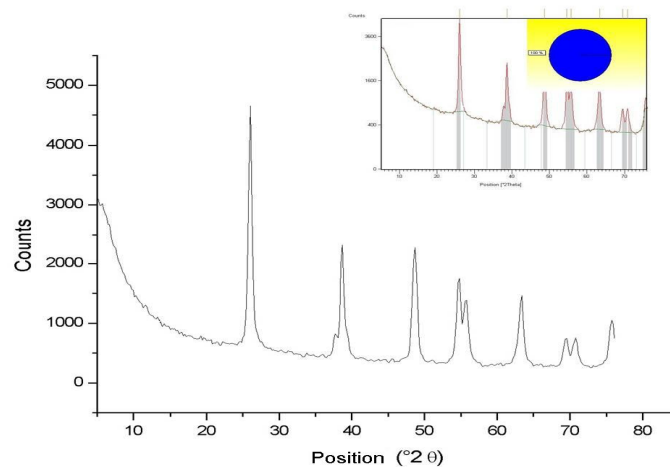


Figure 22 - XRD pattern of Synthesis 1

3. 1. 2 .2 - Synthesis 2

Even the XRD pattern of the synthesis n ° 2 shows (Fig. 23) the obtaining of a single phase that appears to be crystalline anatase.

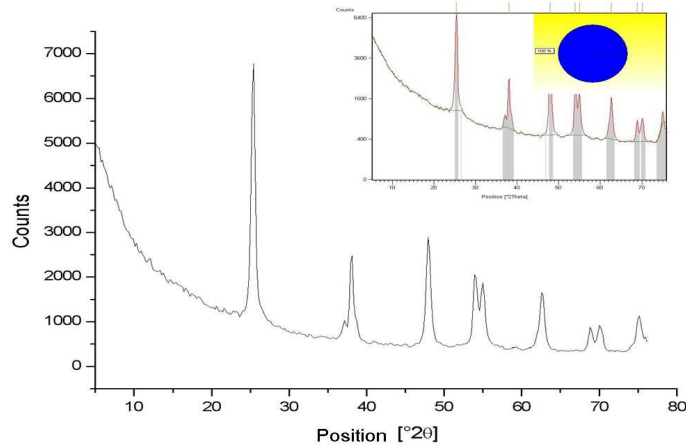


Figure 23 - XRD pattern of Synthesis 2

3. 1. 2 .3 - Synthesis 3

Even the XRD pattern of the synthesis No. 3 shows (Fig. 24) the obtaining of a single crystalline phase of anatase.

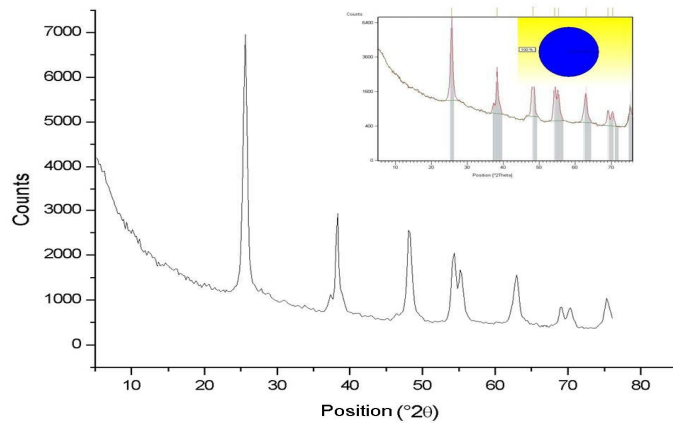


Figure 24 - XRD pattern of Synthesis 3

3. 1.2 .4 - Synthesis 4

The XRD pattern of synthesis No. 4 (Fig. 25) shows also a single phase of anatase crystalline, but has a higher definition of the peaks, then a greater crystallinity than the other synthesis obtained.

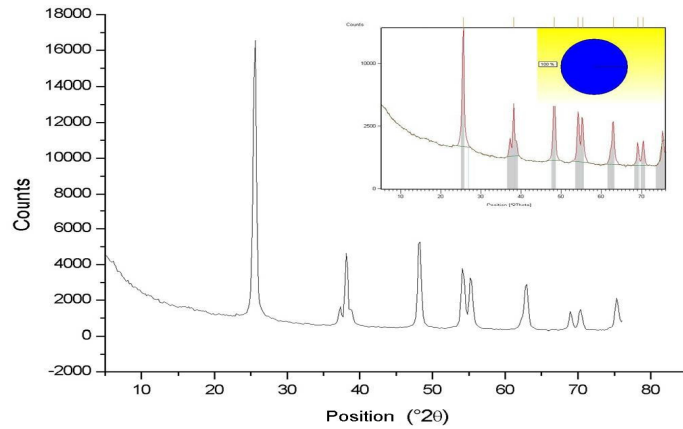


Figure 25 - XRD pattern of Synthesis 4

3. 1.2 .5 - Synthesis 5

Even the synthesis No. 5, from the XRD pattern obtained (Fig. 26) turns out to be composed of a single phase of crystalline anatase

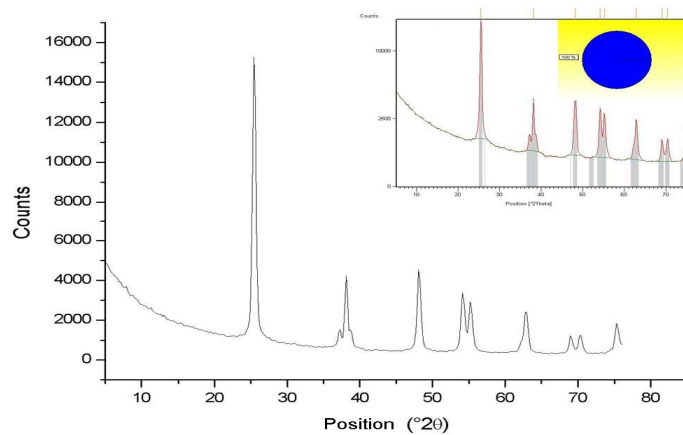


Figure 26 - XRD pattern of Synthesis 5

3.1.2.6 - Synthesis 6

The XRD pattern obtained from the synthesis No. 6 (fig. 27) also shows a single phase of anatase crystalline peaks are very well defined.

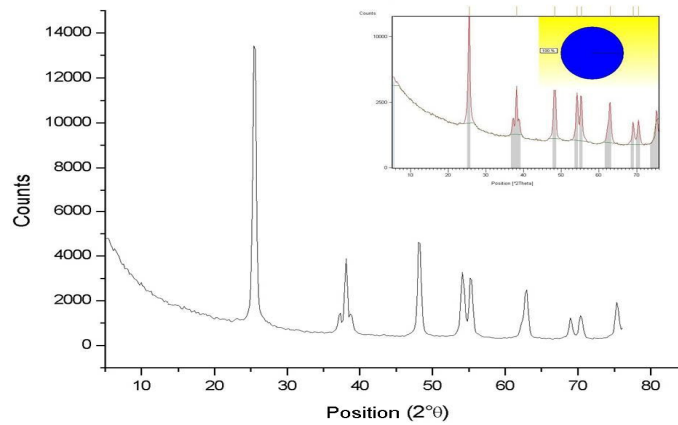


Figure 27 - XRD pattern of Synthesis 6

3.1.2.7 - Synthesis 7

The XRD pattern of the synthesis No. 7 (Fig. 28) obtained at a lower temperature than the other, showing the prevalence of an amorphous phase which covers eventually characteristics reflections of waiting phase as anatase

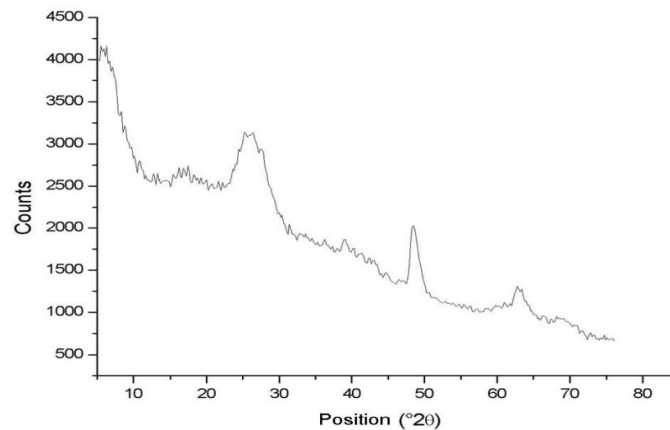


Figure 28 - XRD pattern of Synthesis 7

3. 1.2 .8 - Synthesis 7 heat-treated

The XRD pattern of the synthesis No. 7 heat treated at 400 ° C for 4 hours (Fig. 29), shows how the previously product consisting predominantly in amorphous material, is converted into crystalline material composed of two phases such as rutile and anatase. Mostly, the material is composed of rutile (77%), with a small fraction of anatase (23%). Rutile reference used is ICSD collection code 082081(01-089-0552).

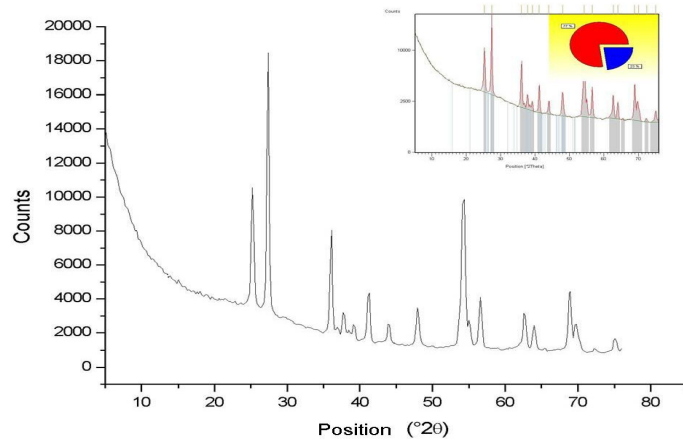


Figure 29 - XRD pattern of Synthesis 7 heat-treated

3. 1.2 .9 - Synthesis 4 heat-treated

The XRD pattern of the synthesis 4 thermally treated (Fig. 30), also shows a single crystalline phase consisting of anatase.

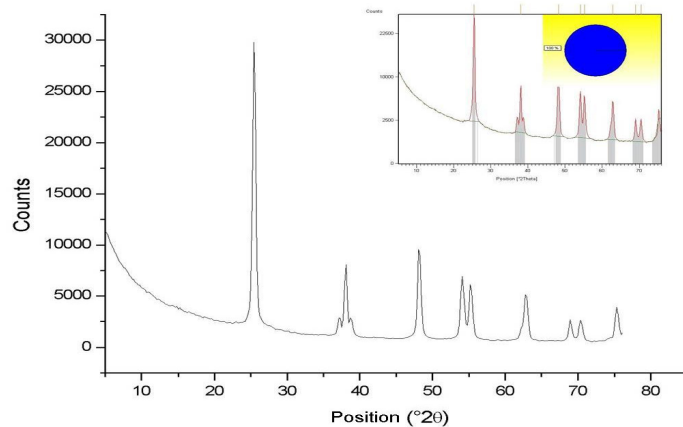


Figure 30 - XRD pattern of Synthesis 4 heat-treated

3.1.2.10 - Synthesis 6 with ultrasound treatment

The XRD pattern of synthesis 6 treated with ultrasound (Fig. 31), also shows in this case that the sample is composed of a single crystalline phase of anatase

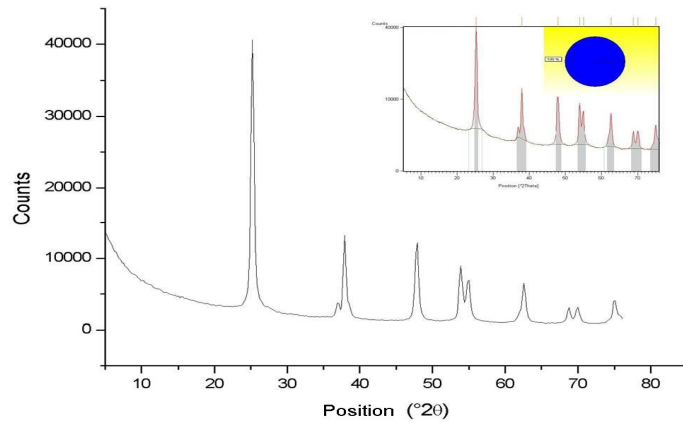


Figure 31 - XRD pattern of Synthesis 6 US-treated

3.1.2.11. - Comparison of the products obtained

Comparing the diffraction patterns (fig. 32) of the products obtained can be seen that the products obtained using as a precursor of titanium Ti (IV)- butoxide (Syntheses No. 1, 2, 3) all give a single crystalline phase of anatase.

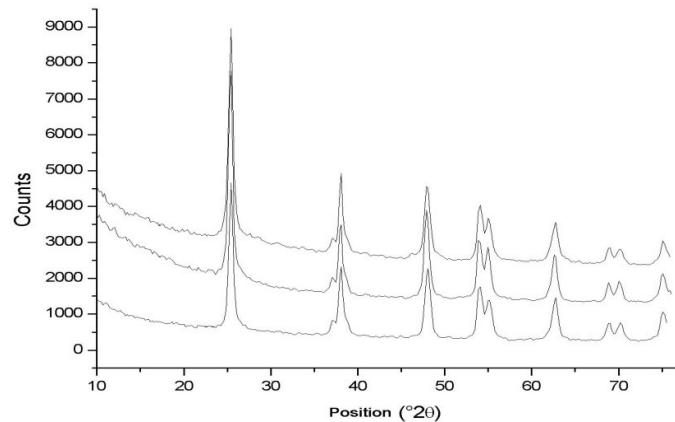


Figure 32 - XRD pattern comparison syntheses 1,2,3

Synthesis No. 2, obtained at pH greater than the synthesis 1 and 3, doesn't shows any differences compared to the other synthesis, indicating that the variation of pH has no influence on the formation of the crystalline structure of the product . (fig. 33)

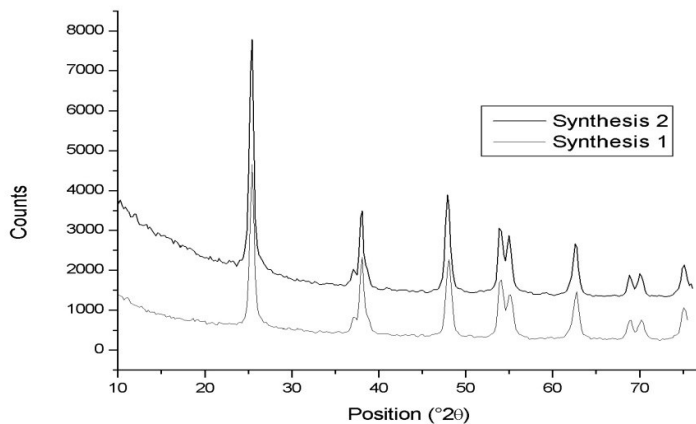


Figure 33 - XRD pattern comparison syntheses 1,2

Also the comparison between different reaction timing does not show substantial differences; can be seen only a slight increase of the definition of the peaks, and then of crystallinity for the synthesis No 1. obtained with more reaction time. (fig. 34)

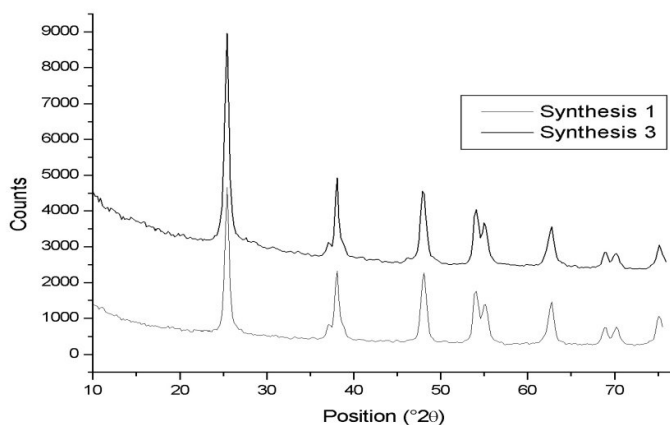


Figure 34 - XRD pattern comparison syntheses 1,3

Comparing XRD pattern of the synthesis No. 1 and No. 4, obtained with the same synthesis parameters, but changing the titanium alkoxide, it is seen that both samples are constituted by a single phase of crystalline anatase. (fig. 35)

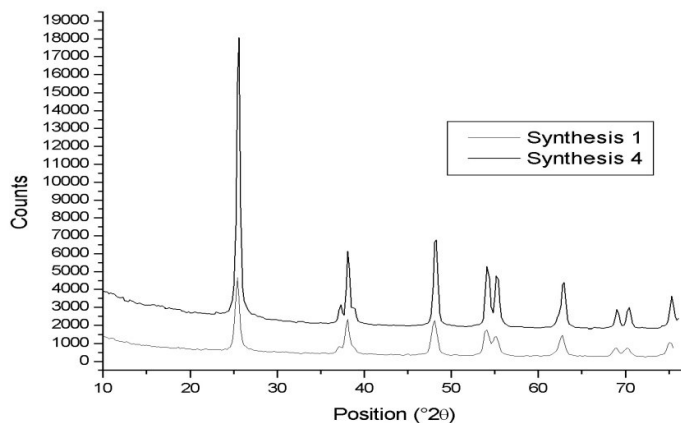


Figure 35 - XRD pattern comparison syntheses 1,4

3.1.2.12 – Thermal treatment

It is known as the XRD pattern of the synthesis No. 4 present signals much more defined than the synthesis No. 1; then the alkoxide used has influence, albeit in a very limited manner on the crystalline structure of the product obtained; this could be given by different kinetics of hydrolysis and condensation of alkoxides. In fact alkoxides with big alkyl groups have very slow kinetics of hydrolysis and diffusion. Since the polymerization reaction of the network of titanium, to create the corresponding oxide, needs a partial hydrolysis reaction and diffusion, in alkoxides with big alkyl residues, it has a lower formation of the corresponding oxide [114].

The two alkoxides used in this work does not differ much as the length of the alkyl chain, but being the linear butoxide and isopropoxide branched, the latter probably can hydrolyze with faster slightly kinetics providing more training to the corresponding oxide, so dioxide of titanium.

Even the synthesis prepared with Ti (IV) isopropoxide (No. 4, 5, 6) were put into relation and as the XRD patterns show, for each one is obtained by a single phase of crystalline anatase. There were no significant differences. (fig. 36)

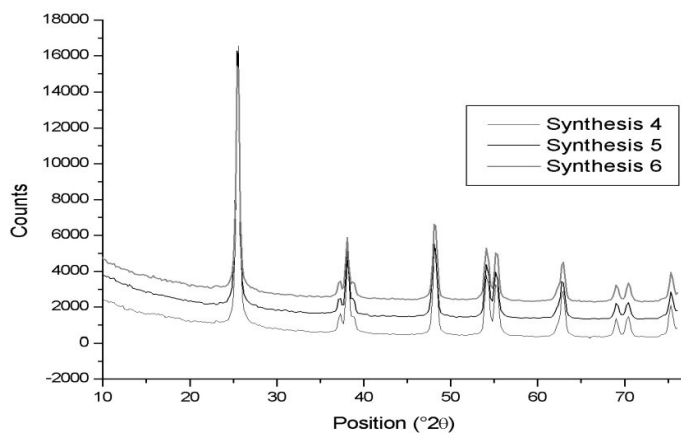


Figure 36 - XRD pattern comparison syntheses 4,5,6

It was also performed a test to see the effect of the synthesis temperature on the properties of the product.

The synthesis No. 7, was obtained using the same parameters of the synthesis No. 6, but varying the temperature synthesis from 160 ° C to 120 ° C. As seen above, the temperature effect is remarkable, in fact at a temperature of 120 ° C do not get a crystalline product or in any case a phase expected as it is obtained from the previous synthesis, but is obtained a product predominantly amorphous. In fact the product after the reaction, was found to have even the characteristics of a gel, the same as it was before the hydrothermal treatment

Probably, such hydrothermal conditions, are not thermodynamically sufficient to obtain complete conversion of the gel obtained by the first part of the synthesis in which the hydrolysis takes place of titanium alkoxide.

It has thus tried to make a heat treatment on the synthesis obtained, to see if by such processing is unable to obtain a crystalline material, providing the conditions for complete conversion of the gel into nanoparticles of titanium dioxide. The treatment carried out in circular oven at a temperature of 400 ° C for 4 hours creates the condition to form rutile phase according to literature that indicate that hydrothermally crystallized titanium dioxide gel, obtaining anatase at lower temperatures and rutile at higher temperatures.

The XRD pattern (fig. 37) shows that you have obtained a very crystalline, but composed mainly of rutile. Due the conditions of thermal treatment, such d anon will allow the conversion of anatase in rutile, it is assumed that the hydrothermal synthesis performed at a temperature of 120 ° C has favored from the point of view of the thermodynamic, an initial formation of rutile together to amorphous material, while the subsequent heat treatment has favored the formation and transformation of the amorphous material in anatase.

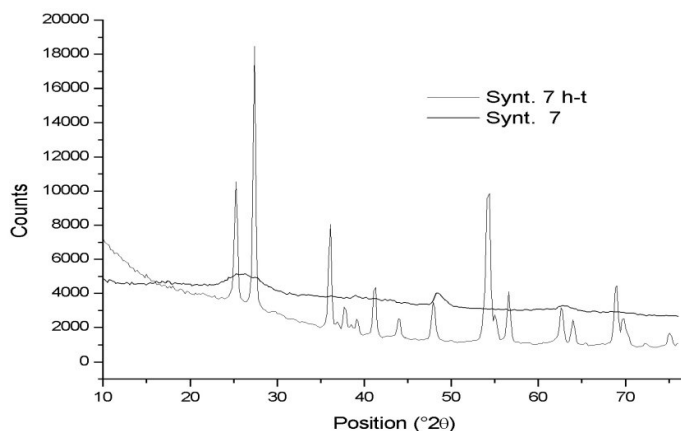


Figure 37 - XRD pattern comparison syntheses 7, 7 h-t

In order to verify the effects of a successive thermal treatment to the synthesis, it was decided to try to treat at 400 ° C for 4 hours, also one of the products obtained which was already composed of a single crystalline phase of anatase. (fig. 38)

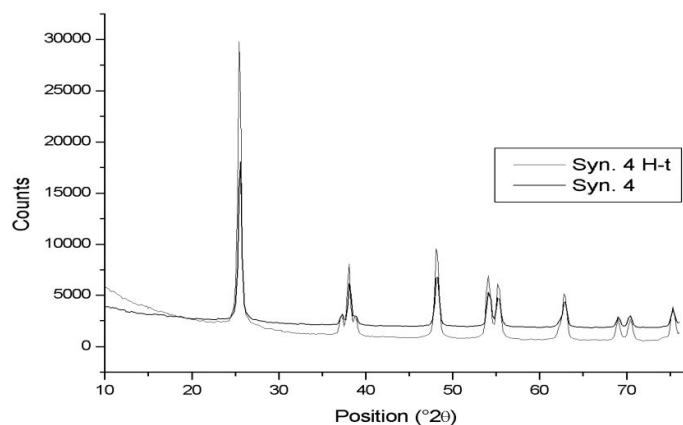


Figure 38 - XRD pattern comparison syntheses 4,4 h-t

This has been done on the synthesis treatment No. 4, the comparison of the XRD patterns shows that there are substantial differences. Only a very little increase of signals in synthesis treated. Probably hydrothermal synthesis in those conditions has reached the necessary thermodynamics conditions for obtaining a crystalline material.

3.1.2.13 - Use of ultrasound

It was also tried to add the effect of ultrasound during the process of hydrolysis of Alkoxide with water. It has been made a synthesis under the same conditions of synthesis No. 6, by adding to the hydrolysis process the effect of foreign ultrasonic (19 KHz), in order to assess any changes in the chemical-physical characteristics.

The comparison of the XRD patterns show that the product obtained using ultrasound results to have peaks slightly more defined: it is likely that the ultrasound accelerate the hydrolysis and condensation processes in the formation of titanium dioxide. (fig 39)

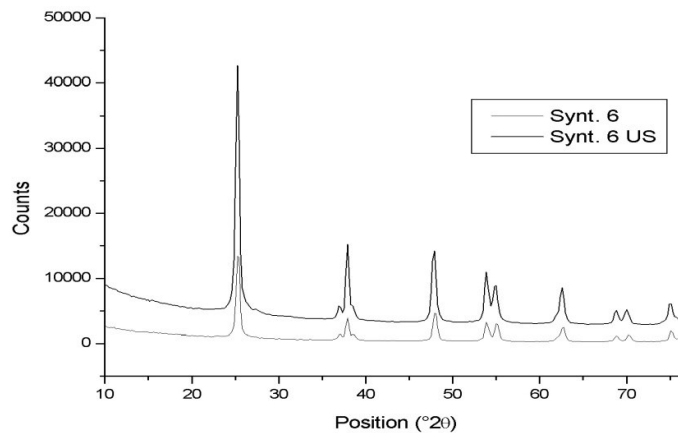


Figure 39 - XRD pattern comparison syntheses 6,6US

3.1.2 – Morphologic Characterization

The morphological characterization to see the size and shape of the particles of titanium dioxide obtained with the different synthesis was performed by TEM microscopy.

It's put themselves in relation the characteristics of the various particles with their method of synthesis.

The samples obtained by hydrothermal treatment using titanium butoxide, slightly differ both in form and in size.

The nanoparticles of anatase obtained from the synthesis No.1, appear to have a variable flat and ellipsoidal shape s enough with a dimension of individual nanoparticles are between 20 and 50 nm.

The plots obtained from synthesis 2, obtained with a different pH compared to the synthesis 1, were found to have a different shape. Indeed, such particles appear to have a more rounded shape but expecially elongated.

This effect is mainly due to triethanolamine is used as a stabilizer. Indeed, as reported in the literature, the triethanolamine is adsorbed more strongly to the face of the crystal parallel to the c-axis of the tetragonal system with respect to face C. This

explains the arrest of the growth of the particles of titanium dioxide in the direction perpendicular to the c axis, leading to the formation of elongated particles.

It happens because at this basic, the triethanolamine is more deprotonated, then with a molar ratio of triethanolamine neutral very large which goes to adsorb on the particles of titanium dioxide.

This large adsorption of triethanolamine hinders the growth along the direction perpendicular to c-axis giving particles of ellipsoidal shape; such a mechanism is not the case at pH lower when a large part of the triethanolamine is in protonated form, thus not free to adsorb on the particles to which their growth is equal in all directions. Such particles as well as having a shape elongated have a size greater; in fact their size is about 50-80 nm.

The particles obtained by the synthesis No. 3 in which the parameters are the same as the synthesis No. 1 except for the lower reaction time, turn out to have the same flat morphology of apticelle synthesis of 1, but are much smaller, because such particles have dimensions comprised between 10 and 25 nm. (fig. 40)

This is probably due to the reaction time and to complete the kinetics of formation of particles, because the particles of Synthesis No. 1, with a time of 14 hours, were able to form completely and grow up to have reached an equilibrium, while the particles obtained from the synthesis 3, have not formed totally throughout and have not reached their size optimal based on the kinetics of the synthesis.

It would also explain the fact that the X-ray diffraction, the product obtained from the synthesis of the peaks have 1 is much more defined than those obtained by the product of synthesis 3; this fact may be due to the fact that since the particles of the synthesis 3 much more small, give a lower diffraction, then a slight broadening of peaks.

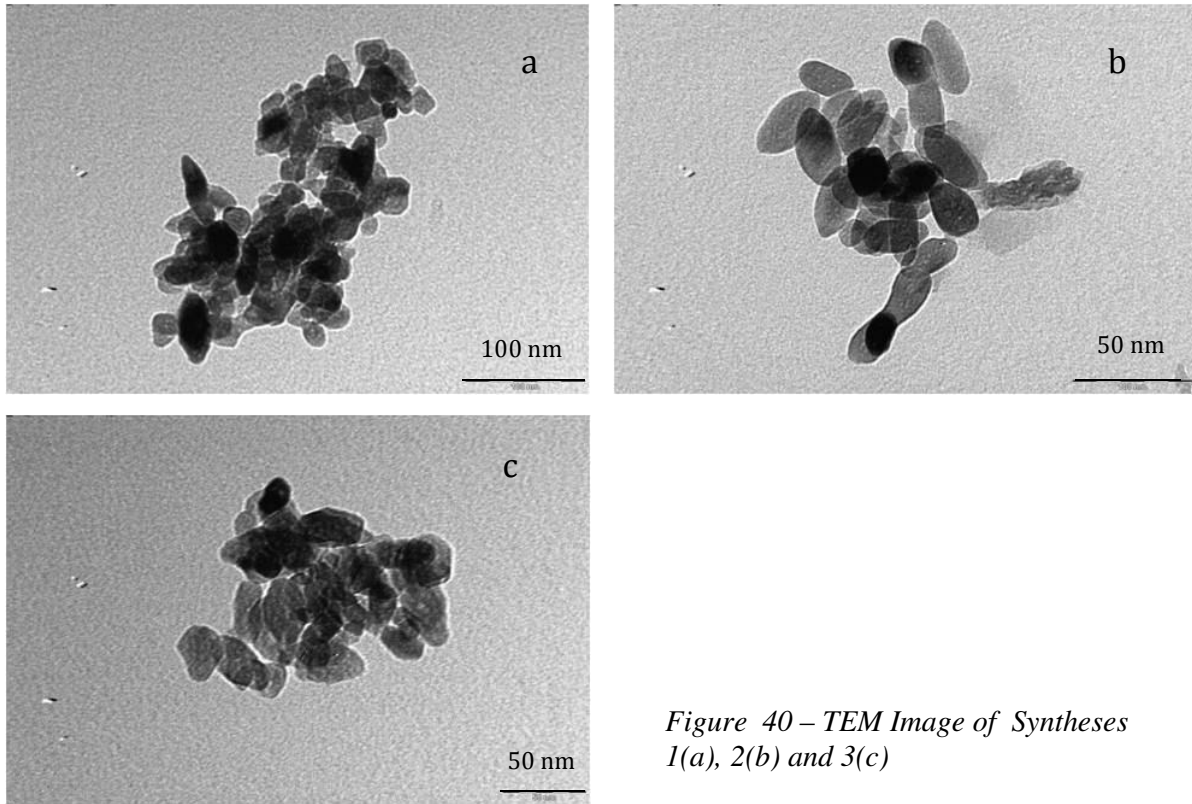


Figure 40 – TEM Image of Syntheses 1(a), 2(b) and 3(c)

TEM investigation carried out on the particles obtained by the synthesis No. 4, in which is used the Titanium-isopropoxide, shows that these particles have a morphology similar to the particles obtained with the synthesis 1, but have a size slightly smaller; fact these particles have a dimension of between 25 and 50 nm (fig. 41).

This could depend on, as mentioned earlier, by the fact to have a kinetic different with which the 2 different alkoxides are able to hydrolyze.

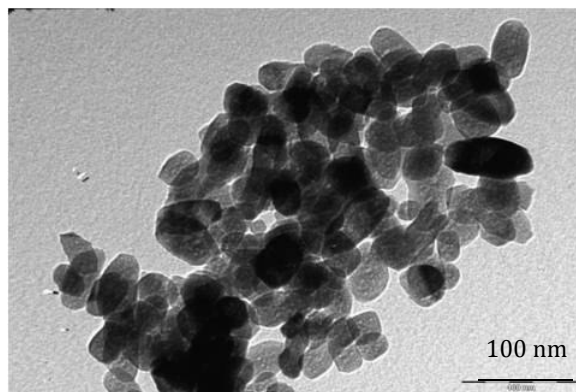


Figure 41 - TEM microscope picture of synthesis 4

TEM investigation carried out on the particles obtained by synthesis No. 5 (fig. 42) in which it had a pH greater than, equal to that of the synthesis No. 2, also shows in this case that the variation of pH has considerable influence on the morphology of the particles. In fact, even in this case we obtain particles of elongated shape, but the phenomenon is more marked as are observed particle morphology not only ellipsoidal, but elongated up to have a needle-like morphology.

The explanation could be passed the same, previously given for the synthesis No. 2, but in this case, the phenomenon is much stronger. This could be due to the fact that being the isopropoxide titanium slightly less cumbersome of titanium butoxide, for which the triethanolamine could adsorb in a greater manner on the parallel face axis C inhibiting drastically the grow along the perpendicular direction to that axis.

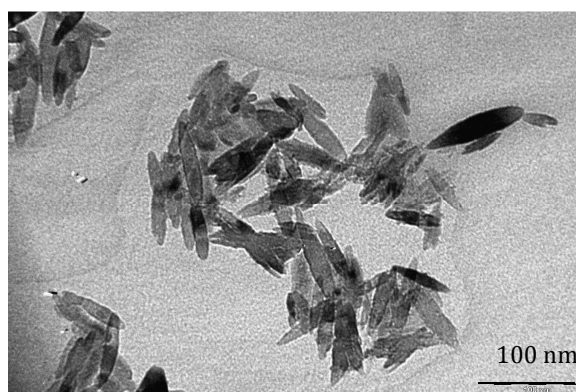


Figure 42 - TEM microscope picture of synthesis 5

In this work, it is tried to make the heat treatment of one of the products obtained, in order to evaluate the effect and the impact on the chemical-physical characteristics. it was decided to treat the sample No. 4 at 400 ° C for 4 hours; as already seen above, this treatment has no effect on the structure and crystalline phase of the product, but instead the TEM analysis shows that it has a strong effect of surface modification, because the particles after being treated appear to have morphology and dimensions similar to those of the untreated sample, but with an apparently porous surface. (fig. 43)

This could be due to the fact that the particles obtained after the hydrothermal synthesis have residues of triethanolamine superficially adsorbed; heat treatment decomposes the triethanolamine that, during synthesis, has acted as templating agent not permitting growth formation of a homogeneous surface, but an uneven surface, only visible just after you delete this molecule by heat treatment.

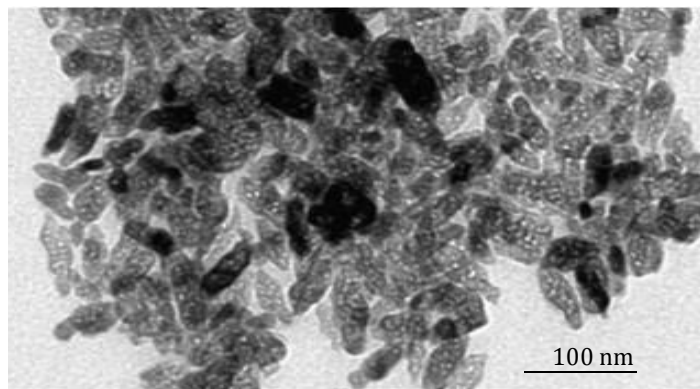


Figure 43 - TEM microscope picture of synthesis 4 h-t

Evaluating the effect of ultrasound, is seen as analysis TEM analysis (fig. 44) shows that the particles obtained with this variation are slightly smaller than those obtained with the same synthesis methodology but without Ultrasound. It's not showed substantial differences, both in morphology and in size.

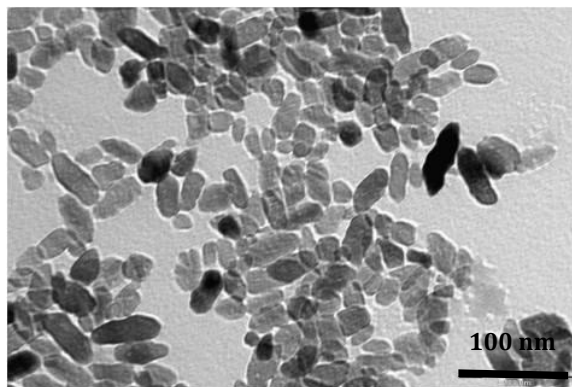


Figure 44 - TEM microscope picture of synthesis 6 US

3.1.3 – FT-IR Characterization

The particles obtained were subjected to FT-IR analysis to better understand if on the surface of nanoparticles there was some residual adsorbed triethanolamine.

All samples obtained show very similar spectra, then, it is taken as an example the synthesis No. 4 which was then heat treated to see if this treatment has had effect on the removal of triethanolamine possibly adsorbed on the surface.

In fact from the spectrum (fig. 45), are observed in the bands attributable to both at anatase and triethanolamine.

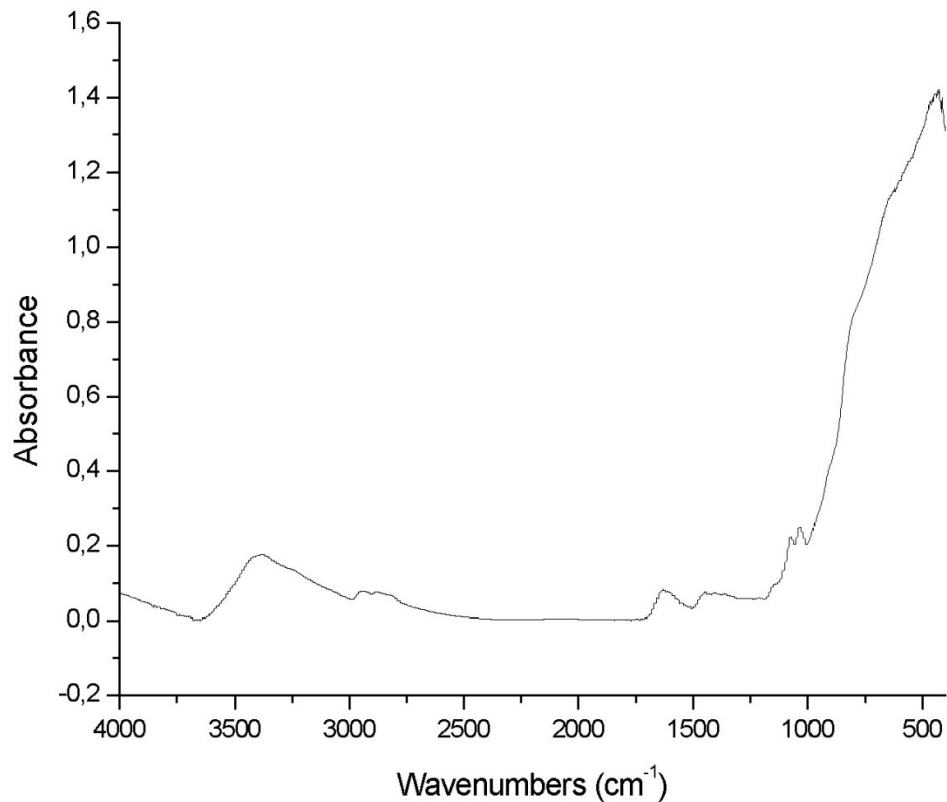


Figure 45 - FT-IR spectra of synthesis 4

It is observed a band between 2800-3600 cm^{-1} due to stretching of H_2O , the band at 1610 due to stretching of water adsorbed, while the band between 450-900 cm^{-1} is attributable to anatase [116].

But you can see the other bands. These bands are to be considered due to the fact triethanolamine. Are noticed in fact the bands at 3056-2923 (2952) cm^{-1} , due to the stretching of the CH triethanolamine, the band from 1506 to 1456 (1506) cm^{-1} attributable to the CH Bendig of triethanolamine and the band from 1136 to 1135 (1123) cm^{-1} due to stretching of the CN bond of triethanolamine. [117] Comparing the spectrum with the database of the instrument, the instrument associated with the spectrum obtained spectrum of triethanolamine.

These considerations confirm that on the surface of the particles obtained by hydrothermal synthesis there are residues of triethanolamine superficially adsorbed.(fig. 46)

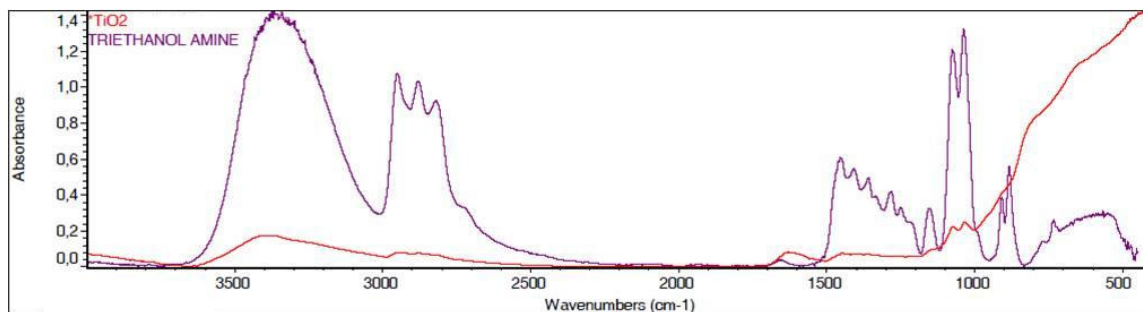


Figure 45 - Comparison FT-IR spectra with Triethanol amine refernce

The hypothesis is still confirmed by comparison with the FT-IR spectrum of the sample obtained with the same synthesis, after heat-treated at 400 ° C for 4 hours.

The spectrum of this sample (fig. 47) in fact does not have the characteristics of bands such as triethanolamine 3056-2923 (2952) cm^{-1} , 1136-1135 (1123) cm^{-1} present in the untreated sample, but shows only a small band on 1506-1456 (1506) cm^{-1} , indicating that the heat treatment eliminates the residual amine adsorbed on the surface, confirming the hypothesized TEM analysis.

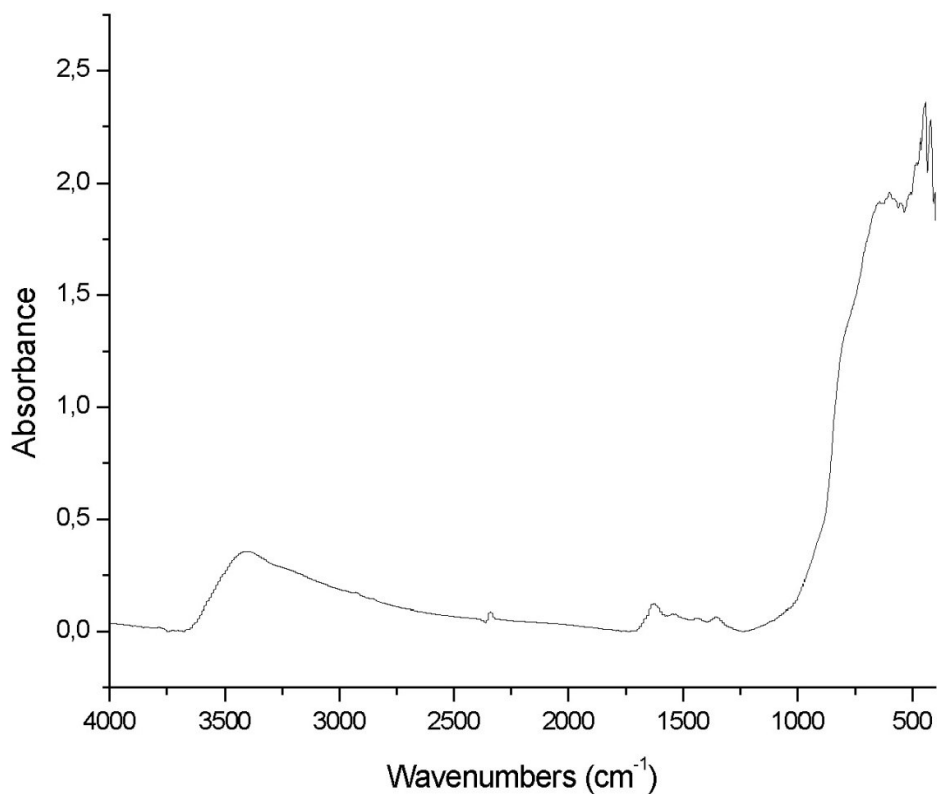


Figure 47 - FT-IR spectra of synthesis 4 h-t

In fact, comparing the two spectra obtained with the treated sample and the untreated sample (fig. 48), it can see how the triethanolamine is gone, while the band 900-450 cm₁, due to anatase, these signals much clearer and also confirming what it was seen from the comparison with the DRX in which were observed also in that case the peaks slightly more precisely defined due the fact that the triethanoalamine has disappeared.

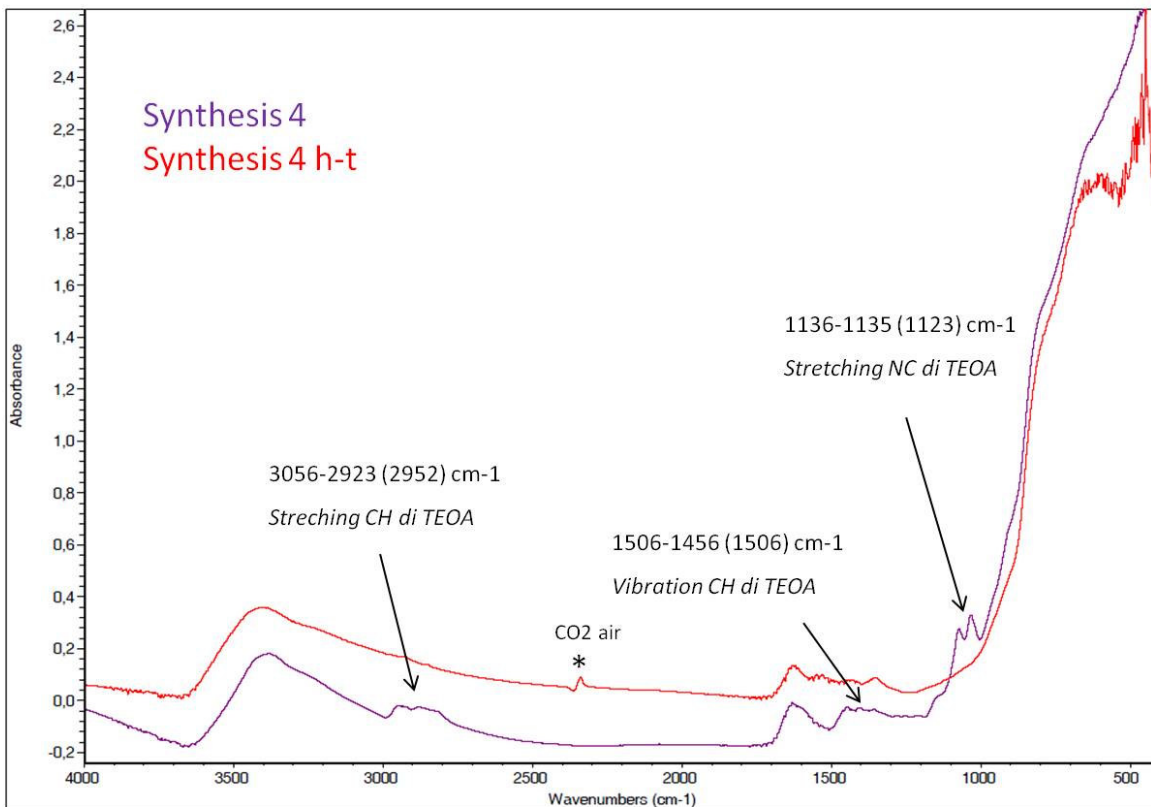


Figure 48 - Comparison FT-IR spectra of syntheses 4, 4 h-t

3.1.4 - Photocatalytic Test

3.1.4.1 – Degradation of Methylene Blue

The samples obtained were carried out tests to see their photocatalytic property and to see if there was a correlation between the results obtained and the different chemical-physical properties of each sample.

The samples obtained with this test does not have given very satisfactory results, since, in confirmation of what that you previously discussed, the samples have a surface that is covered with triethanolamine remaining adsorbed on the surface after synthesis.

This probably does not allow to have an effective photocatalytic activity;

In fact almost all of the samples is has a very low photocatalytic effect almost non existent.

The tests have not allowed then to appreciate significant variances between the various synthesis developed, though instead have highlighted variations in physico-chemical properties.

The best results however have been obtained by the synthesis carried out with the aid of ultrasound (fig. 49). This product is also the only one capable of giving a significant kinetic profile.

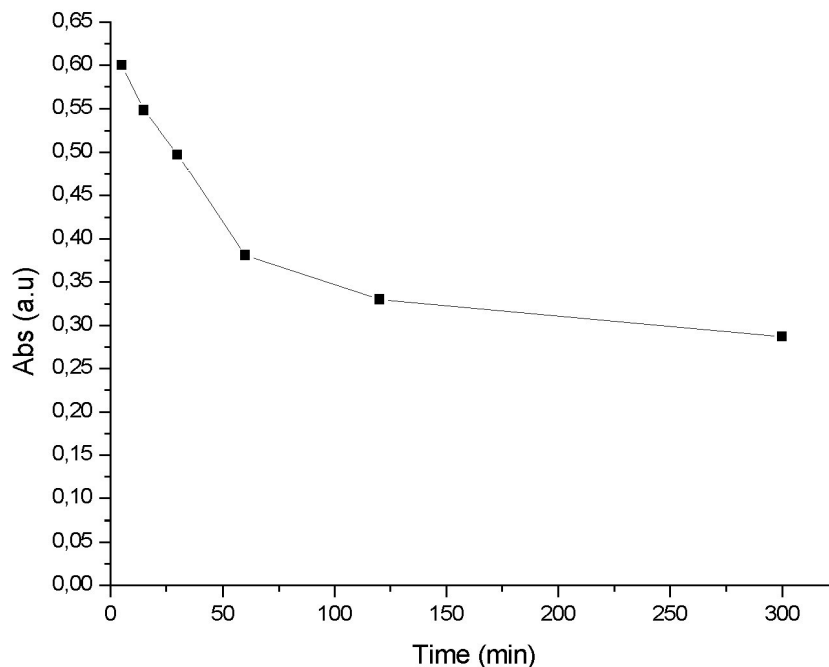


Figure 49 - Degradation test synthesis 6 US

In order to assess which then had the effect due to triethanolamine, tests were carried out by relating photocatalytic activity synthesis of No. 4 and No. 4 that of the synthesis thermally treated (fig. 50).

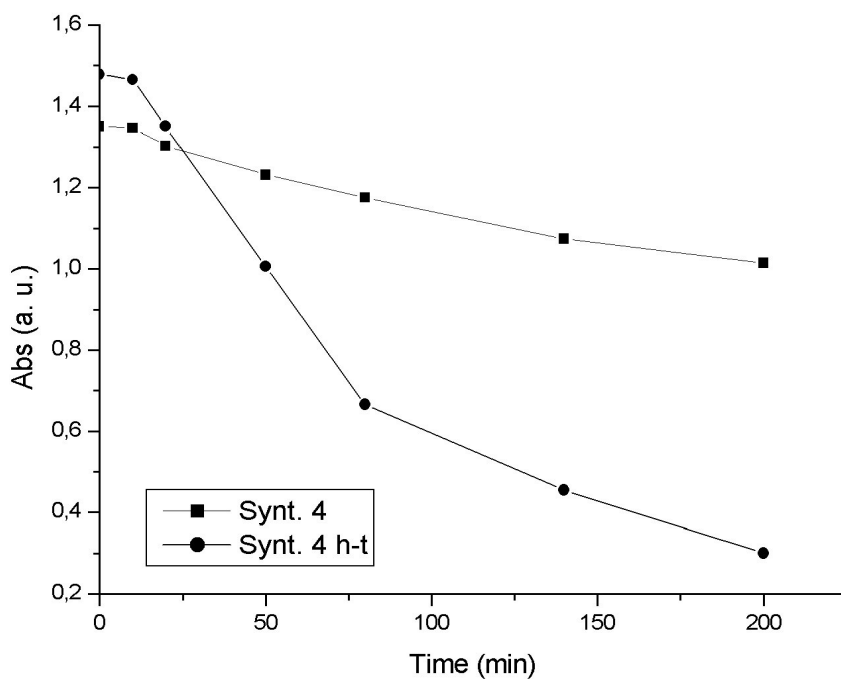


Figure 50 - Comparison degradation tests syntheses 4, 4 h-t

The tests carried out show clearly how the triethanolamine adsorbed on the surface of the particles, both from hindrance and obstacles the photocatalytic effect of nanoparticles .

Removing thermally triethanolamine, it have a product with very high photocatalytic properties.

This it must be partially to triethanolamine, but also to the fact that, as shown by the TEM images, the particles after undergoing heat treatment, show a porous surface, and this may increase the contact surface, and therefore the photocatalytic effect.

3.1.5 – Discussion

Then, as has been discussed above, the particles obtained by hydrothermal synthesis using triethanolamine as a stabilizing agent reflect the influence of the synthesis

parameters that are reflected in their physicochemical properties such as crystalline phase, size and morphology.

The reaction time has no influence on the size as for shorter times are obtained smaller size.

The reaction temperature influences the crystalline phase; as seen previously, with the same reaction time, a temperature of 120 ° C is not sufficient to obtain a crystalline product; this requires a temperature of 160 ° C

The pH influence in a very sharp particle morphology giving rise to elongated ellipsoidal particles and also in the case of needle-like particles obtained with titanium isopropoxide.

The titanium alkoxide slightly influence the size of the particles; fact particles obtained with isopropoxide have slightly smaller dimensions than the particles obtained with the butoxide.

The effect of ultrasound have insignificant influence on the size of the particles, but it allows to obtain discrete results of photocatalytic activity.

The particles obtained with this synthesis methodology are composed by a unique phase of crystalline titanium except that for the synthesis obtained at lower temperatures.; For all other synthesis, obtained at 160 ° C, it can be said that this condition is necessary so that it obtains the complete formation of anatase crystalline; conditions guarantees this is independent of the reaction time, then the parameter that has more effect on the synthesis is certainly to temperature. According to literature, it's can suppose that formation of anatase under hydrothermal conditions should be regarded as a consequence of sluggish reaction kinetics or metastable crystallization [118].

Furthermore, the tests showed that the particles are covered in superficie from residues of triethanolamine were adsorbed during synthesis; this effect was confirmed by the analysis especially FT-IR, but also the survey of TEM microscopy shows that particles with a surface irregular.

As evidence of this, the fact that the particles thus obtained have a low photocatalytic activity, while the particles thermally treated to remove the 'eventual triethanolamine adsorbed have a substantial photocatalytic building activity, confirming also in this case that the particles obtained with this type of synthesis are superficially coated with triethanolamine residues.

To obtain particles with a higher photocatalytic activity, has been developed a new type of synthesis without the use of triethanolamine.

3.2 – SYNTHESIS IN WATER

The synthesis obtained without the hydrothermal process has been developed as described before previously in the experimental part.

The particles obtained through this methodology have also been characterized and both from the point of view chemical-physical that from the point of photocatalytic activity with various tests.

3.2.1 – XRD Characterization

The synthesis obtained without the hydrothermal process has been developed as described before previously in the experimental part.

The particles obtained through this methodology have also been characterized and both from the point of view chemical-physical that from the point of photocatalytic activity with various tests.

XRD pattern shows that with this synthesis was obtained a material consisting of 2 phases; between anatase phase, in this synthesis is obtained a proportion of 3% of brookite (fig. 51).

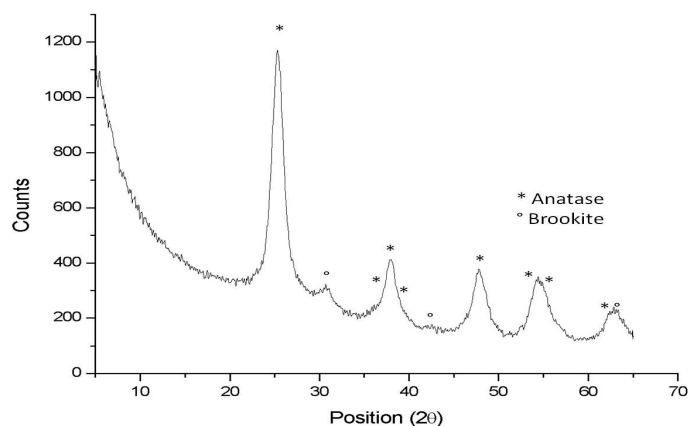


Figure 51 – XRD-pattern of TiO₂ nanoparticles

Anatase is formed because despite the mild reaction conditions, the synthesis involves the use of a temperature of 80 ° C. This temperature, such conditions not excessive, leading to the formation of anatase, which is a metastable phase, and being therefore such metastable conditions, inevitably lead to the formation of anatase. At this temperature and ambient pressure, it has also the formation of small amounts of brookite that is formed at low temperatures and pressures. Furthermore, in this synthesis was used isopropyl alcohol as a stabilizer, a molecule not very cumbersome and that may have affected the formation of a small amount of brookite.

3.2.2 – Morphological Characterization

TEM microscopy investigation (fig. 52) , shows that the particles obtained with this synthesis have a flat morphology and a size ranging from 5 to 10 nm. This could be due to the fact that the geometry of the synthesis, in which is added dropwise, an adduct of Ti-isopropoxide and isopropyl alcohol to a large volume of water under stirring. as the drops of the adduct are in contact with the water, immediately it has undergone a dispersion that does not allow the complete formation of the gel phase. So, there is the formation of particles of a very small size due it has an immediate dissolution of the polymer network of the alkoxide. Furthermore, we note that the particles once formed tend to aggregate together. This could depend on the fact that in this synthesis there is used a capping agent, or a large molecule cumbersome able to allow complete dispersion of the particles; in this synthesis was used isopropyl alcohol to stabilize the alkoxide, then the particles tend to aggregate with each other.

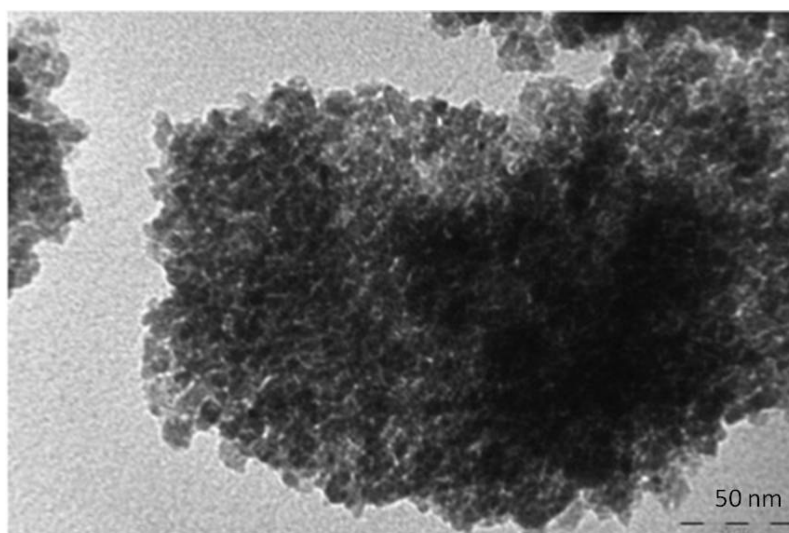
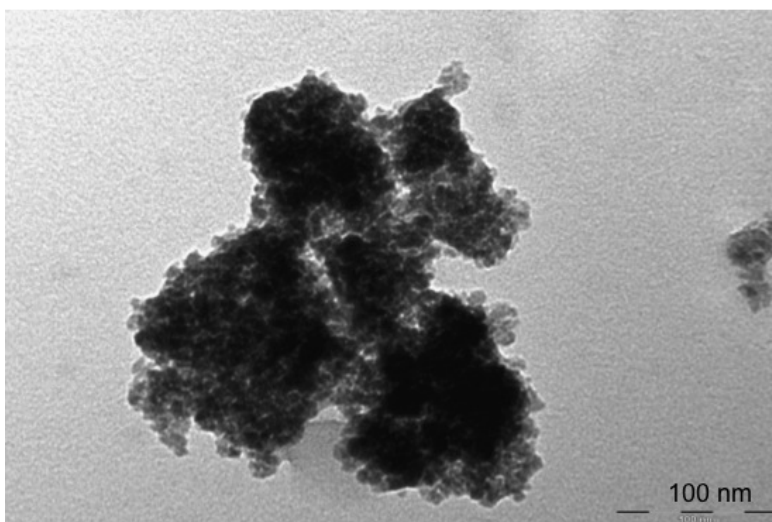


Figure 52 – TEM images of TiO₂ nanoparticles

3.2. 3 – Surface area

The measurement of the surface area calculated with the BET method, confirms what was seen both from DRX in which peaks are seen many widened, both TEM survey in which the particles are found to have a very small size, because the measure with effects at the BET detects a value of surface area of the particles of $214 \pm 20 \text{ m}^2 / \text{g}$. Although this finding correlated with the other analyzes was due to synthesis routes.

3.2.4 – FT-IR Characterization

FT-IR Spectra (fig. 53) shows a band between 2800-3600 cm^{-1} due to stretching of H_2O , the band at 1610 cm^{-1} due to stretching of water adsorbed, while the band between 450-900 cm^{-1} is attributable to anatase.

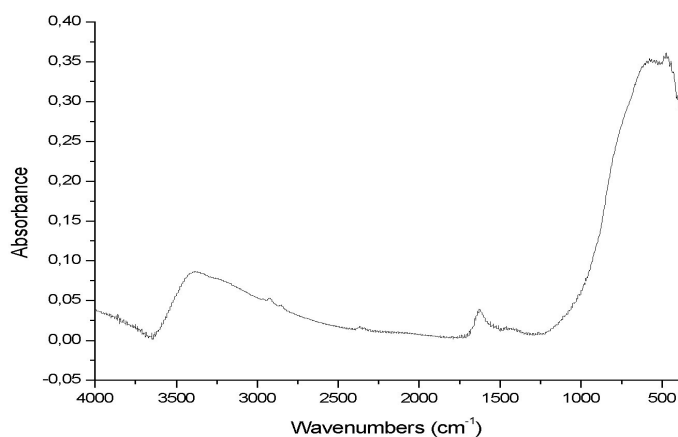


Figure 53 – FT-IR spectra of TiO_2 nanoparticles

3.2.5 - Photocatalytic test

3.2.5.1 – Degradation of methylene blue

As can be seen from the graph (fig. 54), the sample has a velocity photodegradation of the dye very high, because the sample degrades practically all dye already in the first 60 minutes, with a fast kinetics and constant, then gradually coming to a point of plateau to 120 minutes .

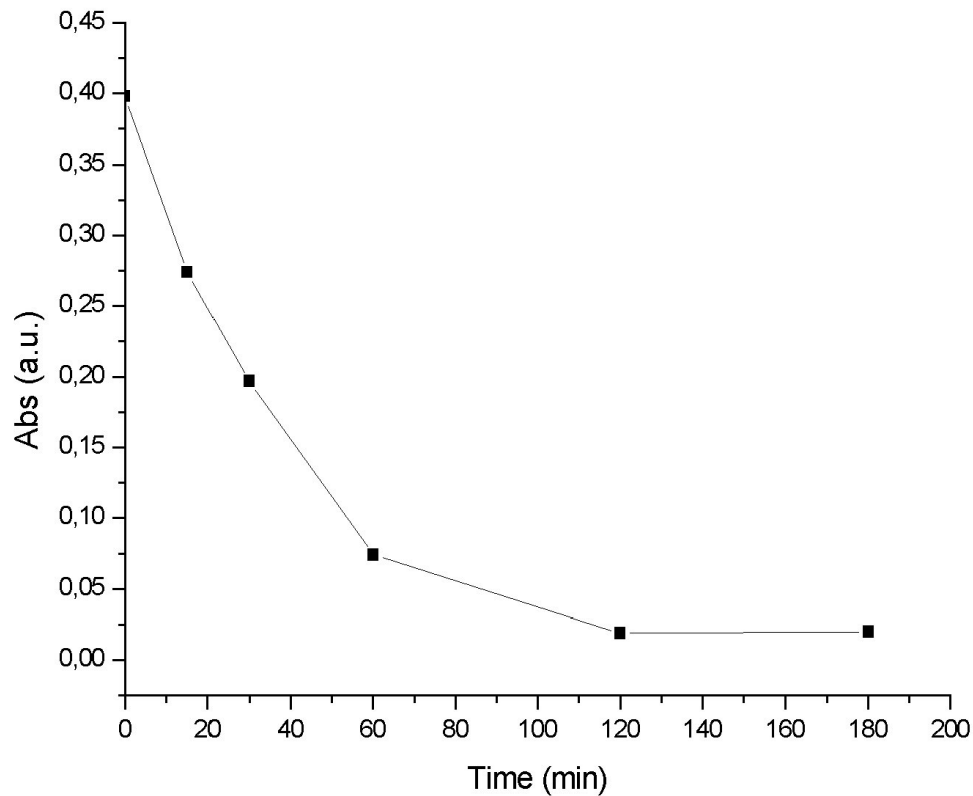


Figure 54 – Degradation of methylene blue test of TiO₂ nanoparticles

This could be due to the fact that the particles are small and have a surface area very high as is confirmed by BET analysis, and thereby high reactivity.

In addition the specimen consists of a small fraction of brookite, then it can be assumed that there is a heterogeneous junction between anatase and brookite having energy-gap values close enough (3.26 eV Brookite, 3.2 eV Anatase) as shown in the literature [119].

This effect together with the size and consequently high surface area, can explain the high photocatalytic activity of the sample obtained.

3.2.5.2 – Degradation of NOx

The data obtained from this analysis, confirm the data obtained with degradation of methylene blue test such as the increasing of activity of photocatalytic; infact also in this test, it sees a very high photocatalytic activity with a very rapid degradation in the first 60 minutes, and then arrive progressively a plateau within 180 minutes (fig. 55)

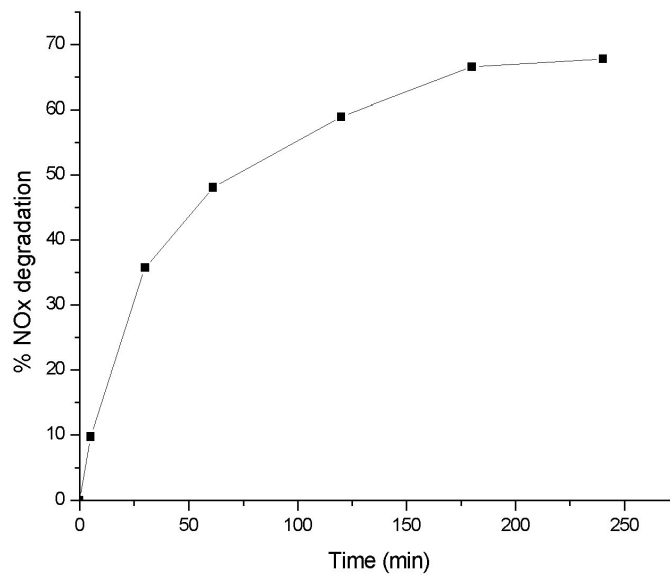


Figure 55 – Degradation of NOx test of TiO₂ nanoparticles

3.3 – SYNTHESIS OF HYDROXYAPATITE

3.3.1 – DRX Characterization

The analysis DRX (fig. 56) shows which is obtained a unique crystalline phase with reflections characteristic of hydroxyapatite (HA) and narrow peaks and well resolved index of high crystallinity

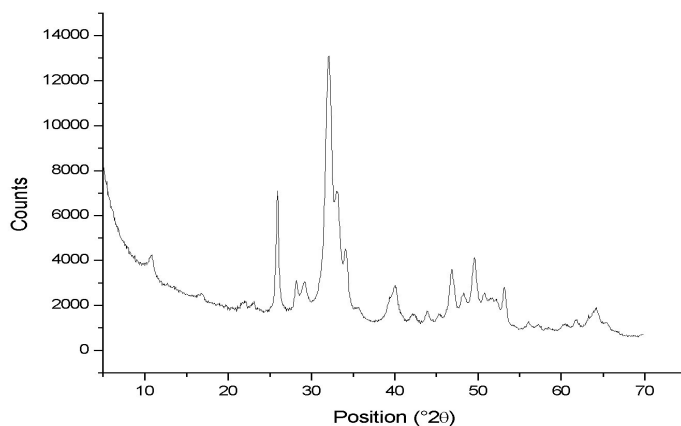


Figure 56 – XRD pattern of hydroxyapatite

3.3.2 – FT-IR Characterization

The FT-IR spectra (fig. 57), shows a band at 3458 cm^{-1} attributable hydroxyl OH, it probably adsorbed water, a band at 1610 cm^{-1} due also to water, a band at 1423 cm^{-1} due to the carbonates present in hydroxyapatite, a band at 1093 cm^{-1} due to the stretching of phosphate groups, a band at 1034 cm^{-1} attributable to symmetrical stretching of P-O phosphate group, and two peaks at 602 cm^{-1} and 563 cm^{-1} attributable to bending of the OH and O-P-O bonds.

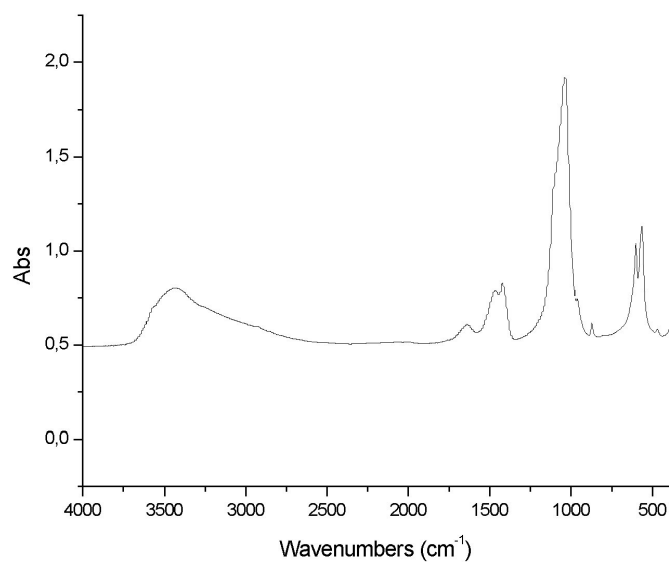


Figure 57 – FT-IR Spectra of Hydroxyapatite

3.3.3 – Morphological Characterization

Survey morphology, carried by SEM microscopy shows that a product obtained has micrometer-size comprised between 3 and 30 micrometers.

The product shows a very irregular surface as desired, a micrometric aggregate of hydroxyapatite crystals.(fig. 58)

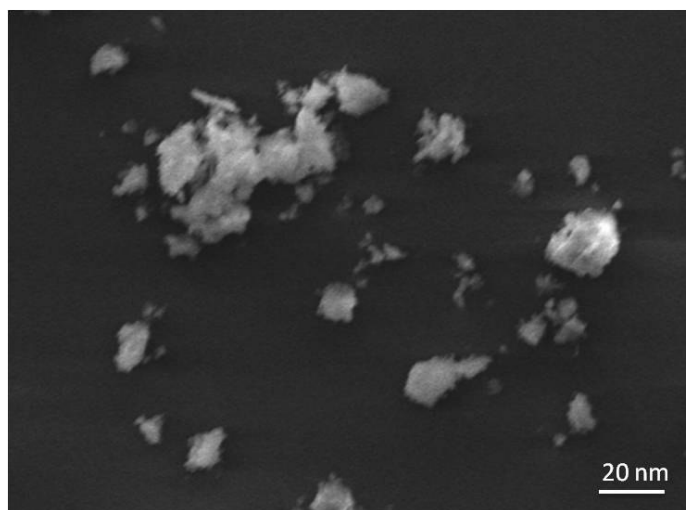


Figure 58 – SEM image of hydroxyapatite nanocrystals

3.6 – FUNCTIONALIZATION WITH HYDROXYAPATITE

3.6.1- XRD Characterization

X-ray diffraction pattern (fig. 59) shows characteristic reflection of both anatase that hydroxyapatite phases. Main peak of hydroxyapatite (002) covers main peak (100) of anatase.

It's also calculated crystal size values as previously described; this values varies from a value of 305 to 285 Å. Calculated on the 4 peaks, the average is 228 Å.

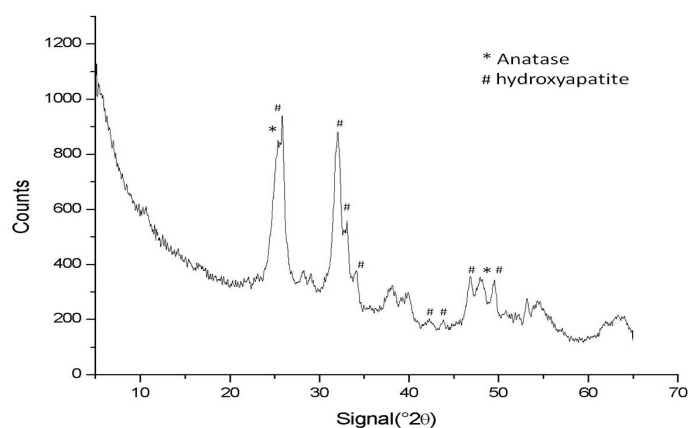


Figure 59 – XRD pattern of TiO₂-HA crystals

Comparing the two XDR patterns (fig. 60) in fact, is seen as anatase peak (100) position is perfectly comparable to the peak (002) of hydroxyapatite

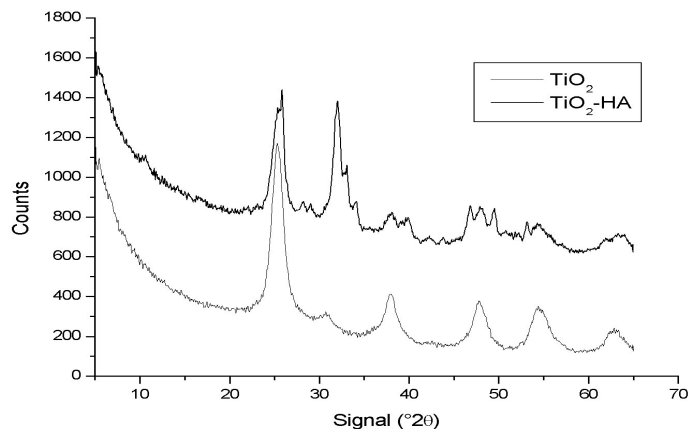


Figure 60 – XRD patterns comparison of TiO_2 -HA crystals and TiO_2 nanoparticles

3.6.2- FT-IR Characterization

FT-IR spectra (fig. 61), shows the characteristic peaks of hydroxyapatite and of anatase.

In fact are the visible band at 435 cm^{-1} characteristic of stretching $\nu\text{Ti-O-Ti}$, the band at 1639 cm^{-1} characteristic of apatite type B, the bands at 1093 and 1025 cm^{-1} relating to the stretching of the apatite phosphates and the bands at 602 and 565 cm^{-1} for the bending of the O-H bonds and O-P-O.

It also note two bands at 2906 , 2855 cm^{-1} attributable to the stretching motions of νCH_2 , CH_3 of isopropyl group present in isopropyl alcohol residue content in solution.

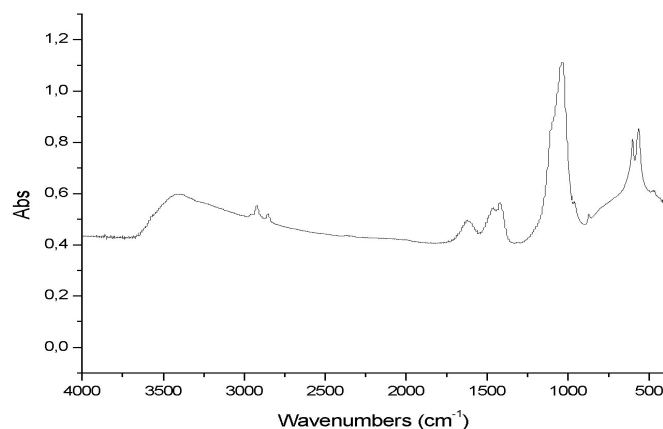


Figure 61 – FT-IR spectra of TiO₂-HA

3.6.3 – Surface Area

Analysis of surface area effected by BET detects a value of $118 \pm 20 \text{ m}^2 / \text{g}$; this value is well below the value obtained with only titanium dioxide, but higher than the value obtained from hydroxyapatite

The value is closer to hydroxyapatite; This could explain the assumptions made or that the particles are arranged on the surface of the microcrystals of hydroxyapatite; For the same weight, the exposed surface area is smaller; TiO₂ particles are arranged superficially to hydroxyapatite instead be free decreasing their surface area exposed.

3.6.4 – Morphologic Characterization

The morphological characterization was performed by SEM microscopy.

Crystals aggregates have all a size micrometer with a distribution that ranges from 3 to 30 mm, according to characteristic shape of hydroxyapatite aggregates as show in (fig. 62).

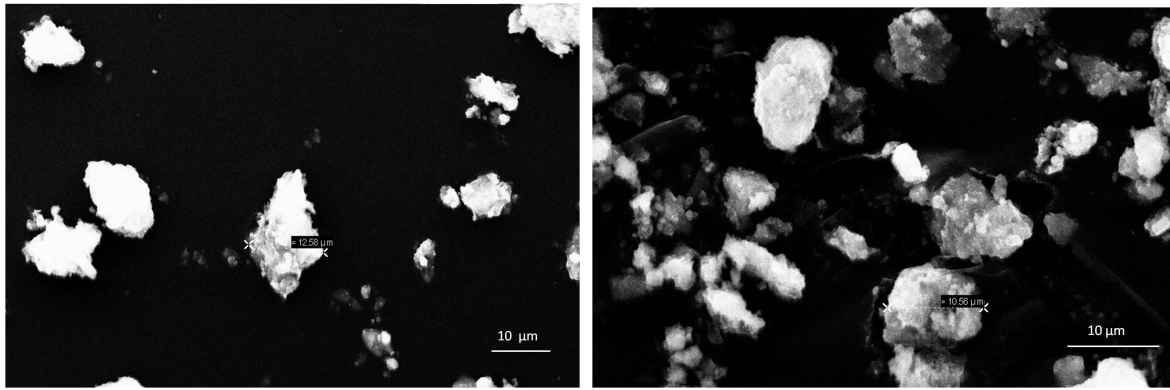


Figure 62 – SEM image of TiO₂-HA crystals

The analysis made by microscopy EDS, shows that crystals, in their elemental composition, consist of calcium, phosphorus and titanium; calcium and phosphorus are in a ratio of about 1.7 calculated on the intensity of the peak. This report is just typical of hydroxyapatite (fig, 63).

Signal of titanium, albeit with less intensity, indicates that on the surface these microcrystals is titanium; This confirms the hypothesis that the particles are arranged on the surface of titanium to hydroxyapatite microcrystals; this result, data signals this so intense, confirm hypothesis that crystals are formed from calcium and phosphorus inside and their quantity is much greater than that of titanium the weak signal which is derived from particles positioned on the surface.

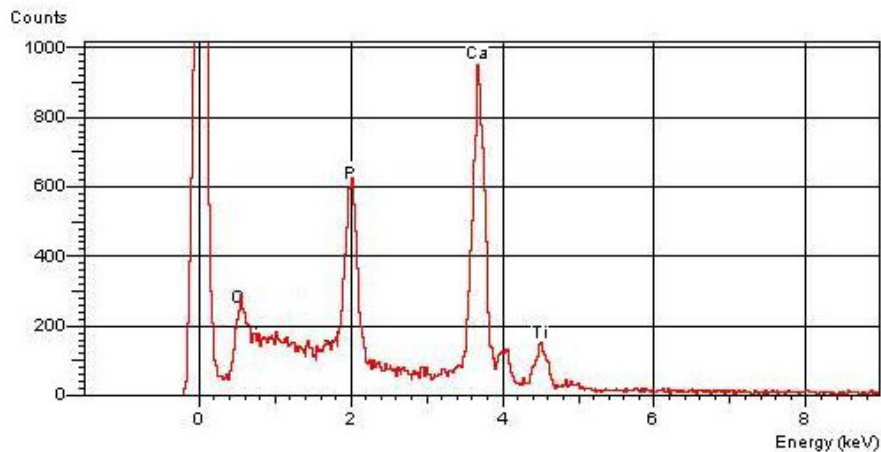


Figure 63 – EDS spectra of TiO₂-HA crystals

3.6.5 – Thermal Analysis

Thermogravimetric analysis (TGA) (fig. 64) reveals loss of weight in the zone comprised between room temperature and 200 ° C of 5.3% due to water absorbed, a loss of 3.7 between 200 and 400 ° C due to water of structure, a loss between 400 and 650 ° C due to the loss of carbonate of hydroxyapatite and an overall loss between 650 and 1000 due to dehydroxylation of hydroxyapatite

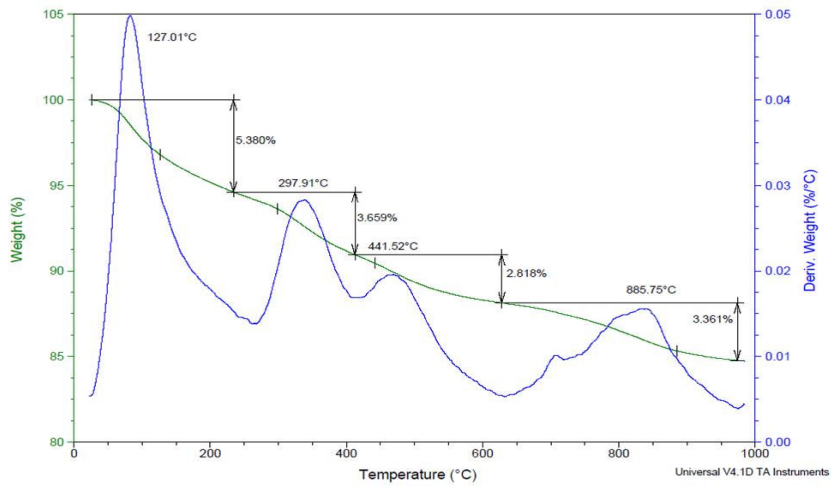


Figure 64 – TGA profile of TiO₂-HA crystals

Even in this case, it is confirmed the hypothesis of titanium dioxide nanoparticles on surface of hydroxyapatite crystals that are the preponderant part of the weight of the entire micro crystal composite.

In fact the weight losses are those characteristics of hydroxyapatite which consists precisely the greater part of the micro crystal.

3.6.3 Photocatalytic Test

3.6.3.1 – Degradation of Methylene Blue

Results of degradation of methylene blue tests (fig. 65), shows also for TiO_2 nanoparticles, a good photocatalytic activity of the product; the rate of degradation in fact, after initial stabilization time, increases steadily during the time; at the end of the test, after 180 minutes the reaction has not yet reached the point of plateau, coming to completely break down all the methylene blue.

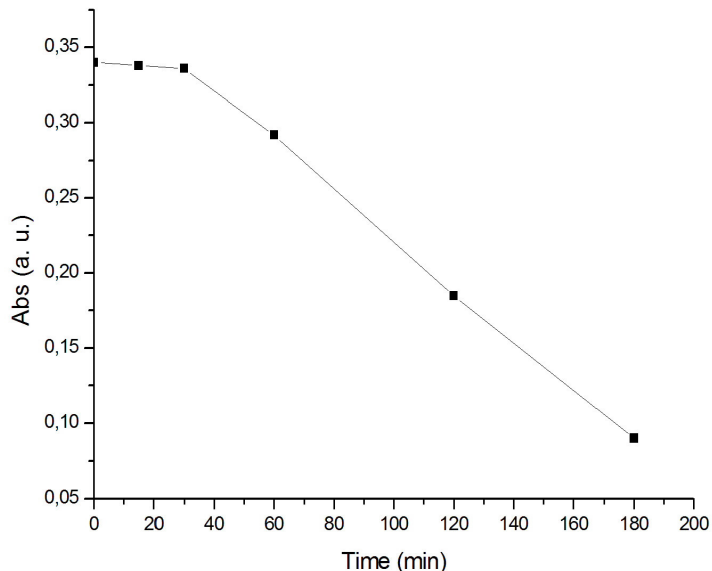


Figure 65 – Graphic of methylene blue degradation test for TiO_2 -HA

Comparing the photocatalytic activity of the obtained compound with that of previously synthesized nanoparticles of titanium (fig. 66), it is seen that activity of sun particles is higher than that of the compound TiO_2 -HA.

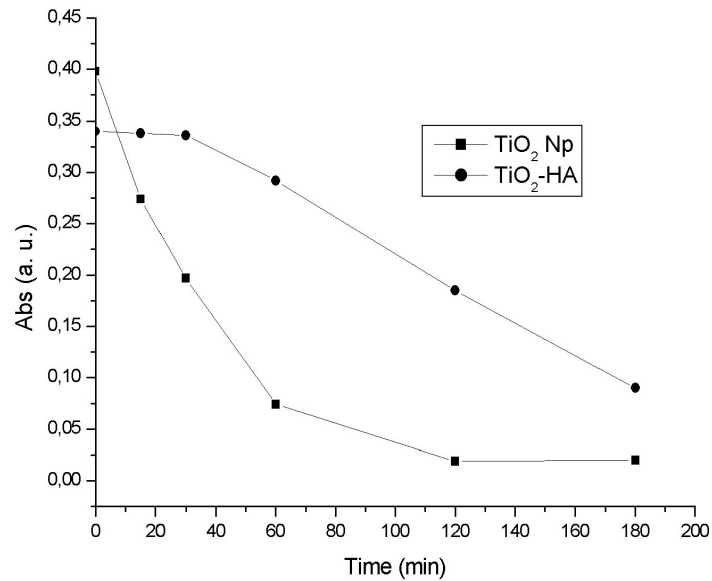


Figure 66 – Comparison between graphic of methylene blue degradation tests for TiO₂-HA and TiO₂ Np

Degradation process of dye by nanoparticles of TiO₂ is much faster initially than that of the microcrystals TiO₂-HA.

TiO₂ nanoparticles, come to plateau already after 120 minutes, while micrometric TiO₂-HA, after 180 minutes are still degrading the dye. Presumably at a long times also latter arrive to degrade completely around the dye.

This different behavior may be due to the fact that the dye molecules are adsorbed also on the possible fraction of the surface remained discovery of microcrystals of hydroxyapatite, slowing the degradation kinetics, which in fact is very slow at first.

Dye molecules then may initially bind instantaneously hydroxyapatite which presents charges in surface and therefore of the points in which the dye molecules may adsorb. subsequently these molecules are released gradually and then degraded by titanium dioxide nanoparticles that are located on the surface of microcrystals.

The kinetics of degradation constant after the first 30 minutes could be confirmed this hypothesis.

3.6.3.2 – Degradation of NOx

As showed from the graph (fig. 67), hydroxyapatite microcrystals functionalized surface with TiO₂, have an initial degradation kinetics of NOx against rising gradually, reaching up to slow down slightly in the vicinity of 180 minutes when it has already knocked down 80% of the NOx concentration; in the remaining 60 minutes of test duration, microcrystals arrive to degrade virtually all of the NOx reaching a value of degradation of 98%.

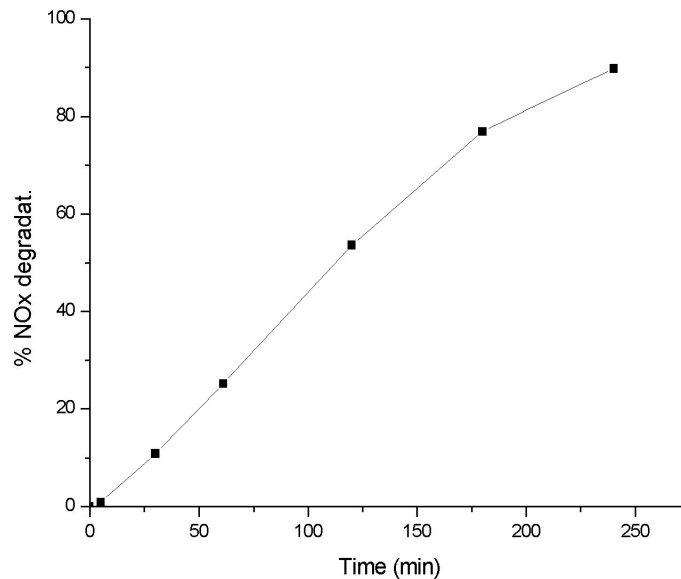


Figure 67 – Graphic of NOx degradation test for TiO₂-HA

Comparing these results with those obtained in the same test (fig. 68) with the nanoparticles of TiO₂, it have the confirmation of what has been seen with the test of degradation of methylene blue. In fact, also in this case, the kinetics are completely different initials reflecting what was seen in the test with methylene blue. Even titanium dioxide nanoparticles have a kinetic extremely fast in the first minutes and then reach a point of plateau already after only 100 minutes. Nanoparticles,

however, do not come to degrade the totality of the concentration of NO_x present reaching a value of 68%. This value can be considered the limit photocatalytic activity of the particles in their free form in respect of NO_x.

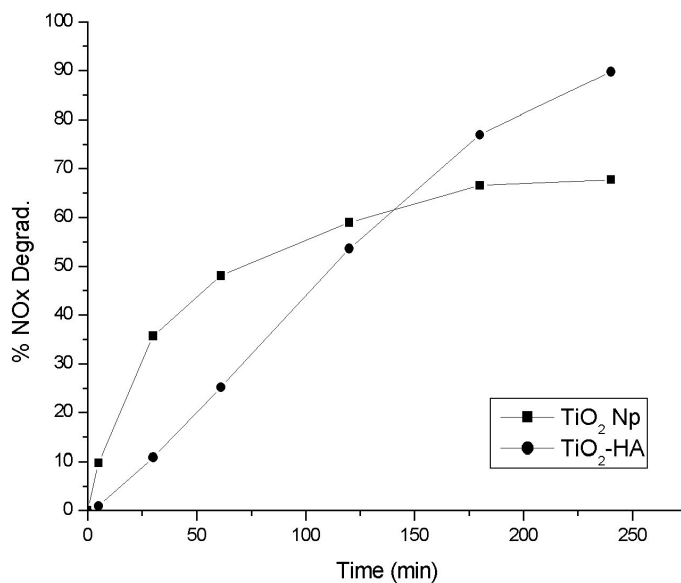


Figure 68 – Comparison between graphic of NO_x degradation tests for TiO₂-HA and TiO₂ Np

The microcrystals instead have a slower initially kinetic compared to nanoparticles confirming the hypothesis made for the tests of methylene blue, for which, some portion of surface hydroxyapatite could be remain free, where immediately adsorb molecules of NO_x, and gradually are released and thus free to be degraded by the nanoparticles of titanium dioxide that are located on the surface of the nanocrystals. In addition, the high % NO_x degraded, practically the totality, confirms the hypothesis initially made, and that has been the target of these research, that nanoparticles of titanium dioxide, being arranged on the surface of the microcrystals of hydroxyapatite may be in some so ranked on it by increasing the exposed surface of the nanoparticles themselves, thus increasing its reactivity.

3.6.3.3 -Antibacterial effect

Given that the product obtained, composed of microcrystals of hydroxyapatite superficially covered with nanoparticles titanium dioxide, has been the subject of interest for the development of products in the biomedical field has been done further tests to confirm the photocatalytic effect based on antibacterial effect.

The tests carried out by reference to E. Coli, show that for both types of tests carried out and described in the experimental section, there is a substantial reduction of this bacterial strain. (table 1 (a),(b))

SAMPLE	Bacteria : Escherichia coli			
	Initial Microbial concentration T ₀ (UFC/ml)	UVA 2h	Final Microbial Concentration (UFC/ml)	Reduction %
Water	1,2x10 ⁸		1,2x10 ⁸	-
TiO ₂ -HA (on plate) 4ml	1,2x10 ⁸		1,3x10 ⁷	89,17%
Ecoactive (in suspension) 4ml	1,2x10 ⁸		2,5x10 ⁶	97,9%

SAMPLE	Bacteria: Escherichia coli			
	Initial Microbial concentration T ₀ (UFC/ml)	UVA 3h	Final Microbial Concentration (UFC/ml)	Reduction %
Water	1,2x10 ⁸		1,2x10 ⁸	-
Ecoactive (on plate) 4ml	1,2x10 ⁸		1,7x10 ⁷	85,84%
Ecoactive (in suspension) 4ml	1,2x10 ⁸		2,5x10 ⁶	97,9%

Table 1 – Antibacterial tests results with 2 (a) and 3(b) hours UV light exposure

This results shows once again the high photocatalytic activity of hydroxyapatite micro-crystals coated of titanium dioxide. In fact, the only UV light has no effect on bacteria, while the micro-crystals have a high effect, almost reaching a total effect reduction of 97.9% in just 2 hours, because the same test was repeated at 2 and 3 hours of irradiation under UV lamp showing results almost identical, demonstrating that already after 2 hours it has the highest photocatalytic effect against bacteria.

3.6.4 – Biological and cellular tests

Given the importance of the crystals synthesized, which have gained great interest for biomedical applications, are also conducted of biological thesis to verify the antioxidant activity and the possible toxicity in comparison of cellular organisms

3.6.4.1 - Antioxidant Activity

Antioxidant test was previously described.

Test shows that TiO₂-HA has a high antioxidant activity. (tab. 2) (fig. 69)

	mmol trolox/100g dw
TiO ₂ -Np	0,028 ± 0,01
TiO ₂ -HA	0,540 ± 0,004

Table 2 – Results of antioxidant activity test for TiO₂ Np and TiO₂ -HA

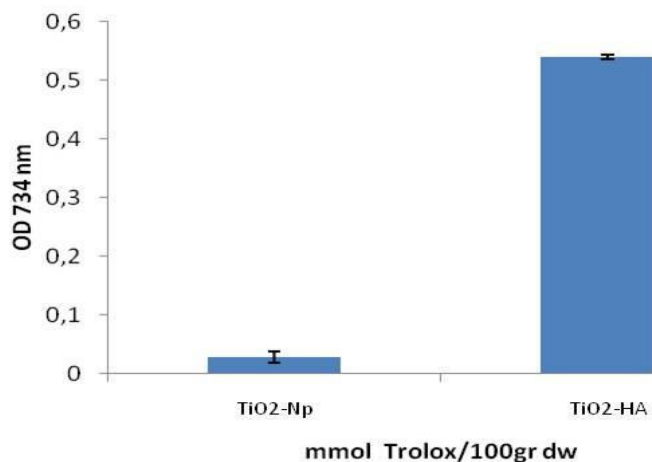


Figure 69 – Graphical Results of antioxidant activity test for TiO₂ Np and TiO₂ -HA

Microcrystals of TiO₂-HA have a good antioxidant activity (expressed in equivalents of Trolox, TEAC). This activity could be compared to that of carrot; little relevant is that instead of titanium dioxide nanoparticles. The assay was carried out using the method ABTS "quencher" which involves the measurement of the antioxidant activity directly on the matrix to be analyzed without extraction.

The antioxidant activity of TiO₂-HA can probably be attributed to the presence of Zn²⁺ cation present in Hydroxiapatite. In fact, the sample consists only of TiO₂ has antioxidant activity irrelevant.

3.6.4.2 - Toxic activity

The concentration used for carrying out tests for toxicity (300µg/ml) represents the MIC (minimum inhibitory concentration) obtained by the tests of antibacterial activity carried out on Gram + and Gram-(Staphylococcus aureus, Listeria monocytogenes, Salmonella enterica paratyphi B and Escherichia coli). The tests carried out on the samples analyzed it was shown that both TiO₂ and TiO₂-HA that are not hemolytic, show no cytotoxicity when exposed to the presence of human

cells. Cell viability is greater than 80% after 72h exposure (Tab.3); and finally the production of LDH is low for both samples analyzed with respect to LDH positive control provided by the kit (Figure 70). The data obtained demonstrate that TiO₂ and TiO₂- HA are non-toxic.

Time (h)	THP-1 (no treatment)	THP-1+TiO ₂ Np300µg/ml	THP-1 + TiO ₂ -HA 300µg/ml
24h	97%	90%	93%
48h	95%	85%	90%
72h	92%	81%	89%

Table 3 – Results of toxic activity test for TiO₂ Np and TiO₂ -HA

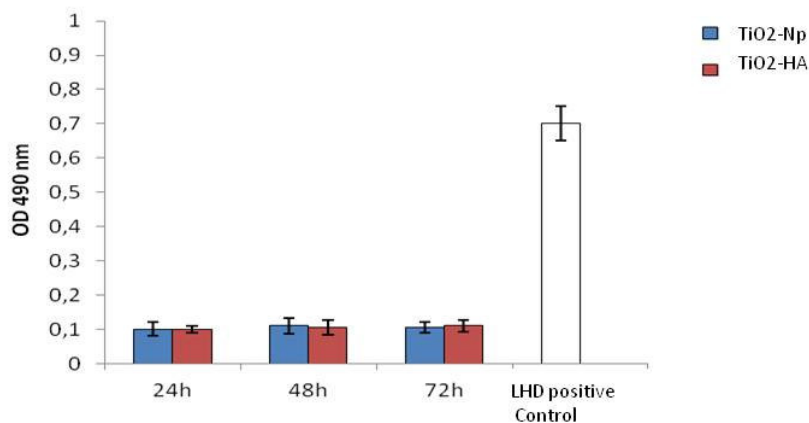


Figure 70 – Graphical Results of antioxidant activity test for TiO₂ Np and TiO₂ -HA

3.6.5 - Discussion

It's was synthesized titanium dioxide nanoparticles with a high photocatalytic activity due both to the high surface area, and to the fact that the product contains anatase phase and a small percentage of brookite and this could leads to a heterogenic conjunction. These two effects are derived from the particular type of synthesis obtained under mild conditions with temperatures of 80 °C, which promotes the formation of metastable phases such as anatase and brookite; also the fact to add an adduct titanium isopropoxide-isopropil alcool to a large volume of water leads to formation of very small particles, this indicates that in this process does not have a complete formation of gel phase, but the polycondensation takes place very quickly, forming very small particles as confirmed by the enlargement of the peaks found by DRX analysis and TEM analyzes, that shows also that nanoparticles tend to aggregate since they were not synthesized with add of an capping agent.

The FT-IR shows that the particles do not contain residues of any kind adsorbed on the surface and this is found in the high photocatalytic activity.

By reacting these particles with microcrystal aggregates of hydroxyapatite, it has a link with the nanoparticles of titanium dioxide as shown by the tests of chemical-physical characterization such as DRX, FT-IR; SEM with relative microanalysis, and the analysis of surface area show as such particles are disposed on surface of hydroxyapatite microcrystals. This is confirmed by the photocatalytic tests where it's encounter very different kinetics, showing that not all the surface of hydroxyapatite microcrystals is completely covered, but there may be small pieces of free surface, where the object of the molecule degradation can immediately adsorbed thanks hydroxyapatite which is not stoichiometric, and these molecules are then degraded by titanium dioxide nanoparticles on the surface that is assumed dispose themselves in such a way as to expose the most active surface and this explains the increase of photocatalytic activity compared to that of the free Titanium dioxide nanoparticles.

So, the particular mode of synthesis allows to obtain nanoparticles extremely efficient with a high surface area; the addition of hydroxyapatite, though drastically decreases

the value of surface area, increases the photocatalytic effect of the particles of titanium dioxide confirming that this last coordinate on the surface in an orderly and exposing their more reactive face. In fact the value of surface area of the nanoparticles decreases approximately half indicating that a planar face is engaged on the surface of the microcrystals of hydroxyapatite.

3.6.2 – Functionalization with oxidized resorcinol

3.6.2. 1. - XRD Characterization

XRD pattern (fig. 71) of the of titanium dioxide nanoparticles functionalized with oxidized resorcinol, shows how it is perfectly superimposable with that obtained from the only nanoparticles, then a XRD pattern where are visible reflections characteristic of anatase and brookite .

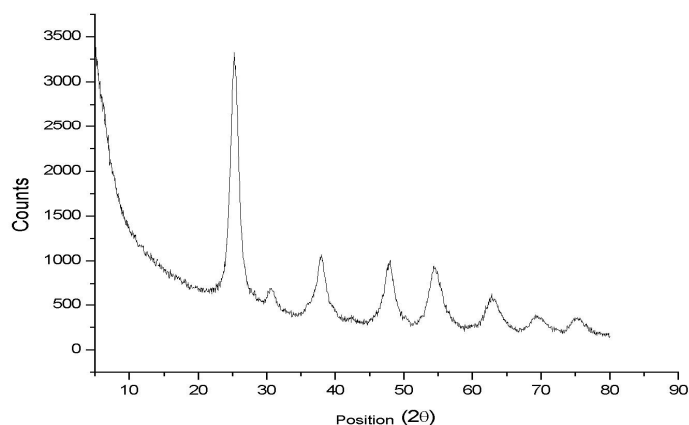


Figure 71 – XRD pattern of TiO_2 nanoparticles functionalized with oxidized resorcinol

Comparing the diffractograms obtained for nanoparticles of titanium dioxide and those coated with oxidized Resorcinol, there was no difference in the position and intensity of the peaks. (fig. 72)

Instead it's shows a shadow of the peaks XRD pattern of functionalized nanoparticles, It may probably be ascribed to the presence around the TiO₂ nanoparticles of a surface coating of Ti (IV) complexes of oxidized resorcinol.

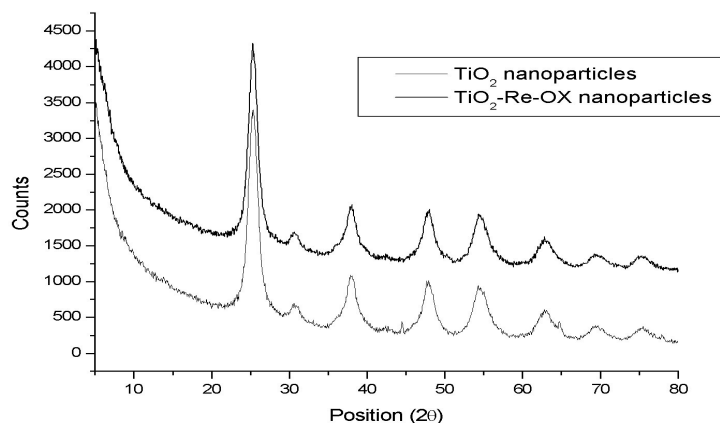


Figure 72 – Comparison of XRD patterns of TiO₂ nanoparticles functionalized with oxidized resorcinol and TiO₂ Np

3.6.2.2 - FT-IR Characterization

FT-IR analysis of TiO₂ nanoparticles (Fig. 73) shows absorption at 3600-2800 with maximum at 3450 cm⁻¹, arising from the superposition of the νOH mode of interacting hydroxyl groups and the symmetric and anti symmetric νOH modes of molecular water coordinated to Ti⁴⁺ cations. The band at 1633 cm⁻¹ is assigned to the molecular water binding mode. The absorption at 900-450 is ascribed to titanium dioxide.

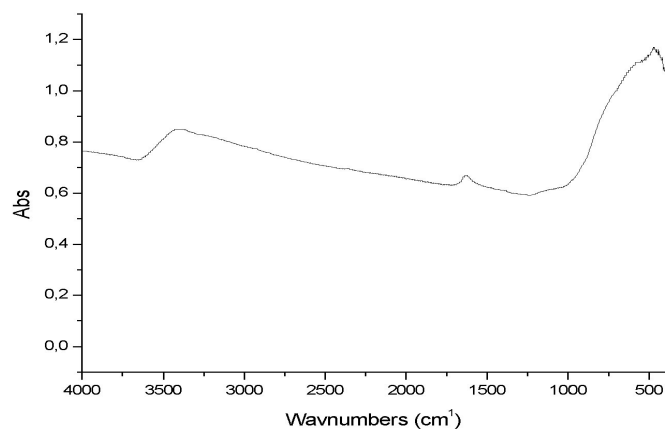


Figure 73 – FT-IR spectra of TiO_2 nanoparticles functionalized with oxidized resorcinol

Comparing FT-IR spectrum of TiO_2 nanoparticles surface complexed with oxidized resorcinol and FT-IR spectrum of TiO_2 nanoparticles before their surface complexation, (fig. 74) it's can't be observed appreciable differences between the spectra of TiO_2 nanoparticles and the spectra of TiO_2 nanoparticles surface complexed with oxidized resorcinol.

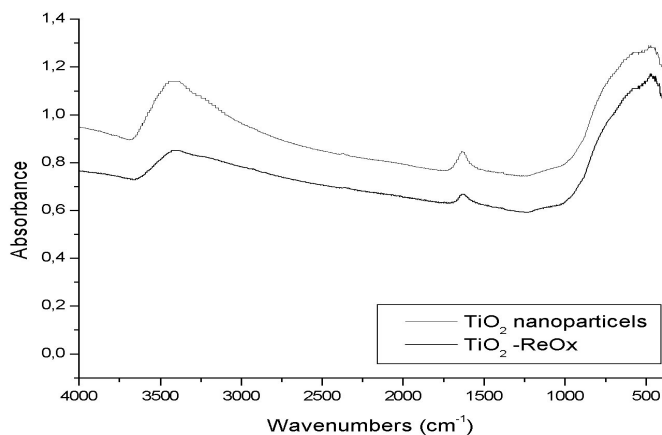


Figure 74 – Comparison of FT-IR spectra of TiO_2 nanoparticles functionalized with oxidized resorcinol and TiO_2 Np

3.6.3 – Morphologic characterization

TEM images of TiO₂ nanoparticles surface complexed with oxidized resorcinol (fig. 75) reveal the same morphology described previously for TiO₂ nanoparticles.

In fact, it's also observed nanoparticles having a dimension of 5-12 nm and a plate like morphology. Lamellar shaped nanoparticles tend to aggregate to form aggregates of 50-100 nm in dimension.

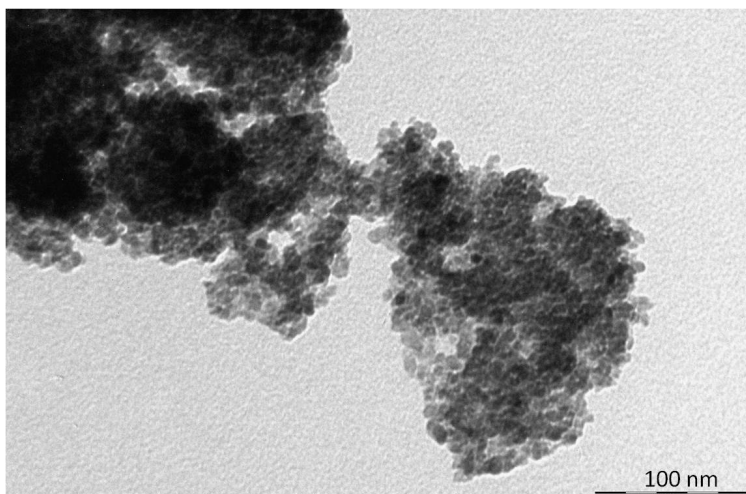


Figure 75 – TEM image of TiO₂ nanoparticles functionalized with oxidized resorcinol

3.6.4 – Thermal treatment

Then to highlight the possible presence of resorcinol due to the fact, however, the particles appear to have a chromatic variation, nanoparticles functionalized were thermally drawn at various temperatures (200, 300, 450 °C for 2 hours) in order to evaluate if this effect is able in some way to eliminate or modify the resorcinol oxidized.

It was made then previously a thermogravimetric analysis to see if the differences and understand the temperature at which the oxidized resorcinol undergo some changes.

3.6.4.1 – Thermogravimetric analysis

As can be seen from the comparison between TGA analysis (fig. 76) carried out on the nanoparticles of titanium dioxide and the analysis performed on nanoparticles functionalized, TiO₂ product has 2 points of weight loss: on at 58°C and on 306 °C probably due to loss of OH binded on Ti nanopartecles surface.

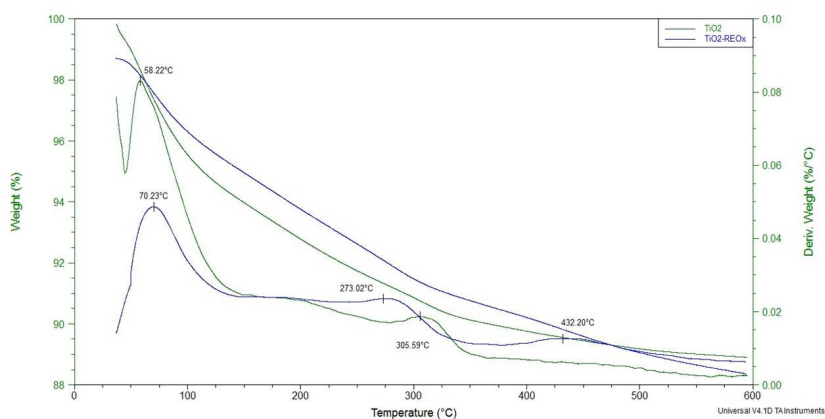


Figure 76 – TGA analysis of TiO₂ Np functionalized with oxidized resorcinol

Product TIO2-ReOX, has 3 points of weight loss:

Similar to TiO₂ product, when interate with Oxidate resorcinol the initial loss is shifted 70 °C; there are also a loss at 273 °C probably due to loss of OH binded on aromatic ring of surfacial oxidate Resorcinol, and a loss at 432 probably due to the loss of residual oxidate resorcinol.

3.6.4.2 –XRD Characterization

Comparison of the diffraction patterns obtained with the samples at different temperatures, it is not observed substantial variations in the crystalline phases, in fact all the samples have the same reflexes, nor in the intensity and in the peak width. (fig 77)

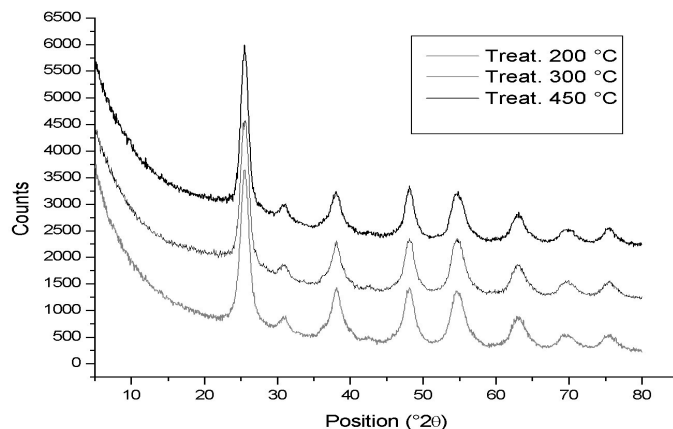


Figure77 – Comparison XRD patterns of Np treated at 200, 300,450 °C

3.6.4.3 - FT-IR Characterization

The comparison of FT-IR spectra (fig. 78) shows that with the increase of temperature, there is a decrease of the band around 3600-2800 with maximum at 3450 cm^{-1} , arising from the superposition of the νOH mode

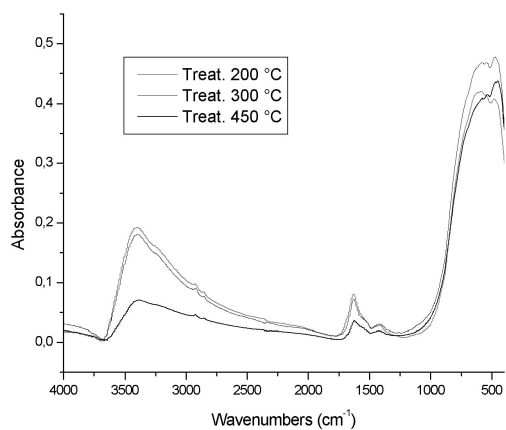


Figure 78 – Comparison XRD patterns of Np treated at 200, 300,450 °C

The FT-IR spectrum of TiO_2 nanoparticles complexed with oxidized resorcinol heated at 450 °C confirmed a degradation of resorcinol structure individuated in TGA

analysis; in fact, there is the decrease of the band with maximum at 550 cm^{-1} and the increase of band with maximum at 490 cm^{-1} ascribed to anatase.

3.6.5 - Photocatalytic Test

3.6.5.1 - Degradation of Methylene Blue

The photocatalytic tests, carried out on a restricted time in order to better evaluate the dye degradation in the first minutes, comparing the results obtained with the non-functionalized nanoparticles of TiO_2 , shows that the particles functionalized with the resorcinol superficially oxidized have a kinetic reaction such faster than the particles not functionalized.(fig 79)

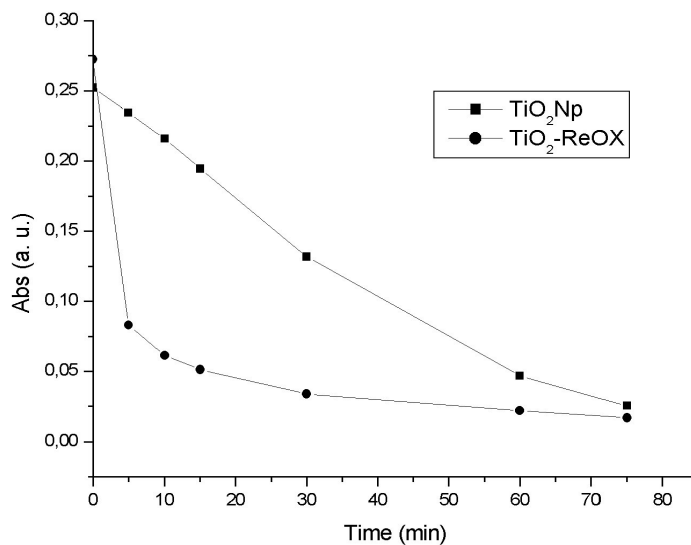


Figure 79 – Comparison of photocatalytic activity of TiO_2 Np functionalized with oxidized resorcinol an TiO_2 Np

TiO₂ nanoparticles are very efficient . In fact, it is possible to appreciate a very fast and regular kinetic of degradation along exposure time 75 min where the initial concentration of Methylene Blue is completely destroyed. TiO₂ nanoparticles surface complexes with oxidized resorcinol shows an higher photocatalytic activity; the kinetic of Methylene Blue degradation is very fast in the first 5 minutes, where it is degraded up to the 77% of methylene blue while in the following 70 min. this value increases up to 94% .

3.6.5.2 - NO_x degradation

NO_x degradation test (fig. 80) shows that TiO₂ nanoparticles are very efficient versus NO_x degradation. In fact, it is possible to appreciate a very fast kinetic of degradation during the first 30 min. where the NO_x degradation rises up to 47% and up to 56% in the following 30 min. This value increases only up to 68% during the following 2 h. NO_x degradation test carried out with TiO₂ nanoparticles surface complexes with oxidized resorcinol shows an higher photocatalytic activity; the kinetic of NO_x degradation is very fast in the first 60 minutes, where it is degraded up to the 92,7% of NO_x, while in the the following 30 min. this value increases up to 99% and remains constant for the following 60 min.

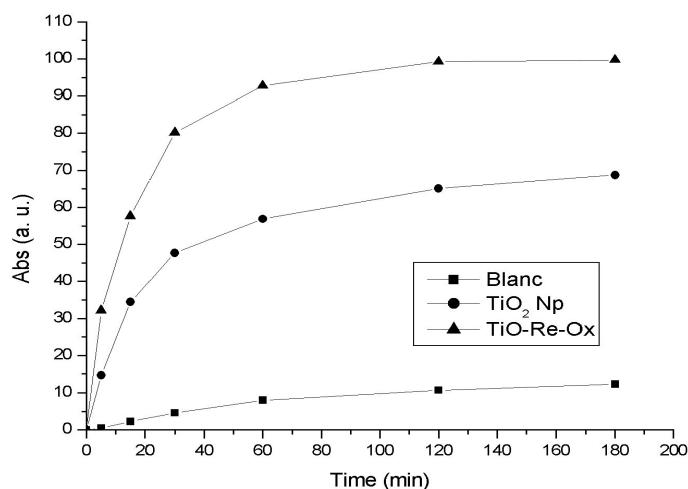


Figure 80 – Comparison of NO_x degradation tests of TiO₂ Np functionalized with oxidized resorcinol an TiO₂ Np

3. 6. 6– Discussion

The structural, morphological and spectroscopic characterization of TiO₂ nanoparticles surface complexed with oxidized resorcinol reveals not appreciably differences respect the TiO₂ characteristic. This finding can be explained assuming that the surface oxidized resorcinol coating is too thin to be evidenced by DRX, TEM and FT-IR. However its presence is consistent with an evident chromatic effect exhibited by the TiO₂ nanoparticles surface complexed with oxidized resorcinol, which appear ochre coloured. The TiO₂ nanoparticles appear ochre coloured only after a thermal treatment at 110 °C changing its previous purple red colour. The heat treatment produces a water desorption in the aqueous purple red surface coating containing oxidized resorcinol TiO₂ nanoparticles allowing the formation of a Ti⁴⁺ oxidized resorcinol coordination complex ochre coloured. The presence of weakly adsorbed water on the TiO₂ nanoparticles has been previously widely demonstrated. [120].

Thermal treatment at 450 °C remove resorvinol as shows bay FT- IR and XRD.

The results of the photocatalytic tests show that the TiO₂ nanoparticles surface complexed with oxidized resorcinol have an high photocatalytic efficiency. Their photocatalytic activity results 30% more reactive than pure TiO₂ nanoparticles revealing the important role exhibited by the resorcinol oxidized form bounded directly to Ti⁴⁺ chemically available after the water desorption from the TiO₂ particles surface.

Probably the increase of photocatalitic effect is due to the fact that aromatic ring attack ·OH; when oxidized resorcinol is linked at ·OH radicals, can react directly with photogenerated holes and O₂^{·-} radicals, being the later ones a less relevant process [121, 122]. Consequently, resorcinol and m-cresol substituents can generate three doubly activating positions [123].

Oxidized resorcinol coating has to be imagined as a surface continuous polymeric net linked to Ti⁴⁺ on the TiO₂ nanoparticles surface forming a hybrid organic-inorganic coordination complex by Ti (IV) (fig. 81)

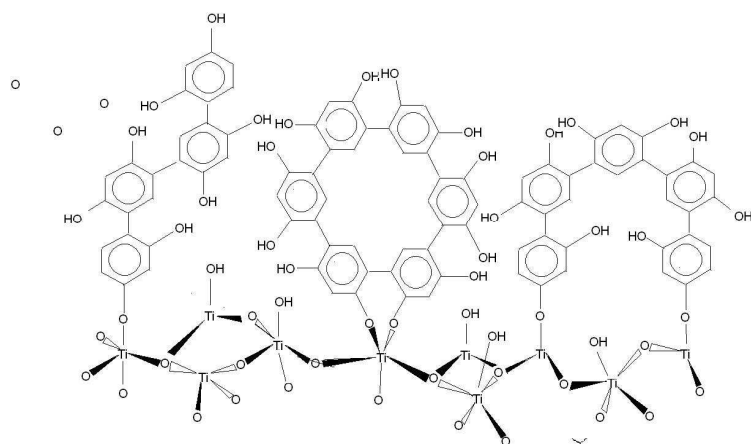


Figure 81– Hypothesis of TiO₂ – oxidized resorcinol cluster

3.7- SYNTHESIS WATERLESS

3.7.1 - DRX- Characterization

TiO₂ in the anatase crystalline form has been synthesized by a waterless synthetic method by an hydroxylation of Ti(IV)- tetrabutoxide(TiTB) with water molecules generated “in situ” by an esterification between formic acid (FA) and octanol (Oc). Changing opportunely the FA/Oc molar ratio it is possible obtain anatase with different chemical-physical properties.

XRD pattern of samples obtained decreasing the FA/O molar ratio from: a) 2.5, b) 1.25, c) 0.80, d) 0.4 up to e) 0.17 (fig. 81) while the TiTB concentration has been maintained constant (10 mmols) during all the different synthesis. XRD patterns do not show any rutile or brookite diffraction maxima, but only the diffraction maxima of anatase which results present in the sensitized powder as the single pure phase. As it can be deduced by the comparison of XRD patterns reported in Fig.1 the anatase sample decrease in crystallinity decreasing the FA/Oc molar ratio utilized during the synthesis.

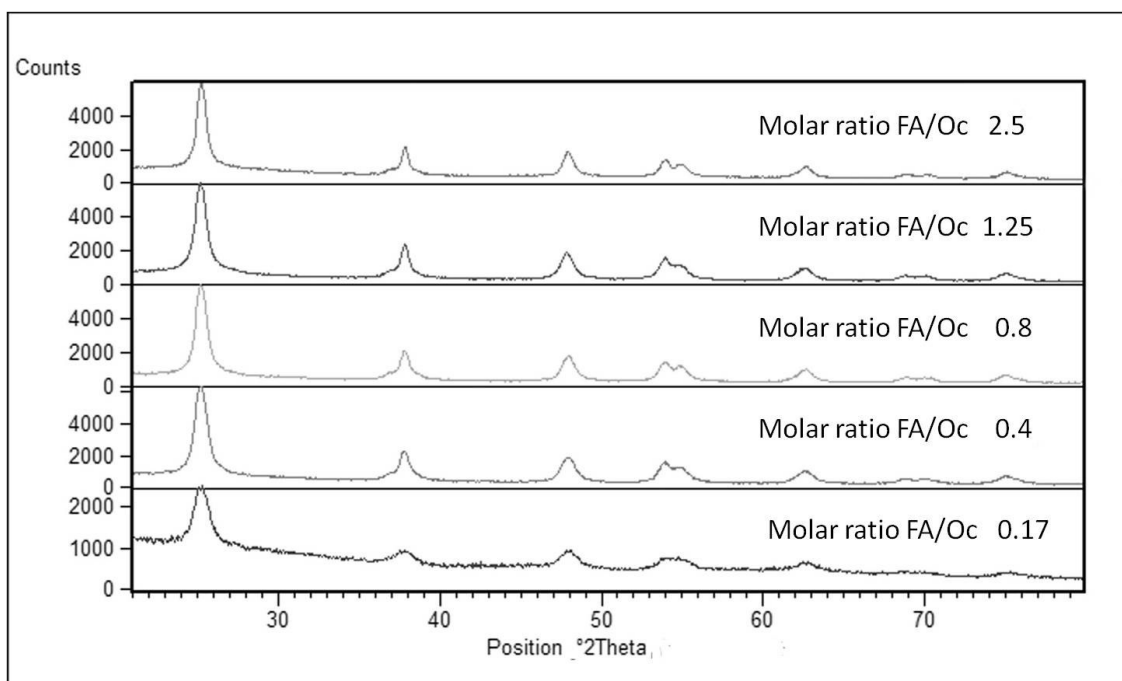


Figure 81 – XRD patterns of nanoparticle obtained with different molar ratio FA/Oc

XRD patterns (fig. 82) of the products obtained by the same synthetic method maintaining constant the amount of TiTB, but without the utilization of Oc and without the utilization of FA, shows that obtained products prevalently amorphous do not show the anatase diffraction maxima revealing that the utilized synthetic method to prepare crystalline anatase needs the water molecules formation “in situ” by the esterification between formic acid and octanol.

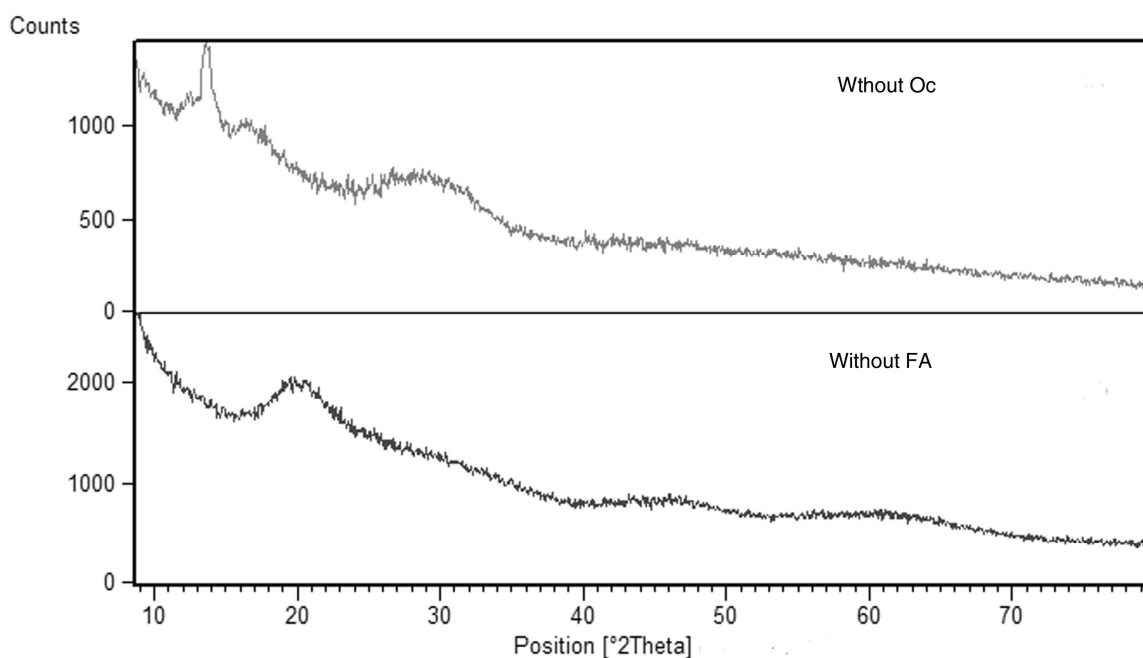


Figure 82 – XRD patterns of product obtained without FA and without Oc

The most intense (101) peak of the anatase at 2 theta 25.2° can be observed in all the X-ray diffraction patterns reported in fig. 88 revealing a preferential development of (101) planes in the anatase structure. Using Scherrer’s formula, the crystallites size along (101) orientation has been evaluated in samples synthesized with a decrescent FC/O molar ratio obtaining respectively the following values:18.4, 19.7, 27.7, 20.7 and 7.1 nm as reported in Tab.3.

Molar ratio FA/Oc	Crystal size d (101) nm
2.50	18.4
1.25	19.7
0.80	27.7
0.40	20.7
0.17	7.8

Table 3 – Cristal size of sample obtained with different molar ratio FA/Oc

3.7.2 -FT-IR Characterization

In fig. 83 comparison of FTIR analysis of samples at different molar ratio of FA/Oc : a) 2.5, b) 1.25, c) 0.80, d) 0.4, e) 0.17, f) synthesis in absence of FA and g) synthesis in absence of O .

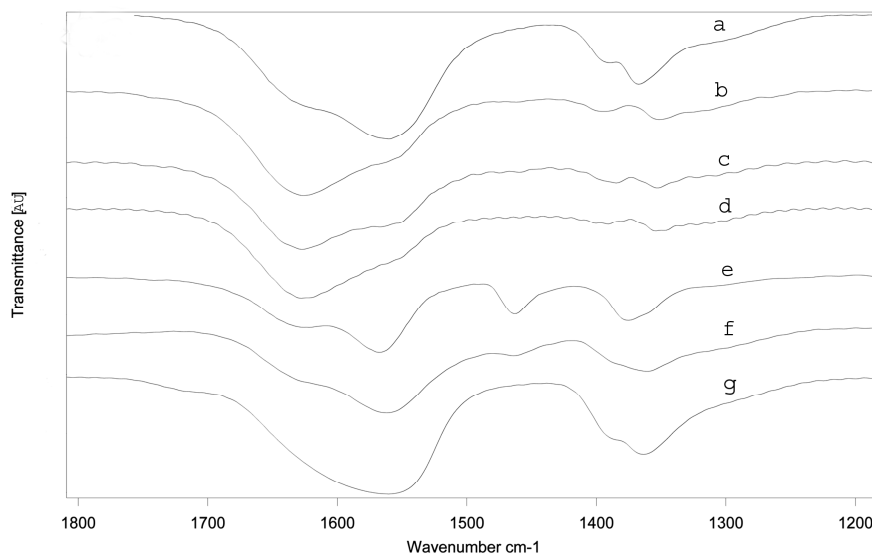


Fig 83 – Comparison of FT-IR spectra of sample obtained with different molar ratio FA/Oc

In the range $1615-1625\text{ cm}^{-1}$ the absorptions band are ascribed to O—H bending vibrational modes, while the asymmetric carboxylate and symmetric carboxylate stretching are ascribed in the ranges $1560-1564\text{ cm}^{-1}$ and $1349-1395\text{ cm}^{-1}$

respectively. Absorptions ascribed to carboxylate antisymmetric stretching and H₂O bending vibrational modes in absence of octanol (fig. 83 g) appear completely fused giving rise to an intense band with a transmittance minimum at 1560 cm⁻¹. This band has also a shoulder on the left side at about 1720 cm⁻¹ ascribed to formic acid bonded to the complex.

3.7.3 - Morphologic Characterization

Morphology characterization was performed by TEM microscope on samples with molar ratio FA/Oc a) 2.5 b) 0.8 c) 0.4 d) 0.17 (fig. 84) The anatase crystals show nanosized dimensions very close to their main crystal size estimated by the XRD line broadening revealing that these crystals are prevalently constituted of a single crystal domain. The morphology of all the anatase nanocrystals is planar revealing the highest development of a family of planes which may be identified as the (101) considering the highest relative intensity of the 101 anatase X-Ray diffraction maximum.

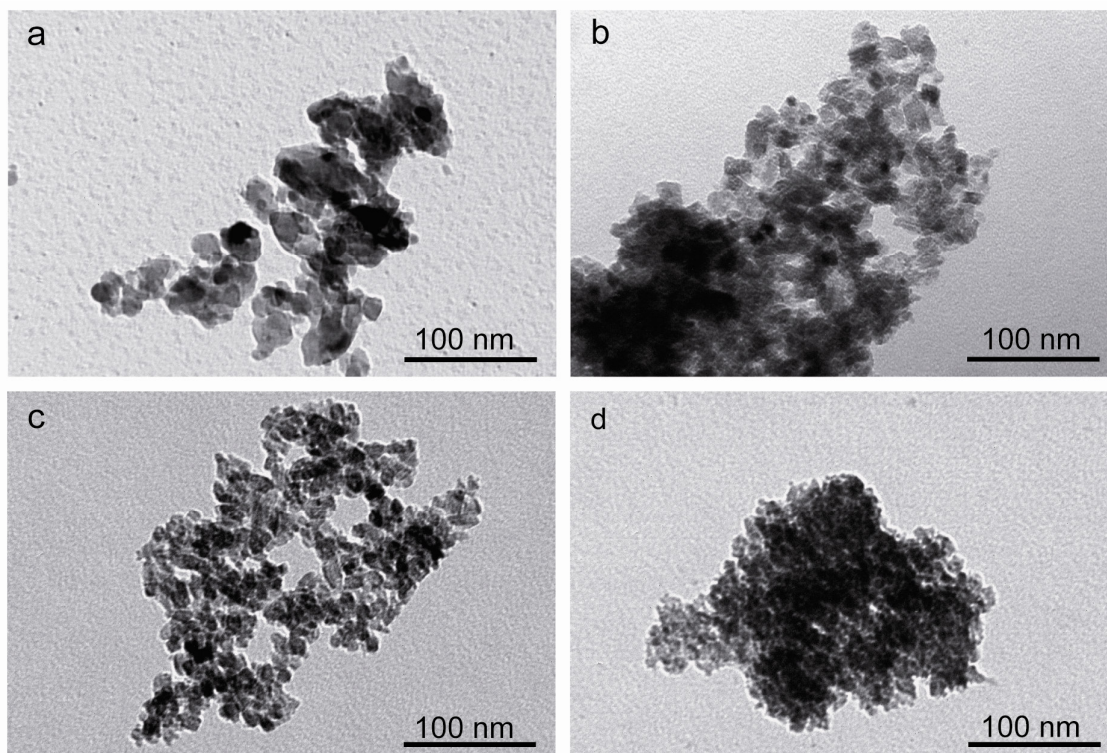


Figure 91 – TEM image of nanoparticles obtained with different molar ratio FA/Oc a) 2.5 b) 0.8 c) 0.4 d) 0.17

3.7.4 – Surface Area

The surface area of the different samples of anatase synthesized using different FA/O molar ratio has been determined by BET and the results reported in Tab 4. The surface area of the anatase samples synthesized using a FC/Oc molar ratio ranging from 2.5 up to 0.4 appears very large and about four times larger than the surface area of the usual commercial products. In all syntheses we observe the formation of plate-like shaped nanoparticles with dimensions according to the crystal size value that decreases with the decrease of the molar ratio.

Molar ratio FA/O	BET measured (m ² /g)
2.50	219
1.25	172
0.80	208
0.40	211
0.17	62

Table 4 – Surface area nanoparticles obtained with different molar ratio FA/Oc

3.7.5 - Photocatalitical test

3.7.5.1 - Degradation of Methylene Blue

photodegradation methylene blue tests did not give significant results; infact for each sample was observed a sinusoidal curve showing increase and decrease of the concentration of methylene blue.

This suggests that on the surface of nanoparticles occur phenomena of adsorption and desorption, but not of degradation.

This could be due to the fact that the surface of the particles there are any residues that can lead to this effect, and this fact is confirmed by FT-IR in which it is seen that for each samples are present residues and formiate anions of alcoxide together with TiO-OH groups.

3.7.6. – Thermal treatment

As in the case of the hydrothermal synthesis, to confirm if there were actually residues of synthesis adsorbed on the surface of particles as hypothesized, we proceeded with a heat treatment at 450 ° C in order to see the effect that these residues have on the properties photocatalytic particles

3.7.6.1.– XRD Characterization

X-ray pattern of nanoparticles treated thermally (fig. 85) shows a spectrum with a single crystalline phase with the characteristic peaks of anatase. Peaks are very narrow and intense index of high crystallinity degree .

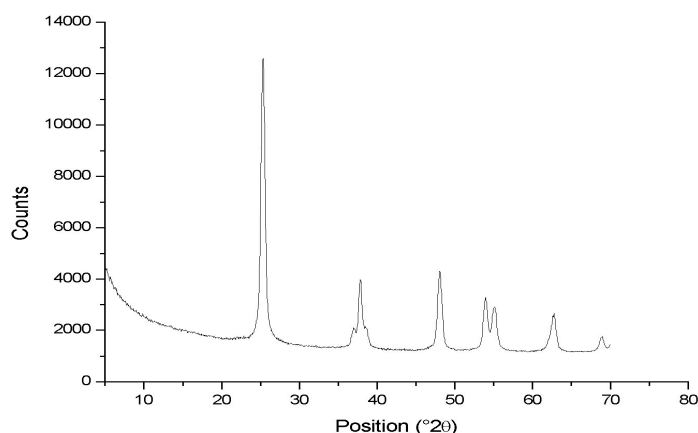


Figure 85 – XRD pattern of functionalized Np thermally treated

Comparing the spectrum obtained with thoe of nanoparticles not heat treated (fig 86) it is observed that the spectra are perfectly superimposable, indicating that treatment had no influence on the crystalline phase.

Heat treated nanoparticles have peaks pier more intense and well defined respect to particles untreated presenting peaks broadened and poorly defined. This confirms what hypothesized, namely that nanoparticles synthesized are covered by a layer of carboxyl residues, while the particles untreated, are devoid of these residues, giving notes very defined peaks.

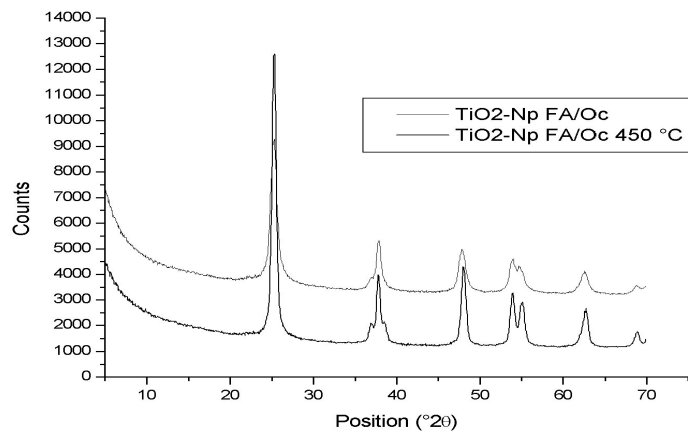


Figure 86 –Comparison XRD patterns of functionalized Np thermally treated and untreated

3.7.6.2 – FT-IR Characterization

Even the FT-IR analysis confirms the assumed and already demonstrated with the analysis DRX. Comparing the spectra of the particles in fact treated thermally with the spectrum of untreated ones, we see how the heat treatment has removed any residual adsorbed on the surface of the nanoparticles. (fig. 87)

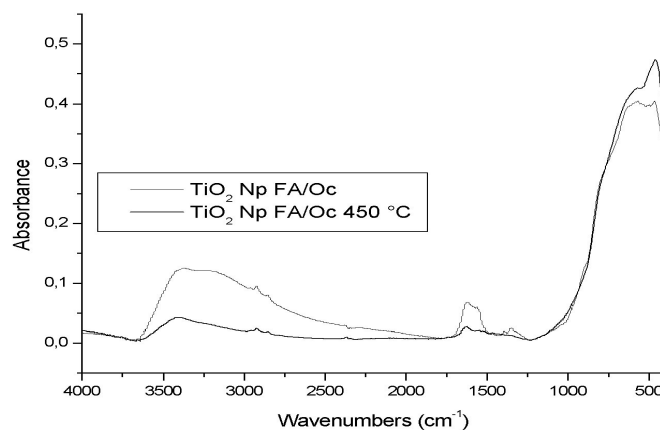


Figure 87 –Comparison FT-IR spectra of functionalized Np thermally treated and untreated

Even the FT-IR analysis confirms the assumed and already demonstrated with the analysis DRX.

Comparing the spectra of the particles in fact treated thermally with the spectrum of untreated ones, we see how the heat treatment has removed any residual adsorbed on the surface of the nanoparticles.

In the spectrum of particles heat treating, there are no characteristics bands of asymmetric and symmetric stretching of the carboxylates that are in the ranges $1560-1564\text{ cm}^{-1}$ and $1349-1395\text{ cm}^{-1}$ respectively.

Moreover, in the spectrum of the heat-treated particles is the most intense band with a peak at 470 cm^{-1} attributable to anatase.

This shows how the heat treatment has completely removed the residual carboxylic superficially adsorbed to the nanoparticles. This then confirms that this type of synthesis produces nanoparticles covered on the surface by carboxyl residues.

3.7.7.1-Photocatalytic Test

3.7.7.1.1- Degradation of Methylene blue

We also made photocatalytic test to find further confirmation

Comparing the test results obtained with the particles treated and those untreated, is seen as particles untreated give a phenomenon of adsorption and desorption of molecules of methylene blue as previously described (fig. 88).

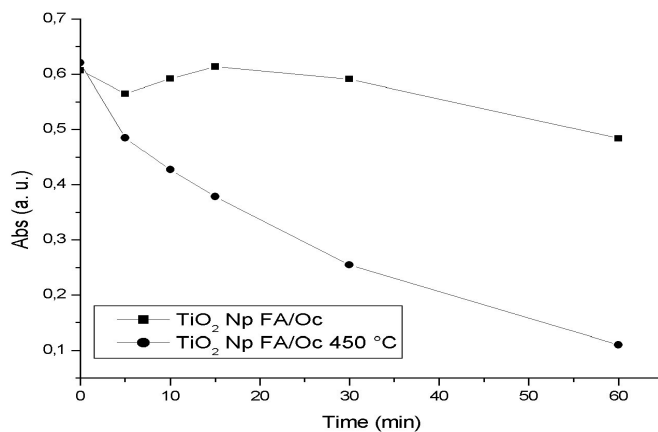


Figure 88 – Comparison of degradation test of methylene blue of Np treated and no treated

This fact is assumed to be due to the carboxylic residues present on the surface of nanoparticles as confirmed by XRD and FT-IR of the particles dealt with in a thermally, which adsorb and release the molecules without degrade them.

However this effect is not observed for the treated particles that show a good photocatalytic activity with a curve of photodegradation profile similar to the particles of titanium dioxide obtained by the synthesis in water.

This once again confirms that the type of synthesis without water, produces particles that are functionalized with surfacial carboxylic residues.

3.7.8 - Discussion

A waterless synthetic method by an hydroxylation of Ti(IV)-isopropoxide with water molecules generated “in situ” by an esterification between formic acid and 1-Octanol has been performed to prepare as unique phase, TiO₂ nano crystals with tailored chemical-physical properties such as planar morphology, high surface area, crystallinity and photocatalytic activity which can be modulated as a function of the degree of carbosilation present on the surface. Anatase crystals have a grain size observed by TEM ranging from 5 nm to 20 nm practically equal to their crystalline domains, which have been estimated from the broadening of the (101) diffraction line.

FTIR analysis performed on the samples allows us to determine how the surface of anatase nanocrystals are functionalized by carboxylic group from FA.

As octanol fraction increases, bands of progressively decreasing intensity begin to separate.

Resolved and weaker absorptions appear in the spectra relative to c and e (fig 90). These absorptions have almost the same intensities. Band at 1622 cm⁻¹ is more intense than that at 1563 cm⁻¹ in spectrum of c, while the reverse is observed for e.

Referring to Fig. 83, a strong absorption due to symmetric carboxylate stretching at 1362 cm^{-1} with a shoulder at 1385 cm^{-1} is present in the spectrum relative to e (absence of octanol). Two weak and well resolved bands of almost the same intensity appear in the spectra of b (1393 cm^{-1} , 1349 cm^{-1}) and d (1395 cm^{-1} , 1352 cm^{-1}) while only one weak band at 1376 cm^{-1} is present in that of E along with another one at 1462 cm^{-1} , probably due to scissoring vibrational mode of the C—H bonds.

FTIR spectra also shows that residual formate and alcoxo anions are present on the nanocrystal surface of all samples along with Ti—O—H titanol groups. This means that only the nanocrystal core is made of pure crystalline anatase while Ti(IV) alcoxo and hydroxo formates and titanolates. Ti—O—H form a coating on the nanoparticle surface.

In fact, in test of methylene blue (BM) degradation (data not showed) an initial and rapid decrease was observed followed by an increase to the initial levels in solution absorbance. A direct interaction BM-anatase is consequently prevented and only a rapid physical adsorption of the BM molecules on the above said layer occurs followed by a slower desorption.

This reversible reaction can be attributed to the nature of the nanoparticles surface.

Thermal treatment at $450\text{ }^{\circ}\text{C}$ confirm that surface of nanoparticles is coated by carboxylic residuals.

Changing opportunely the FA/O molar ratio it is possible to obtain anatase with tailored chemical-physical properties such as planar morphology, high surface area, crystallinity which can be modulated as a function of the carboxylation degree present on the surface.

CHAPTER 4 - CONCLUSIONS

Years of researches led to the understanding of the mechanism of synthesis of titanium dioxide nanoparticles, the influence of synthesis parameters on chemical - physical properties and how these influence photocatalytic properties of the nanoparticles .

The study followed different synthesis methods.

A type of hydrothermal synthesis, from which titanium dioxide anatase phase nanoparticles are obtained directly, has been developed; the synthesis was studied by changing parameters and conditions. The results show that only temperature is a limit to obtain anatase nanoparticles, while other parameters, such as titanium alkoxide, pH, reaction time, effect of ultrasound do not modify the crystalline phase. At temperatures than lower 120 °C, the synthesis remains in the gel phase and the subsequent heat treatment leads to the formation of rutile, given the different kinetics reactions.

Titanium alkoxide and ultrasound have effect on the nanoparticle size, while pH has an influence on the morphology making elongated particles; this is due primarily to the fact that all the syntheses involve the use of a stabilizing agent which is the triethanolamine. This molecule remains on the particles' surface after the synthesis inhibiting photocatalytic activity, which otherwise would be high as shown by the tests obtained with particles thermally treated in which triethanolamine has been completely removed.

Given these results the strategy has been changed and a new synthesis in very mild conditions in water has been developed to obtain anatase nanoparticles with high photocatalytic activity, and to avoid the use of triethanolamine or other stabilizing

agents, using instead only isopropyl alcohol which is a product of hydrolysis reaction between titanium alkoxide and water.

The conditions of this synthesis permit the formation of the desired product, with high photocatalytic activity; these conditions are important to obtain a crystalline phase consisting of anatase, which is a metastable phase and a small brookite percentage. Geometry and condition of the synthesis also allow to obtain a particle size of about 5 nm with a high surface area. These two factors may explain the high activity of the photocatalytic particles, because the brookite formed could lead to an effect of hetero-junction with anatase, while high surface area allows the high reactivity.

This type of synthesis is free of any residue and it has been subject of interest for biomedical applications, but there is yet a problem of size and toxicity, for which it was decided to make micrometer-sized particles which, however, retained a high photocatalytic activity.

To achieve this purpose, we proceeded with the study and realization of an innovative material composed of an inorganic micrometric core on the surface of which titanium dioxide nanoparticles obtained with the synthetic methods described above are arranged.

As inorganic core, biomimetic Zn-substituted hydroxyapatite micrometric aggregates studied in our research group were used; from the experience I had with my previous thesis work, these crystals were studied as drug-delivery devices capable to bind drug molecules on the surface and amplify the effect as shown by the results obtained and published. [98]

Microcrystals consisting of hydroxyapatite were deposited on the surface covered by titanium dioxide nanoparticles. This was demonstrated by physico-chemical characterization in particular XRD analysis and EDS microanalysis made with probe.

The values of surface area obtained from BET analysis confirm this hypothesis.

The results obtained from photocatalytic tests have shown how these product have a higher photocatalytic activity than particles themselves; in both tests carried out, it

was demonstrated that TiO₂-HA microcrystals have a slower degradation kinetics at short times compared to nanoparticles. This is probably due to immediate adsorption of molecules on possibly hydroxyapatite microcrystals surface remained uncovered so that these molecules can be degraded by titanium dioxide nanoparticles on microcrystals' surface; longer in timing TiO₂-HA microcrystals arrive at much higher degradation values, thus achieving the purpose of this work and confirming the choice of microcrystals of hydroxyapatite which, as seen with the drug molecules, have the same effect with nanoparticles.

The innovativeness of the product obtained has allowed patenting for these crystals of TiO₂-HA [124] and consecutively also patented biomedical application of these microcrystals was made, [125] from which two products were produced and are already on the market.

Ti-HA microcrystals also were tested from the antioxidant and cytotoxic activity point of view, and it is seen that they have a strong antioxidant activity in dark conditions and practically no toxicity.

In order to increase the performance of titanium nanoparticles obtained by synthesis in water, these have been functionalized with a molecule, resorcinol, but it was decided to use its oxidized form not to have problems of molecule degradation.

An ochre color on the particles appeared which is obtained only after they have been treated at 110 °C indicating that water is necessary for the molecules desorption from the nanoparticles surface to adhere to the molecule, a process that would otherwise not occur .

Characterization techniques such as XRD, FT-IR not detect these molecules, indicating that probably a very thin layer was created, thus not detectable; there is a chromatic evidence confirming that heat treatment, above all, by the evidence of photodegradation in which higher performances are found compared to the untreated particles, thus realizing the purpose of this search.

Finally we have studied a new waterless synthesis process with an "in situ" esterification which allows to obtain nanoparticles consisting of anatase single phase

coated with a layer of carboxyl residues capable of binding molecules. Were studied various syntheses by changing molar ratio formic acid / octanol. It is seen that in absence of one of two reagents there is no formation of anatase nanoparticles.

Changing molar fraction, we obtain particles with different surface area and size, and different residues on surface; it is possible to synthesize particles of tailor-made properties, by modulating molar fraction of synthesis reagents then, adsorption mode of molecules.

To confirm that the particles are coated with a carboxyl residues layer, a thermal treatment of one of synthesis was carried out. Tests have shown that the heat treatment removes the coating of nanoparticles confirming that they are actually coated.

Such particles can be synthesized and to be functionalized in order to adsorb a wide range of different molecules to be used in various fields especially in technological application

Resuming, in these years a synthesis method has been developed for obtaining innovative photocatalytic crystals both for biomedical use, as has already occurred with use of synthesized TiO_2 -HA microcrystals in products for bleaching treatment of dental care, and for uses in technology field especially in energetic application with possibility to obtain materials with high photocatalytic efficiency and that they can absorb a broader spectrum of radiation in order to activate the photocatalytic process.

REFERENCES

- [1] A. Mills, H.R. Davies, D. Worsley, *Chem. Soc. Rev.* 22 (1993) 417.
- [2] P.-C. Maness, S. Smolinski, W.A. Jacoby, *Appl. Environ. Microbiol.* 65 (1999) 4094.
- [3] Y. Paz, Z. Luo, L. Rabenberg, A. Heller, *J. Mater. Res.* 10 (1995) 2842.
- [4] I. Poullos, P. Spathis, P. Tsoumparis, *J. Environ. Sci. Health* 34 (1999) 1455.
- [5] R. Cai, K. Hashimoto, K. Itoh, Y. Kubota, A. Fujishima, *Bull. Chem. Soc. Jpn.* 64 (1991) 1268.
- [6] A. Fujishima, R. Cai, K. Hashimoto, H. Sakai, Y. Kubota, *Trace Met. Environ.* 3 (1993) 193.
- [7] H. Sakai, R. Baba, K. Hashimoto, Y. Kubota, A. Fujishima, *Chem. Lett.* (1995) 185.
- [8] O. Legrini, E. Oliveros, A.M. Braun, *Chem. Rev.* 93 (1993) 671.
- [9] D. Bahnemann, J. Cunningham, M. A. Fox, E. Pelizzetti, P. Pichat, N. Serpone, Photocatalytic treatment of waters, in: G. Helz, R. Zepp, D. Crosby (Eds.), *Aquatic and Surface Photochemistry*, CRC Press, 1994, 261pp.
- [10] D.Y. Goswami, Engineering of the solar photocatalytic detoxification and disinfection processes, in: K.W. Boer (Ed.), *Advances in Solar Energy*, vol. 10, American Solar Energy Society, Boulder, CO, 1995, 165 pp.
- [11] A. Heller, *Acc. Chem. Res.* 28 (1995) 503.
- [12] M. Hoffman, S. Martin, W. Choi, D. Bahnemann, *Chem. Rev.* 95 (1995) 69.
- [13] G. Sheveglieri (Ed.), *Gas Sensors*, Kluwer Academic Publishers, Dordrecht, 1992.
- [14] P.K. Dutta, A. Ginwalla, B. Hogg, B.R. Patton, B. Chwieroth, Z. Liang, P. Gouma, M. Mills, S. Akbar, *J. Phys. Chem.* 103 (1999) 4412.
- [15] Y. Xu, K. Yao, X. Zhou, Q. Cao, *Sens. Actuators B* 13±14 (1993) 492.
- [16] Kronos International, 1996.
- [17] L.G. Phillips, D.M. Barbano, *J. Dairy Sci.* 80(1997)2726.
- [18] J. Hewitt, *Cosmet. Toiletries* 114 (1999) 59.
- [19] Mickael Gratzel *Inorg. Chem.* 2005, 44, 6841-6851
- [20] Jamieson JC, Olinger B. *Am Min* 1969;54:1447.
- [21] Norman N. Greenwood, A. Earnshaw, *Chemistry of the Elements*, first ed., Pergamon, Oxford, 1984, pp. 1117–1119.
- [22] A. Vittadini, A. Selloni, F.P. Rotzinger, M. Gratzel, *Phys. Rev. Lett.* 81 (1998)
- [23] M. Lazzeri, A. Vittadini, A. Selloni, *Phys. Rev. B* 63 (2001) 155409/1.

- [24] M. Lazzeri, A. Vittadini, A. Selloni, *Phys. Rev. B* 65 (2002) 119901/1.
- [25] R. Hengerer, B. Bolliger, M. Erbudak, M. Gratzel, *Surf. Sci.* 460 (2000) 162.
- [26] J. Woning, R.A. van Santen, *Chem. Phys. Lett.* 101 (1983) 541.
- [27] A. L. Linsebigler, G. Lu, J. T. Yates Jr., *Chem. Rev.*, 95, (1995), 735.
- [28] Gerischer, H. In *Photocatalytic Ollis*, D. F., Al-Ekabi, H., Eds., Elsevier: Amsterdam, (1993).
- [29] Fujishima A, Hashimoto K, Watanabe T. *Fundamentals and applications*, 1st ed. Tokyo: BKC; (1999).
- [30] Mardare D, Tasca M, Delibas M, Rusu GI. *Appl Surf Sci* 156, (2000), 200.
- [31] Halley JW, Kozlowski M, Michalewicz M, Smyrl W, Tit N. *Surf Sci* 226, (1991), 397.
- [32] Radecka M, Zakrewska K, Czternastek H, Stapinski T, Debrus S. *Appl Surf Sci* 1993;65/66:227.
- [33] Madhusudan Reddy K, Gopal Reddy CV, Manorana SV. *J Solid State Chem* 158, (2001), 180.
- [34] Kumar PM, Badrinarayanan S, Sastry M. *Thin Solid Films* 358, (2000), 122.
- [35] Bard J. *Science* 201, (1980), 139.
- [36] Matthews, R. W. *J. Catal.* 113, (1988), 549.
- [37] Mahdavi F, Burton TC, Li Y. *J Org Chem*, 58, (1993), 744.
- [38] Li Y. In: Kamat PV, Meisel D, editors. *Semiconductor nanocluster*. Amsterdam: Elsevier; (1993) [Stud Surf Sci Catal 103].
- [39] Ferry JL, Glaze WH. *Langmuir* 14, (1998), 3551.
- [40] Pichat P. *Catal Today*, 19, (1994), 313.
- [41] Hermann JM. *Catal Today* 53, (1999), 115.
- [42] Vuilliet E, Emmelin C, Chovelon JM, Guillard C, Hermann. *Appl Catal B: Environ* 38, (2002), 127.
- [43] Maurino V, Minero C, Pelizzetti E, Vincenti M. *Colloids Surf A: Physicochem Eng Aspects* 151, (1999), 329.
- [44] Hermann JM, Guillard C, Disdier J, Lehaut C, Malato S, Blanco J. *Appl Catal B: Environ* 35, (2002), 281.
- [45] Balcioglu A, Getoff N, Bekbolet M. *J Photochem Photobiol A: Chem* 135, (2000), 229.
- [46] Tanaka K, Robledo SM, Hisanaga T, Ali R, Ramei Z, Bakar WA. *J Mol Catal A: Chem*, 144, (1999), 425.
- [47] Tanaka K, Reddy KSN. *Appl Catal B: Environ*, 39, (2002), 305.
- [48] Hermann JM, Tahiri H, Guillard C, Pichat P. *Catal Today*, 54, (1999), 131.
- [49] Hisanaga T, Harada K, Tanaka K. *J Photochem Photobiol A: Chem*, 56, (1990), 113.

- [50] Ohtani B, Ueda Y, Nishimoto S, Kagiya T, Hschisuka H. *J Chem Soc Perkin Trans, 2*, (1990), 1955.
- [51] Konstantinou IK, Sakkas VA, Albanis TA. *Appl Catal B: Environ*, 34, (2001) 227.
- [52] Tahiri H, Ait-Ichou Y, Hermann JM. *J Photochem Photobiol A: Chem* 114, (1998), 219.
- [53] Maillard C, Guillard C, Pichat P. *New J Chem*, 18, (1994), 941.
- [54] Low GKC, Mc Evoy SR, Matthews RW. *Environ Sci Technol*, 25, (1991), 460.
- [55] Bianco Prevot A, Vincenti M, Banciotto A, Pramauro E. *Appl Catal B: Environ*, 22, (1999),149.
- [56] Sakkas VA, Albanis TA. *Appl Catal B: Environ*, 46, (2003),175.
- [57] Pramauro E, Vincenti M, Augugliaro V, Palmisano L. *Environ Sci Technol*, 27, (1993),1790.
- [58] Kerzhentsev M, Giullard C, Pichat JP, Hermann JM. *Catal Today*, 27, (1996), 215.
- [59] Konstantinou IK, Sakellarides TM, Albanis TA. *Environ Sci Technol*, 35, (2001), 398.
- [60] Hermann M, Matos J, Disdier J, Guillard C, Laoine J, Malato S, et al. *Catal, Today* 54, (1999), 255.
- [61] Turchi CS, Ollis DF. *J Catal*, 122, (1990), 178.
- [62] Para S, Olivero J, Pulgarin C. *Appl Catal B: Environ*, 36, (2002), 75–85.
- [63] Minero C, Catozzo F, Pelizzetti E. *Langmuir*, 8, (1992), 481.
- [64].Q. Liu, S.W. Tao, Y.S. Shen *Sens. Actuators B*, 40 (1997), pp. 161–16.
- [65] A.M. Taurino, M. Epifani, T. Toccoli, S. Iannotta, P. Siciliano *Thin Solid Films*, 436 (2003), pp. 52–63.
- [66] Y. Nakatani, M. Matsuoka, *Jpn. J. Appl. Phys.*, 21 (1982), pp. 1758–1762.
- [67] S. Xue, W. Ousi-Benommar, R.A. Lessard, *Thin Solid Films*, 250 (1994), pp. 194–201.
- [68] Y. Liu, W. Zhu, O.K. Tan, Y. Shen, *Mater. Sci. Eng. B*, 47 (1997), pp. 171–176.
- [69] C.C. Chai, J. Peng, B.P. Yan, *J. Electron. Mater.*, 24 (1995), pp. 799–804.
- [70] F. Edelman et al. *Inst. Electron Technol.*, 33 (2000), pp. 89–107-
- [71] M. Ferroni et al., *Sens. Actuators B*, 58 (1999), pp. 289–294.
- [72] F. Cosandey, G. Skandan, A. Singhal, *J. Mater. Sci. Mater. Electron.* 52 (10) (2000).
- [73] G. Williams, G.S.V. Cole, *MRS Bull.*, 24 (6) (1999), pp. 25–29.
- [74] L. Lü, M.O. Lai, *Mechanical Alloying*, Kluwer Academic Publishers, 1998, pp. 11–21.
- [75] O.K. Tan, W. Cao, W. Zhu, *Sens. Actuators B*, 63 (1–2) (2000), pp. 129–134.
- [76] W. Cao, O.K. Tan, W. Zhu, B. Jiang, *J. Solid State Chem.*, 155 (2000), pp. 320–325.
- [77] J.Z. Jiang, S.W. Lu, Y.X. Zhou, S. Mørup, K. Nielsen, E.W. Poulsen, F.J. Berry, J. McMannus, *Mater. Sci. Forum*, 235–238 (1997), pp. 941–946.
- [78] J.Z. Jiang, R. Lin, W. Lin, K. Nielsen, S. Mørup, K. Dam-Johansen, R. Clase, *J. Phys. D Appl.*

Phys., 30 (1997), pp. 1459–146.

[79] W. Cao, O.K. Tan, W. Zhu, B. Jiang, J.S. Pan, *IEEE Sensors J.*, 3 (4) (2003), pp. 421–434.

[80] A. Verma, S. B. Samant, A. K. Bakhshi, S. A. Agnihotry, *Sol. Energy Mat. Sol. Cells* 88 (2005) 47.

[81] M.C. Carotta, S. Gherardi, C. Malagù, M. Nagliati, B. Vendemiati, G. Martinelli, M. Sacerdoti, I.G. Lesci, *Thin Solid Films* 515 (2007) 8339–8344.

[82] P. P. Phule, S. H. Risbud, *J. Mater. Sci.* 25 (1990) 1169.

[83] Y. Takahaschi, Y. Matsuoka, *J. Mater. Sci.* 23 (1988) 2259.

[84] Y. Takahaschi, K. Kiwa, K. Kobayashi, M. Matsuki, *J. Am.Ceram. Soc.* 74 (1991) 67.

[85] C. Sanchez, J. Livage, M. Henry, F. Babonneau, *J. Non-Cryst. Solids* 100 (1988) 65.

[86] M. Ivanda et al. *J. Mol. Struct.* 480–481 (1999) 645–649.

[87] Y. Watanabe, Y. Moriyoshi, Y. Suetsugu, T. Ikoma, T. Kasama, T. Hashimoto, H. Yamada, J. Tanaka, *J. Am. Ceram. Soc.* 87 (2004) 1395.

[88] K. Elkabouss, M. Kacimi, M. Ziyad, S. Ammar, F. Bozon-Verduraz, *J. Catal.* 226 (2004) 16.

[89] M. Wakamura, K. Hashimoto, T. Watanabe, *Langmuir* 19 (2003) 3428.

[90] J.J. Blaker, S.N. Nazhat, A.R. Boccaccini, *Biomaterials* 25 (2004) 1319.

[91] A. Lopez-Macipe, J. Gomez-Morales and R. Rodríguez-Clemente, *Adv. Mater.*, 10, (1998), 49.

[92] S. Koutsopoulos, *J. Biomed. Mater. Res.*, 62, (2002), 600.

[93] A. F. Lemos, J. H. G. Rocha, S. S. F. Quaresma, S. Kannan, F. N. Oktar, S. Agathopoulos and J. M. F. Ferreira, *J. Eur. Ceram. Soc.*, 26, (2006), 3639.

[94] D. Walsh, L. Arcelli, V. Swinerd, J. Fletcher, S. Mann and B. Palazzo, *Chem. Mater.*, 19, (2007), 503.

[95] S. Manara, F. Paolucci, B. Palazzo, M. Marcaccio, E. Foresti, G. Tosi, S. Sabbatini, P. Sabatino, G. Altankov and N. Roveri, *Inorg. Chim. Acta*, 361, (2008), 1634.

[96] A. Villacampa and J. M. García-Ruiz, *J. Cryst. Growth*, 211, (2000), 111.

[97] R. Ramachandra Rao, H. N. Roopa and T. Kannan, *J. Mater. Sci.: Mater. Med.*, 8, (1997), 511.

[98] M. Iafisco, B. Palazzo, M. Marchetti, N. Marghiotta, R. Ostuni, G. Natile, M. Morpurgo, V. Gandin, C. Marzano and N. Roveri, *J. Mater. Chem.*, 19, (2009), 8385–8392.

[99] Vandermolen, J.; Gomes, W. P.; Cardon, F. J. *Electrochem. Soc.* 127, (1980), 324

[100] Nazeeruddin, M. K.; Kay, A.; Rodicio, I.; Humphry-Baker, R.; Mueller, E.; Liska, P.; Vlachopoulos, N.; Grätzel, M. *J. Am. Chem. Soc.*, 115, (1993), 6382.

[101] T. Sugimoto, X. Zhou, A. Muramatsu, *J. Colloid Interface Sci.* 252 (2002) 339.

- [102] T. Sugimoto, K. Okada, H. Itoh, J. Disper. Sci. Tech. 19 (2–3) (1998) 143,
- [103], Y.Q. Wang, S.G. Chen, X.H. Tang, O. Palchik, A. Zaban, Y. Koltypin, A. Gedanken, J. Mater. Chem. 11 (2001) 521.
- [104] T.J. Mason, Sonochemistry: The Uses of Ultrasound in Chemistry, The Royal Society of Chemistry, 1990.
- [105] G.J. Price, Current Trends in Sonochemistry, The Royal Society of Chemistry, 1992.
- [106] (T. Sugimoto, X. Zhou, and A. Muramatsu, Journal of Colloid and Interface Science 252, (2002), 339–346
- [107] M. A. Rauf, M. A. Meetania, A. Khaleela and A. Ahmeda, ,Chemical Engineering Journal 157, (2010), 373-378.
- [108] M.A. Rauf, S. Salman Ashraf, , Chemical Engineering Journal 151, (2009), 10–18.
- [109] K Ioannis., A. Konstantinou Triantafyllos Albanis, Applied Catalysis B: Environmental 49, (2004), 1-14.
- [110] O. Carp, C.L. Huisman, A. Reller, Progress in Solid State Chemistry, 32, (2004), 33–177.
- [111] D., Mitoraj, A. Janczyk, M. Strus, H. Kisch, G. Stochel, P.B. Heczko and W. Macyk, Photochem. Photobiol. Sci., 6, (2007), 642-648.
- [112] Hiura T. et al., Biomedical Research, 31(2), (2010), 151-154.
- [113] R. Capparelli, F. De Chiara ,N. Nocerino , R. C. Montella, M. Iannaccone, A. Fulgione, A. Romanelli, C. Avitabile, G. Blaiotta, F. Capuano, BMC Immunol., 61, (2012) 17-13.
- [114] E. Y. Bullent, Journal of Materials Science, 21 (1986) 1087-1092
- [115] F. Dacheille, P. Y. Simons and R. Rov, Am. Mineralogist 53, (1968) 1929 -1939
- [116] J. M. Yu, L. Z. Zhang, Z. Zheng, J. C. Zhao, Chem. Mater. 15, (2003) , 2280
- [117] S. Kurtaran *, Đ. Kavlak **, G. S. Kurkcuođlu, Eskiseir Osmangazi Univerisity
- [118] A. Mattew American Mineralogist, Volume 61, pages 419424, 1976
- [119] Y. Liao, W. Que, V. Jia, Y. He, J. Zhang, P. Zhong, J. Mater. Chem., 22, (2012), 7937-7944.
- [120]J. Sanz, I. Sobrados, J. M. Coronado, A. Javier Maira, M. Hernandez-Alonso, and F. Fresno, J. Phys. Chem. C, 111, (2007), 10590-10596.
- [121] ([M.R. Hoffmann, S.T. Martin, W. Chot, D. Bahnemann, , Chem. Rev. 95, (1995), 69–96.
- [122] A.M. Peiro´, J.A. Aylló´n, J. Peral, X. Domenech, , Appl. Catal. B: Environ., 30, (2001), 359–373.
- [123] J. Araña et al. J. Haz. Mat., 146, (2007) 520–528.
- [124] M. Gualandi, E. Foresti, M. Lelli, M. Marchetti, F. Pierini, N. Roveri, S. Vecchiotti, G. Montebugnoli, E. D’amen I.G. Lesci, F. Rinaldi, G. Fracasso, Italian Patent n. MI2011A002384 storage data 23/12/2011 – PCT 05/11/12

[125] P. Gualandi, A. Gualandi, J. Gualandi, M. Gualandi, M. Lelli, M. Marchetti, F. Pierini, N. Roveri, S. Merli, G. Montebugnoli, E. D'amen, F. Rinaldi, Italian Patent n. MI2012A001310 storage data 26/07/2012